

# **The PISCES Program FY04-06 Progress Report**

**George Tynan, Russell Doerner, Farrokh Najmabadi  
and the PISCES Team**

**9 May 2006**



**Center for Energy Research**  
University of California, San Diego  
9500 Gilman Drive  
La Jolla, CA 92093-0420

# **The PISCES Program FY04-06 Progress Report & FY07-09 Research Plans**

Submitted to

The Office of Fusion Energy Science  
Office of Science  
US Department of Energy

By

Dr. George R Tynan  
Professor of Engineering Science,  
Department of Mechanical and Aerospace Engineering  
Principal Investigator

Dr. Russell Doerner  
Senior Research Scientist  
Department of Mechanical and Aerospace Engineering  
Co-Principal Investigator

Dr. Farrokh Najmabadi  
Professor of Electrical and Computer Engineering  
Department of Electrical and Computer Engineering  
Co-Principal Investigator

University of California San Diego  
Jacobs School of Engineering  
Center for Energy Research

9 May 2006

# **The PISCES Program FY04-06 Progress Report & FY07-09 Research Plans**

Contributions from

G. Antar, M. Baldwin, R. Doerner, J. Hanna, C. Holland, E. Hollmann, F.  
Najmabadi, D. Nishijima, R. Pugna\*, G.R. Tynan, K. Umstadter, J. Yu,

University of California San Diego  
Jacobs School of Engineering  
Center for Energy Research

\*US-EU-EFDA Exchange Long-term Visitor  
Max Planck Institute for Plasma Physics of Plasmas  
Garching, Germany, EU

Acknowledgement:

Prof. D. Whyte, UW-Madison for  
A discussion fo the ARRIBA in-situ real-time  
PMI diagnostic

9 May 2006

## **Project Summary**

As the US and World Magnetic Fusion Energy (MFE) programs move into the burning plasma era, there are a number of plasma material interaction (PMI) issues and edge and scrape-off layer (SOL) boundary plasma issues that impact the design and performance of both the core plasma and of plasma-facing components (PFCs) in burning plasma devices, particularly ITER. Strong edge plasma turbulence induces cross-field transport, causing both diffusive-like and convective plasma transport into and through the SOL region. This plasma can then flow either along magnetic field lines or, if cross field transport processes are fast enough, can move this plasma all the way to the first wall where it can sputter wall material. Neutralized plasma particles as well as sputtered material are then ionized and transported back towards the separatrix; a portion of these particles find their way across the separatrix and into the main plasma, while the remainder are transported along the magnetic field down into the divertor region. AS an example, the present ITER PFC design calls for the use of Beryllium for the first wall, Carbon for the divertor strike point, and Tungsten for the divertor armor. These edge and SOL PMI and transport processes lead to the formation of mixed materials on both the divertor and main plasma PFCs. The performance and interaction of these mixed materials with the plasma during steady-state, transient, and off-normal plasma events will then play a critical role in determining PFC lifetime, tritium retention and core plasma performance of ITER.

The SOL and Divertor ITPA Group has identified four high-priority boundary plasma and PMI research tasks that directly impact the design and performance of the ITER PFC system. The PISCES program is addressing three of these high priority issues:

- **Effects of ELMs/disruptions on divertor and first wall structures.**
- **Tritium retention effects in mixed materials and investigating various removal techniques.**
- **Improve measurements & understanding of plasma transport to targets and walls**

The PISCES Program is making important contributions to these critical PMI and Boundary Plasma Science issues. In addition to being responsive to ITPA relevant research requests, the PISCES Program is also integrated into all levels of the US BPO effort. This, coupled to an active engagement of the international ITER team, ensures that PISCES results are directly impacting the ITER design and helping to minimize the risk associated with the ITER project. The overall program objective can be stated as:

***Perform Basic Plasma-Materials Interaction & Boundary Plasma Research Needed for ITER PFC Design Validation and Performance Predictions***

In order to successfully meet this program objective, the PISCES Program uses the PISCES-B facility to perform controlled plasma experiments using ITER candidate materials. This facility is uniquely capable of using Beryllium in mono-material and

mixed material PMI experiments, and thus provides the focal point of the US-European Union European Fusion Development Association (EU EFDA) collaboration, which is focused upon ITER PFC R&D needs. As a part of this collaboration, the ability to apply thermal transients in these PMI experiments was added in FY06, and the first thermal transient PMI experiments are now underway; first results will be presented at the May 2006 PSI meeting in Hefei, China. The program is now prepared to perform controlled PMI studies of Be, C, W mono-materials as well as studies of Be-C, Be-W, C-W and ternary material combinations in both steady-state and ELM-like thermal transient PMI conditions. The program also takes advantage of a number of other laboratory plasma devices at UCSD to develop new PMI experimental capability, develop new edge plasma diagnostics and data analysis techniques, study the essential elements of turbulent cross-field SOL plasma transport, and perform fundamental PMI and divertor plasma physics studies.

**Key results from the FY04-06 time period include:**

- Discovery of Be-W alloy formation under ITER relevant PMI conditions. These alloys have significantly different thermo-mechanical properties that impact ITER divertor performance (US-EU EFDA Collaboration)
- Discovery of a large reduction of C chemical erosion in Be-containing plasmas due to PMI-driven Be<sub>2</sub>C formation in the near-surface region of C targets, and demonstration that Be<sub>2</sub>C mixtures rapidly form between ELMs for expected ITER conditions (US-EU EFDA Collaboration)
- Experimental validation of Monte-Carlo simulations of exit-angle dependence of erosion yield, and validation of Be erosion-redeposition modeling.
- Demonstration of the universal character of intermittent transport events in tokamak edge plasmas and linear PISCES-A plasma device.
- Observation of spontaneous sheared flows driven by small-scale turbulence, verifying recent theory predictions of turbulent transport saturation mechanism in MFE core and edge plasmas

**The primary issues that will be investigated in the FY07-09 time period include:**

- Continue the US/EU EFDA collaboration, with a focus on extending Be/C, Be/W, and Be/C/W mixed material experiments to ELM-like transient thermal loading conditions
- Test and validate edge plasma and PMI models, including WBC and ERO erosion/redeposition models, the UEDGE time-averaged fluid SOL model, and UCSD-developed fluid-based edge, SOL turbulence simulations, to develop deep understanding of mixed material PMI in turbulence SOL plasmas.
- Develop in-situ PMI diagnostics and investigate high priority PMI-related ITER R&D needs such as first-mirror degradation.

This proposal is organized as follows. In part I, a summary of the research results from FY04-06 is given. Part II summarizes our program plans for FY07-09, making reference to the recent results. Each of these portions is organized to first present PMI-related work followed by the boundary plasma research and supporting development work.

**Table of Contents**

|   |           |
|---|-----------|
| <b>Project Summary .....</b>  | <b>1</b>  |
| <b>Part I: Progress Report for FY04-06 .....</b>  | <b>5</b>  |
| Plasma-Materials Interaction Research .....   | 5         |
| I. Introduction .....   | 5         |
| II. Mixed-Material Investigations .....   | 5         |
| II.a. C/Be Mixed-material layer formation on graphite exposed to Be-seeded<br>deuterium plasmas .....                   | 6         |
| II.b. Hydrogen isotope retention in co-deposited C/Be layers.....   | 11        |
| II.d. Parametric studies on carbon chemical erosion mitigation dynamics due to<br>Be seeding deuterium plasma. ....     | 14        |
| Scaling law for protective Be layer formation time.....   | 18        |
| Implications of Be-C Mixed Material PMI Studies for ITER .....  | 20        |
| II.e. Beryllium-tungsten alloy formation on tungsten exposed to Be-seeded<br>deuterium- plasmas .....                   | 20        |
| Implications of Be-W Mixed Material PMI Studies for ITER .....  | 22        |
| III. Mono-materials Investigations.....   | 23        |
| III.a. Angular distribution of sputtered beryllium atoms from a beryllium target<br>exposed to a deuterium plasma ..... | 23        |
| III.b. Angular distribution of sputtered carbon and metal surfaces .....  | 26        |
| III.c. Temperature dependent erosion of beryllium .....   | 28        |
| Supporting Boundary Plasma Science and Hardware Development Accomplishments<br>in FY2004-2006 .....                     | 29        |
| I. Introduction .....   | 29        |
| II. Edge and SOL Turbulence, Transport, and Flows .....   | 30        |
| III. Divertor Physics Studies .....   | 35        |
| IV. Pulsed surface heat deposition system development.....  | 42        |
| <b>Part II: Proposed Work for FY07-09.....</b>  | <b>45</b> |
| I. Introduction .....   | 45        |
| II. Mixed-Material Research.....  | 47        |
| II.a. Binary element combinations .....   | 47        |
| II.a.1. Beryllium-Carbon system.....  | 47        |
| II.a.2. Beryllium-Tungsten system.....  | 49        |
| II.a.3. Beryllium-Nickel system (JET erosion tile marker development).....  | 50        |
| II.b. Tertiary element combinations.....  | 50        |
| II.b.1 Beryllium and methane seeded plasma interactions with graphite targets..   | 51        |
| II.b.1 Tertiary element plasma interactions with tungsten targets .....   | 51        |
| II.c. Codeposited material evaluations.....   | 52        |
| II.c.1. Witness plate samples.....  | 52        |
| II.c.2. First mirror coatings .....   | 53        |
| III. Mono-Material Research .....   | 53        |
| III.a.1. Mixed material sputtering yield via spectroscopy .....   | 54        |
| III.a.2. Angular distribution of sputtered Be atoms .....   | 54        |
| III.a.3. Energy distribution of sputtered Be atoms.....   | 55        |

|  |           |
|--|-----------|
| III.a.4. Importance of Be metastable states for Be spectroscopy in SOL plasmas | 55        |
| III.b. Tungsten plasma-material interactions .....                             | 57        |
| III.c. Carbon mono-material investigation .....                                | 57        |
| III.d. Deuterium migration into molybdenum.....                                | 58        |
| IV. PMI Modeling Code Validation .....   | 59        |
| V. Boundary Plasma Science and Supporting Hardware Development Tasks.....      | 60        |
| Divertor Physics.....  | 63        |
| In-situ Real-time PMI Diagnostic Development .....                             | 66        |
| Hardware Development for Transient PMI Experiments .....                       | 72        |
| <b>References.....</b>   | <b>74</b> |

## **Part I: Progress Report for FY04-06**

The PISCES Program is organized into PMI-related research, boundary plasma research, and supporting hardware and diagnostic development efforts. In Part I of this proposal we summarize the key FY04-06 accomplishments in each of these three program areas.

### **Plasma-Materials Interaction Research**

#### **I. Introduction**

The PISCES Program Plasma-Materials Interaction research effort is focused primarily on the investigation of mixed materials that might be expected to form in the ITER device, namely Be, C and W. This effort is centered on a bilateral US-EU collaboration on mixed-material effects for ITER. In the ITER device, the first wall will be constructed using beryllium tiles. The divertor region will be constructed of tungsten with the high heat flux divertor strike points fabricated from graphite. Material eroded from the first wall will flow into the divertor region along with the diverted plasma fuel. Developing an understanding of the interaction of this beryllium containing hydrogenic plasma with the tungsten and carbon surfaces in the divertor is crucial to accurately predicting the tritium accumulation rate within the ITER vacuum vessel.

In addition to the mixed-material studies, a smaller effort has focused upon the investigation of PMI effects with mono materials. Specifically the erosion of solid, single element surfaces as a function of temperature has been investigated and a theoretical explanation for the observed temperature dependent erosion in a variety of materials has been developed. The angular dependence of erosion of sputtered beryllium atoms and carbon clusters emitted during sputtering events has also been measured. The significant results in all of these areas will be summarized in the following sections.

#### **II. Mixed-Material Investigations**

The progress achieved during the present proposal period (FY04-06) focuses on new capabilities added to the PISCES-B linear plasma simulator. These include a beryllium atom beam source to allow seeding of the deuterium plasma column with controllable amounts of beryllium impurity ions. In addition, a temperature controlled witness plate manipulator has been installed to allow collection of redeposited material in a region shielded from the primary plasma flux. Finally, the capability to deliver large pulses of heat to plasma-exposed samples, along with the diagnostics to accurately measure the resultant surface temperature has been recently developed and demonstrated on the PISCES-B device, opening the way for thermal transient mixed PMI experiments in the coming FY07-09 period.

In ITER, the beryllium impurity concentration in the divertor plasma is expected to be in the 1-10% range. Experiments in PISCES-B find that even a very small beryllium impurity concentration (as low as 0.1%) is sufficient to dramatically reduce the graphite

target chemical and physical erosion rates. Fig. 1a shows the spectroscopic signature of chemical erosion (CD band emission) from a sample exposed at 200°C while Fig. 1b shows the physical sputtering signature (C-I line radiation) from a sample exposed at 700°C to deuterium plasma. Data is presented for cases with and without beryllium seeding of the plasma. Weight loss measurements confirm the spectroscopic signature data and indicate a reduction of the total erosion from the graphite samples by more than an order of magnitude when the beryllium concentration in the plasma is as low as 0.1%.

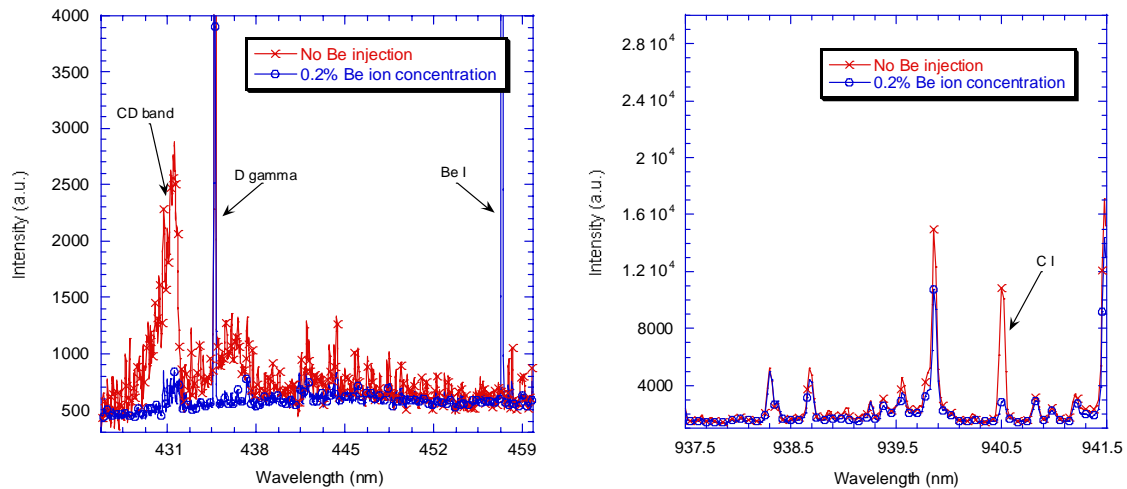


*Fig. 1 – Beryllium impurity seeding of the incident deuterium plasma reduces both a) chemical erosion and b) physical sputtering of graphite target plates.*

The cause of the reduction becomes apparent during post-exposure surface analysis of the graphite targets. Auger electron spectroscopy of the sample surface exposed at 200°C reveals essentially complete (>90%) coverage of the graphite sample by a thin beryllium layer as long as the Be seeding concentration exceeds 0.1% of the plasma density. Similar effects are observed during exposure of graphite samples at 1000°C, although a slightly higher Be seeding rate (>0.3%) is needed to achieve 90% Be surface coverage. This is due to the higher rate of diffusion of Be into the bulk at the higher temperature, as well as an increase in the Be erosion rate at higher temperature [4]. A significant effort during this proposal period has been devoted to understanding the changes in the surface layer that account for the observed changes in the erosion of mixed Be-C samples. The insights gained from these experiments are currently being incorporated into PMI modeling codes to ensure the codes can predict the observed surface behavior in PISCES before subsequently making predictions for what behavior might be expected in ITER.

### *II.a. C/Be Mixed-material layer formation on graphite exposed to Be-seeded deuterium plasmas*

Graphite erosion mitigation is accompanied by fundamental changes in the chemical nature of the surface as beryllium is deposited. Insight into this effect was gained using a comprehensive collection of surface-diagnostic methods. In particular, surface-chemical interaction between mixed-surface elements, mixed-layer composition, and the impact of mixed-materials on hydrogen-isotope retention were explored utilizing facilities located at UCSD PISCES and the DIONOSIS facility at the University of Wisconsin.

Following exposure to beryllium-seeded deuterium plasma, the graphite targets were probed using x-ray photoelectron spectroscopy (XPS) to study the chemical state of the mixed material surface. Shown in Fig. 2 are C-1s and Be-1s XPS spectra for targets exposed to plasma for  $\sim 3000$  s at 450 K, 730 K and 950 K where  $f_{\text{Be}} = 0.001$ . A set of spectra for clean-reference targets that show metallic beryllium and graphitic carbon is also given to facilitate comparison. In all but the lowest temperature case of 450 K, exposed-target surfaces are found to display evidence of chemical reaction with beryllium incident during the exposure. The formation of beryllium carbide ( $\text{Be}_2\text{C}$ ) is readily observed based on comparison with the clean-reference targets and XPS-peak positions stated in the literature [Goldstrass:2001, Linsmeier:2001]. Only the 450 K exposed case shows any sign of elemental graphite and beryllium while targets exposed at higher temperature are found to be fully surface carbidized. Here the graphitic C1 s peak at 284.7 eV is shifted to a carbidic peak at 282.3 eV and the metallic Be 1 s peak at 111.8 eV to 112.2 eV.

The composition of mixed Be/C layers with depth was studied using RBS in a collaboration between the UCSD PISCES group and the UW-Madison DIONYSIS facility. Backscatter spectra for two targets are shown above in Fig. .3. The spectrum of an unexposed graphite standard (STD) target is also shown for reference. In Rutherford Backscattered Spectroscopy (RBS), leading edges in data represent ion-backscatter events from given elements at the very surface of the target. Projectile ions scattered from deeper within the target surface are measured with lower-kinetic energy due to energy loss in the material. The figure contrasts the backscatter spectra for the carbon leading edges of two targets that received different beryllium plasma ion fluences at  $\sim 500$  K in plasmas where  $f_{\text{Be}} = 0.0015$ . The plasma exposure times are 1600 s and 4600 s, corresponding to beryllium-ion fluences of approximately  $3 \times 10^{22} \text{ m}^{-2}$  and  $1 \times 10^{23} \text{ m}^{-2}$ . When compared with the unexposed-graphite target, notable count depletion ( $\sim 0.5\text{--}0.7$  MeV) is observed on those targets exposed to the plasma containing beryllium indicating less carbon at the target surface. This is due to the presence of beryllium on the targets and can be modelled with a layer approximately  $0.6 \mu\text{m}$  thick (as indicated schematically), of beryllium concentration gradient varying from  $\sim 75\text{--}85$  at. % at the target surface, to  $\sim 10\text{--}15$  at. % at the graphite target substrate. The similarity in both layers suggests a saturation of the target surface, at least under the present set of plasma conditions.

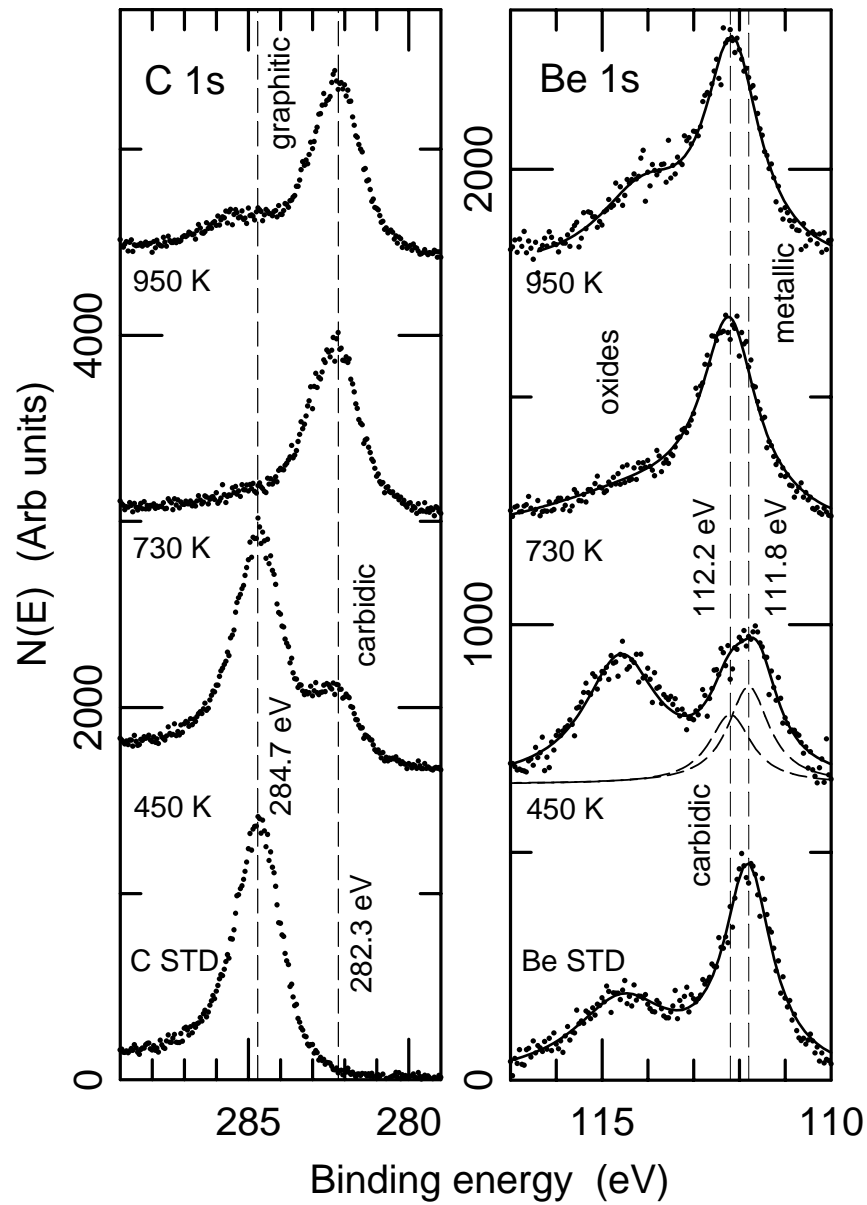


Fig. 2 – XPS analysis of beryllium and carbon binding on the surface of carbon targets exposed to a beryllium containing plasma at different target temperatures. The Be-C bond is seen to be primarily carbidic in nature, suggesting the formation of a beryllium carbide ( $\text{Be}_2\text{C}$ ) surface layer.

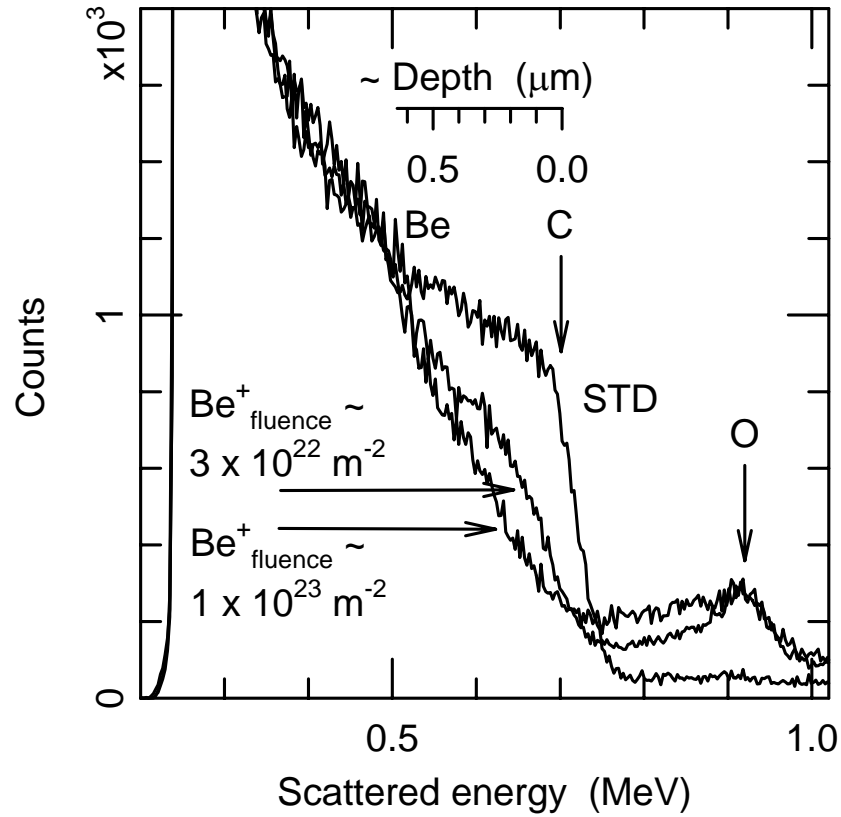


Fig. 3 - Rutherford Backscattered Spectra (RBS) from graphite samples. A notable count depletion for backscattered particles with energy 0.5–0.7 MeV is observed on targets that were exposed to Be-seeded plasma, indicating less carbon at the surface of these targets. Data courtesy of D. Whyte, UW-Madison.

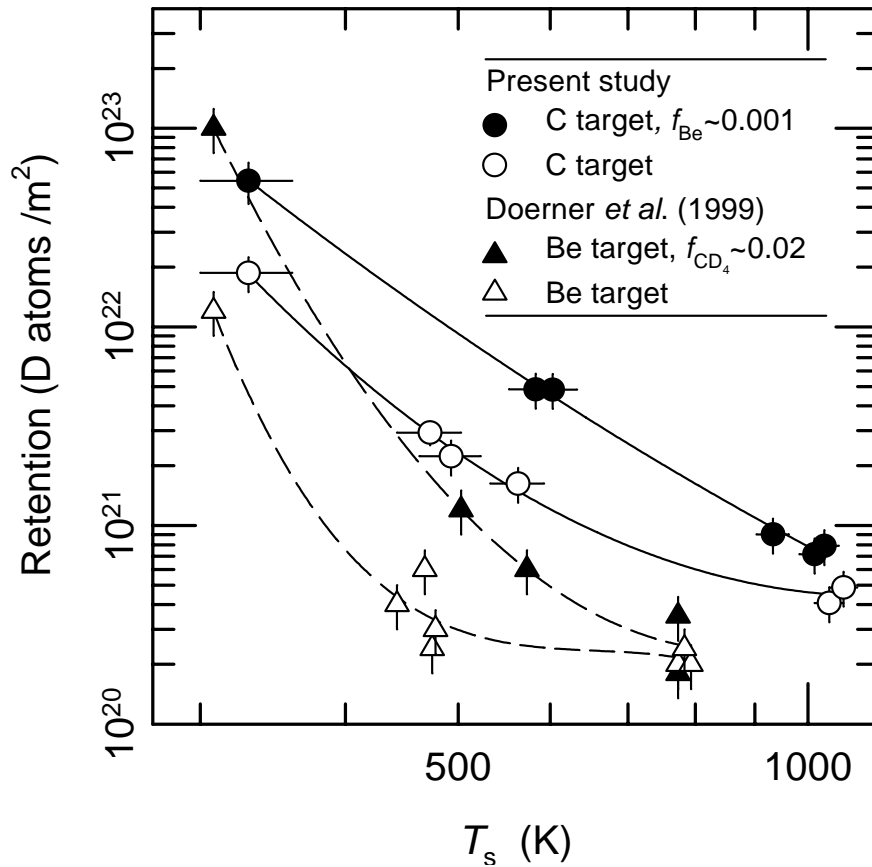


Fig. 4: Deuterium retention determined using TDS, as a function of target-surface temperature during plasma exposure. Data are shown for graphite targets exposed to both pure and beryllium containing ( $f_{\text{Be}}=0.001$ ) deuterium plasma. The plasma fluences vary from  $2-5 \times 10^{26}$  D ions  $\text{m}^{-2}$ . The plot shows that retention falls significantly with exposure temperature.

In Fig. 4 above, deuterium retention in samples that are directly exposed to the plasma, determined using TDS, is plotted against target-surface temperature during exposure. Data are shown for graphite targets exposed to both pure, and beryllium containing,  $f_{\text{Be}}=0.001$ , deuterium plasma while the plasma fluence varies from  $2-5 \times 10^{26}$  D ions  $\text{m}^{-2}$ . The plot shows that retention falls significantly with exposure temperature; a result that, in pure graphite, has also been observed by others [Haasz:1996] and this is also apparently true for mixed material Be/C surfaces. However, targets with a mixed Be/C surface show systematically higher retention than targets without this mixed layer. Retention in targets with a mixed-material surface is increased by a factor of  $\sim 4$  at temperatures below 600 K, while only a  $\sim 2$  increase in retention inventory is seen at  $\sim 1000$  K. Also shown in Fig. 4 are previously published PISCES mixed-materials retention data [Doerner:1999]. In those experiments, pure-beryllium targets are exposed under similar conditions to the present study, and retention is compared for plasma

exposures with and without deuterated methane ( $\text{CD}_4$ , ~2 %) injection. As with the present study, retention is increased in beryllium targets with a mixed-material layer and the difference narrows at temperatures beyond 600 K.

The other primary area of concern for ITER is tritium retention in codeposited layers away from the divertor strike point locations. This issue is addressed in the next section by using the witness plate manipulator, supplied by IPP-Garching as part of the US-EU EFDA collaboration, to collect eroded material during mixed beryllium-carbon sample exposures.

### *II.b. Hydrogen isotope retention in co-deposited C/Be layers*

The major disadvantage to using carbon as a first wall material is its ability to trap hydrogen at a level up to 0.4 H/C in codeposited layers. Chemically eroded  $\text{C}_x\text{H}_y$  species have less than unity sticking probabilities; as a result codeposited layers can form in unexpected locations that are difficult to access by subsequent T removal processes. JET [Coad:2001] and ASDEX Upgrade [Rohde:2001] have reported such observations. In ITER, the inventory of tritium in codeposited layers (limited to 350 g) is a serious issue that must be addressed to meet stringent safety and licensing requirements. The witness plate diagnostic on PISCES-B has been used to sample deposited and codeposited materials in the vicinity of graphite targets exposed to deuterium plasma with an ionized beryllium fraction in order to simulate ITER conditions. Witness plate samples were subsequently analyzed for elemental composition using XPS sputter-depth profiling and deuterium content using TDS.

Fig. 5 shows representative XPS sputter depth profile analysis results. Deposited layers were formed on Ta witness plates by eroding a graphite target with a Be-seeded deuterium plasma ( $f_{\text{Be}}=0.002$ ) at surface temperatures of 600 K and 1000 K. The targets were exposed to ion fluences of  $2.4 \times 10^{26} \text{ m}^{-2}$  while the witness plates were kept at 300 K. The XPS profiles show a reverse history of the plasma exposure of the graphite target. At plasma 'switch on', target erosion leads to a small amount of deposited C on the deposition probe coupons. Increased chemical erosion of the target case at 600 K results in more deposition of C compared to the 1000 K target exposure. Both deposited layers are ~100 nm thick and almost free of O impurities (1–3 at. %). Witness plates kept at 300 K during collection, but with half the Be seeding ( $f_{\text{Be}}=0.001$ ), show similar O content and reduced layer thickness ~50 nm. Higher witness plate temperatures however, revealed O contents up to ~30 at. %. All witness plates samples examined, regardless of temperature, showed low C content throughout the deposited layer (<3 at. %) once graphite target erosion was suppressed by coverage in Be.

The D/Be and O/Be ratios for the deposited films are shown in Fig. 6. The Be rich nature of the co-deposits allows comparison with other data in the literature [Causey:1998, Mayer:1996, Causey:1996] and are also plotted. The D/Be ratios seen in the deposited films in the PISCES data are found to decrease rapidly as the collection temperature is increased and systematically show the lowest deuterium retention compared to the other data. Retention decreases from ~0.1 D/Be at 300 K to ~0.01 D/Be at 600 K. It has been

suggested [Causey:1998] that O content in deposited Be films can have a strong influence on hydrogen isotope retention, effectively increasing the D/Be ratio to values comparable with a:C-H films during room temperature deposition. In Fig. 2, the data of Mayer *et al.* suggest that the D/Be ratios does decrease as O content in the film is reduced. However, the PISCES data are not consistent with this view. Instead, the presence of significant levels of O in the higher temperature co-deposits does not appear to affect the already low deuterium content. The origin of this discrepancy is not yet understood and will be the subject of future work.

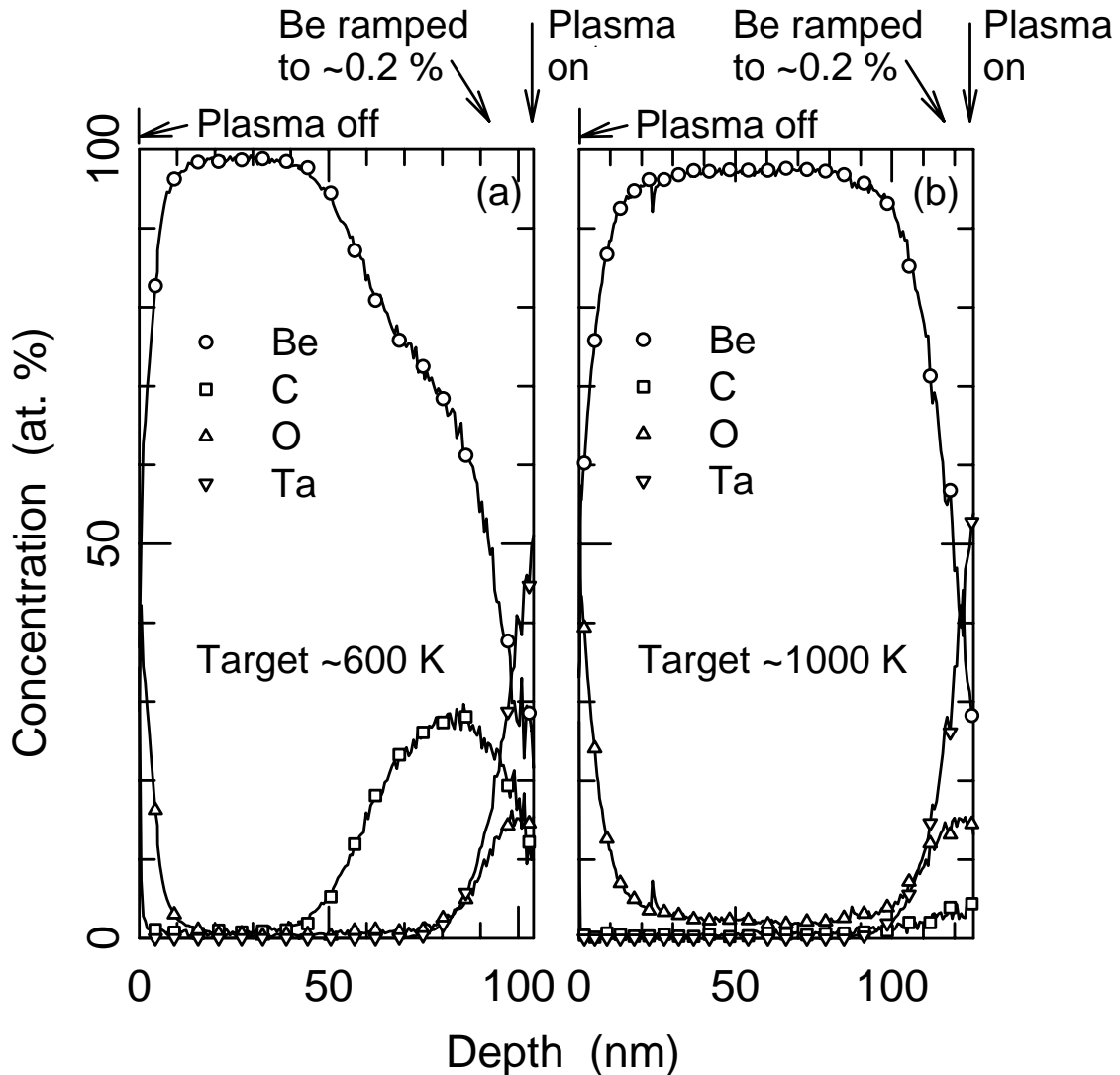


Fig. 5 - XPS depth profiles for deposited material collected on witness plate samples during beryllium containing deuterium plasma bombardment of graphite samples.

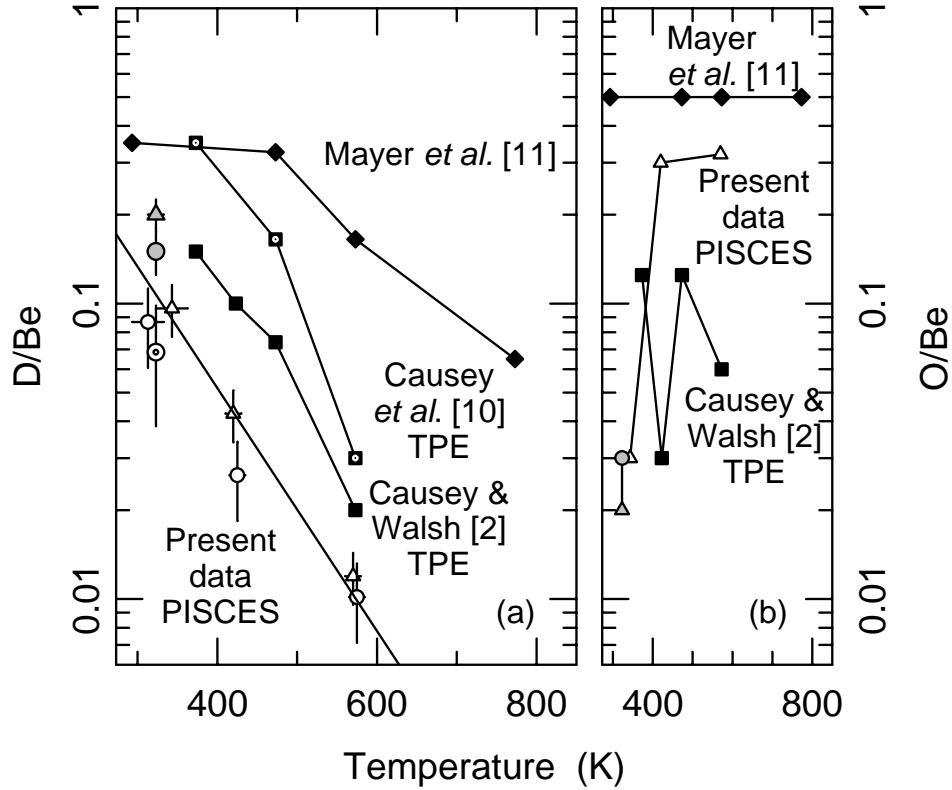


Fig. 6 – D/Be (a) and O/Be (b) ratios for deposited material collected on witness plate samples as a function of the witness plate temperature.

### II.c. Time resolved study of the mitigation of graphite chemical erosion in Be-seeded deuterium plasmas

We previously showed the strong reduction of C chemical erosion by seeding deuterium plasmas with small (<1%) amounts of Be. In order to gain further insight into the dynamics of this effect, the temporal behavior of the suppression of graphite chemical erosion was examined in a series of experiments. Graphite targets were exposed at 600 K to deuterium plasmas with fixed beryllium fractions in the range  $0.0003 \leq f_{Be} \leq 0.011$  while C target chemical erosion was monitored through CD band optical emissions from the target. An example of the temporal evolution of graphite chemical erosion in deuterium plasma containing beryllium is revealed by the optical emission and residual gas traces of Fig. 7 below. The plasma ‘switch on’ and beryllium injection ( $f_{Be} \sim 0.0015$ ) commence simultaneously and the plasma  $D\gamma$  emission is basically constant during the experiment, indicating that the plasma discharge conditions are constant in time.

The temporal behavior of the chemical erosion yield (Fig. 7(a)) is inferred from normalized CD band data (i.e. the ratio of CD/ $D\gamma$  emission), which decreases monotonically with discharge time to a ‘baseline’ value,  $\gamma_{baseline}$ . When this baseline is subtracted to remove background signal effects, the trend in the CD band strength is easily fit with a single decaying exponential term of rate of decay  $1/\tau_{CBe}$ . This behavior is

also qualitatively observed in the partial pressures for masses 18 (CD<sub>3</sub>) and 20 (CD<sub>4</sub>), Fig. 7(c). The change in neutral beryllium emission,  $\delta\text{Be I}$ , rises linearly during these experiments (Fig. 7(a)) and is thought to be associated with the erosion of beryllium that has been deposited on the target surface. Fig. 7(b) & 7(d) are data taken the following day and demonstrate that wall or startup interactions do not cause the observed trends in Fig. 7(a) & 7(c).

Data obtained at other beryllium fractions are found to behave similarly and show the emission decay rate increases as  $f_{\text{Be}}$  is increased, as shown in Fig. 8(a). CD-band data are shown for five different plasma-beryllium fractions. The relationship between  $f_{\text{Be}}$  and the decay rates,  $1/\tau_{\text{CBe}}$  are plotted Fig. 8(b). This plot is best represented by a power law expression  $1/\tau_{\text{CBe}} = \alpha f_{\text{Be}}^\beta$  where a weighted least squares fit yields  $\alpha = 785 \pm 161 \text{ s}^{-1}$  and  $\beta = 2.07 \pm 0.10$ . These empirical fits give good agreement with the data is observed over several orders of magnitude of  $f_{\text{Be}}$ .

#### *II.d. Parametric studies on carbon chemical erosion mitigation dynamics due to Be seeding deuterium plasma.*

A scaling study of C erosion mitigation by Be<sub>2</sub>C formation with relevant exposure parameters in PISCES has been performed in order to extrapolate our results to conditions that might be expected in the ITER divertor. We investigated the variation of the carbon chemical erosion mitigation time  $\tau_{\text{CD}}$  with  $f_{\text{Be}^+}$ , incident ion energy  $E_i$ , surface temperature  $T_s$  and incident ion flux  $\Gamma_i$ . This study contributes to better predictions of Be/C mixed-material effects in the ITER divertor and allows us to determine if Be and Be<sub>2</sub>C layers would form between ELMs.

##### *Be ion concentration dependence*

The Be ion concentration  $f_{\text{Be}^+}$  was scanned by changing the Be oven temperature while keeping other parameters,  $\Gamma_i$ ,  $T_s$  and  $E_i$ , constant. As shown in fig. 9, a fit of power function,  $\tau_{\text{CD}} = \alpha f_{\text{Be}^+}^\beta$ , to the data reveals a relatively strong dependence on  $f_{\text{Be}^+}$ , with a best fit value  $\alpha = 1.27 \times 10^{-3}$  and  $\beta = -2.07$ .

##### *Incident ion energy dependence*

By varying the incident ion energy  $E_i$  while all other parameters are constant, we find that  $\tau_{\text{CD}}$  is nearly proportional to  $E_i$  (Fig. 10). This tendency may be due to the fact that, at higher incident energy, Be deposited on the C target can be more readily sputtered before Be<sub>2</sub>C is formed, resulting in an increased value for  $\tau_{\text{CD}}$ .

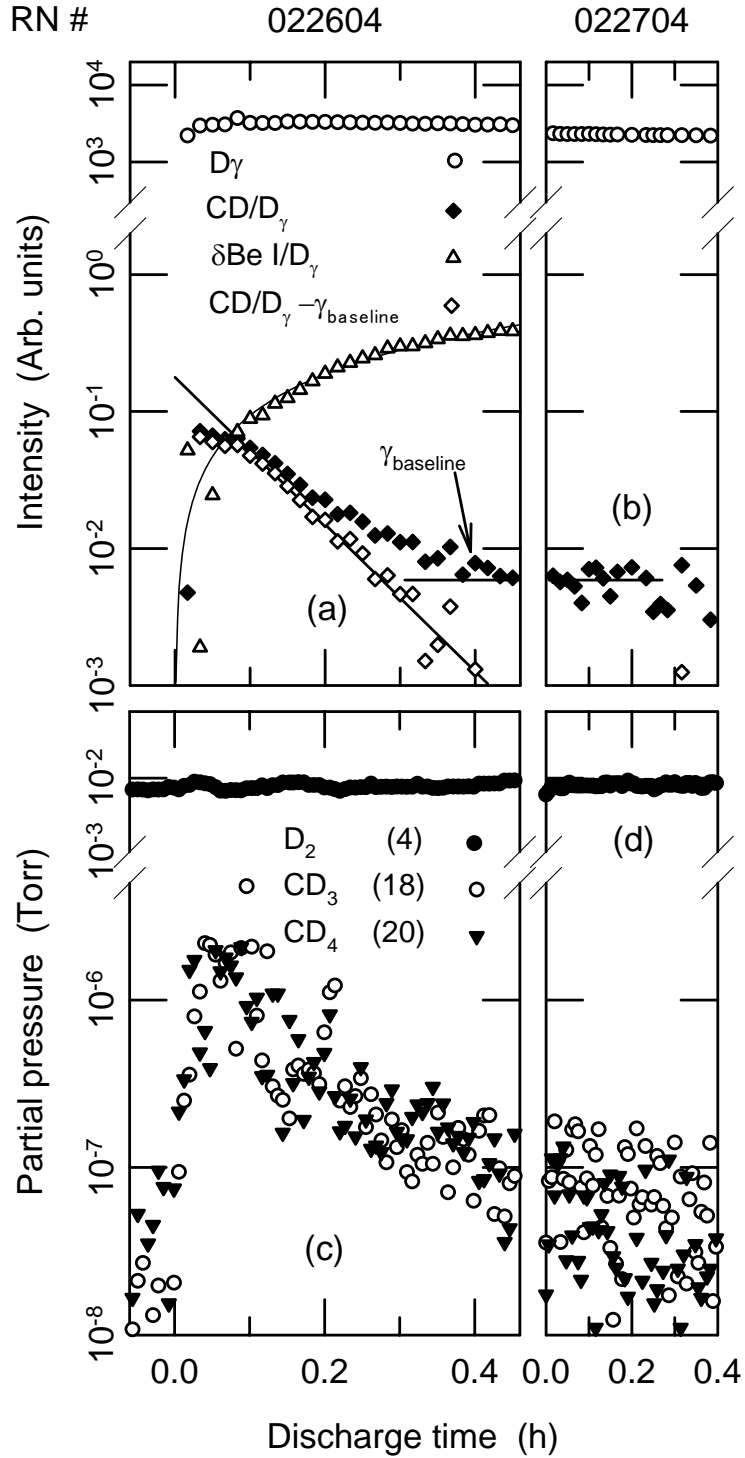


Fig. 7 –Evolution of plasma discharge showing (a&b) CD band and Be I line emission, (c&d) gaseous impurity and plasma gas partial pressures.

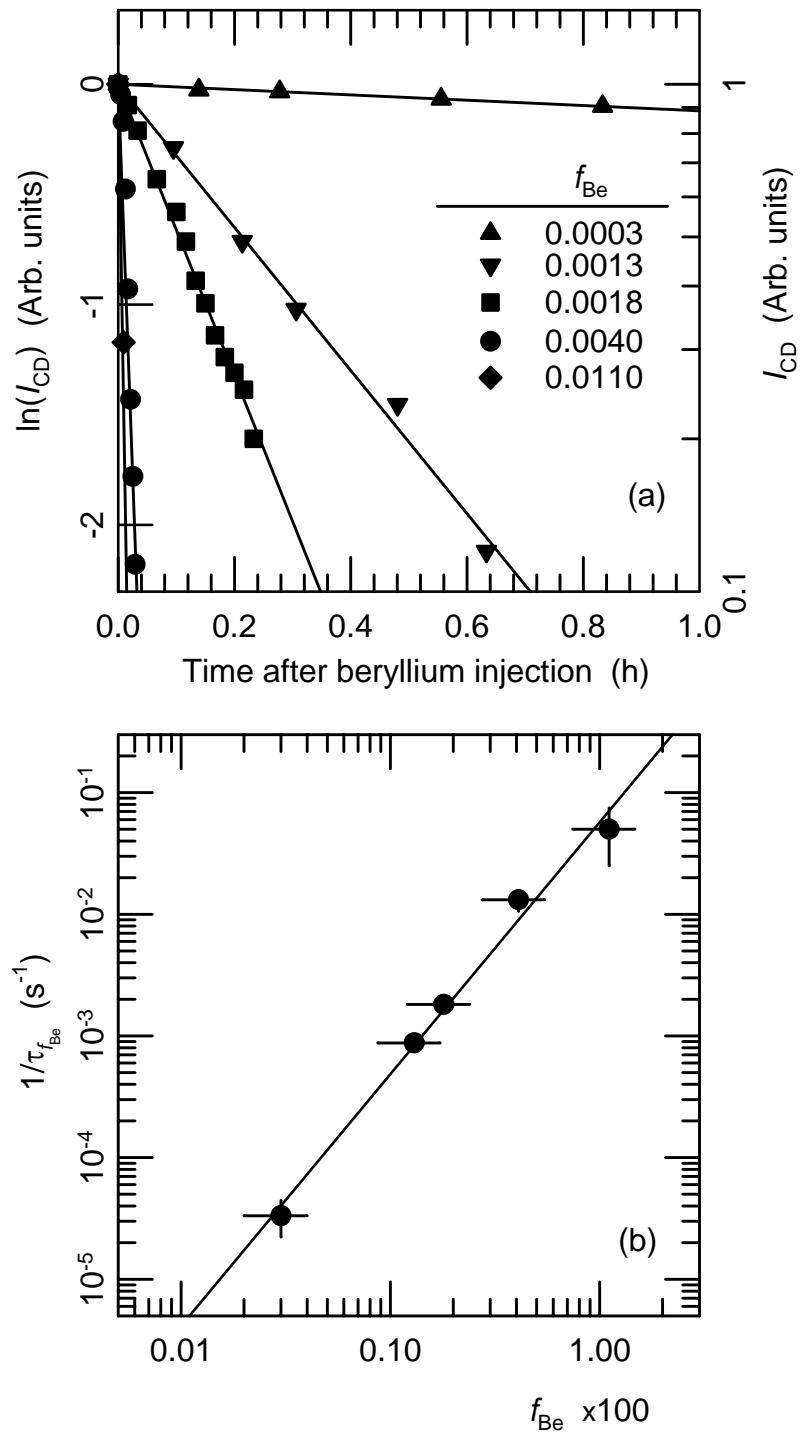


Fig. 8 – Temporal behavior of CD band intensity (a) during plasma bombardment with varying concentrations of Be impurities, (b) least squares fit of CD band decay time.

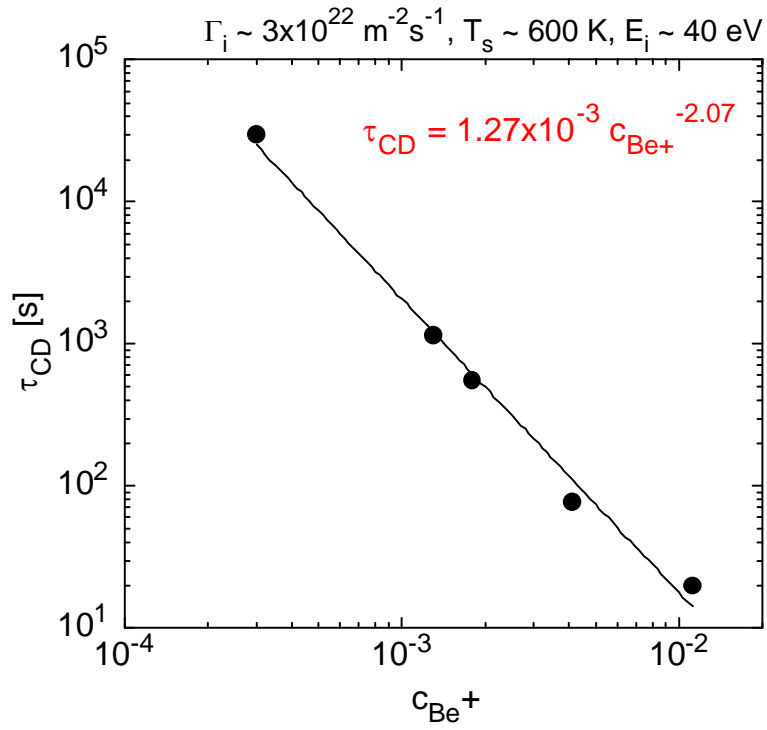


Fig. 9 - Be ion concentration dependence of CD band decay time.

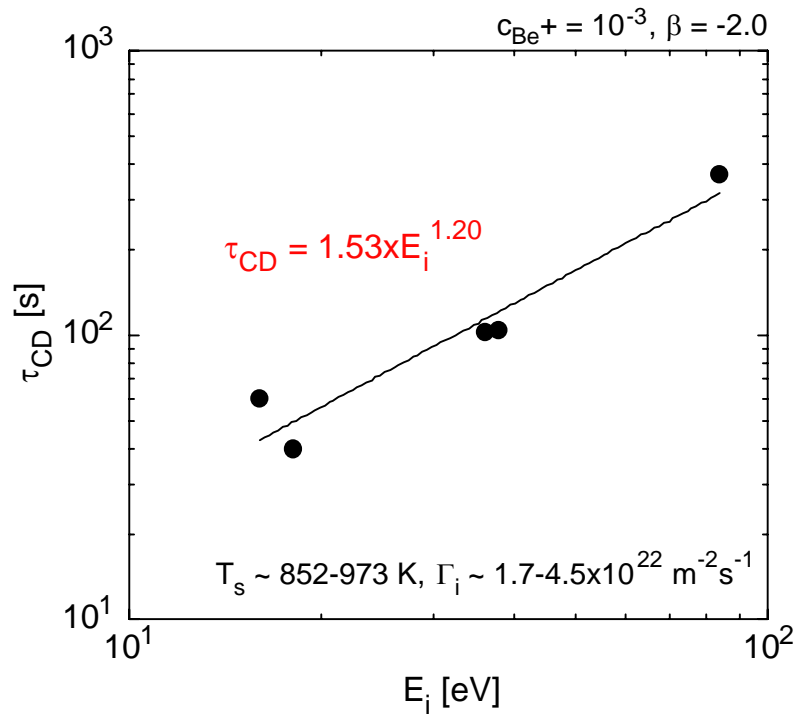


Fig. 10 - Incident ion energy dependence of CD band decay time.

### *Surface temperature dependence*

The decay time is plotted as a function of the inverse of surface temperature in fig. 11. The data is fitted with an Arrhenius exponential function with an activation energy of approximately 0.4 eV (4600 deg K). At a higher surface temperature  $T_s$  of  $\sim 950$  K ( $1/T_s \sim 0.001$  K<sup>-1</sup>),  $\tau_{CD}$  becomes shorter than that at  $T_s \sim 600$  K ( $1/T_s \sim 0.0017$ ) by a factor of  $\sim 20$ , perhaps due to the fact that beryllium carbide (Be<sub>2</sub>C) forms more readily at higher  $T_s$ . As shown in the inset of fig. 4, the parameter  $\beta$  in  $\tau_{CD} = \alpha f_{Be^+}^\beta$  at  $T_s \sim 950$  K is nearly the same ( $\sim 2$ ) as that at  $T_s \sim 600$  K, indicating the same trend with respect to  $f_{Be^+}$ .

### *Scaling law for protective Be layer formation time*

Using these results, we find an empirical scaling for the C-erosion mitigation time given as

$$\tau_{CD}^{\text{scale}} [\text{s}] = 1.0\text{e-}7 f_{Be^+}^{-1.9\pm 0.1} E_i^{0.9\pm 0.3} \Gamma_i^{-0.6\pm 0.3} \exp(4.8(\pm 0.5) \times 10^3 / T_s), \quad (1)$$

where  $f_{Be^+} = n_{Be^+}/n_e$ ,  $E_i$  in eV,  $T_s$  in deg K and  $\Gamma_i$  in  $10^{22}$  m<sup>-2</sup>s<sup>-1</sup>. In fig. 12, the experimentally measured decay time obtained under a variety of plasma conditions is compared with this scaling expression. The experimental values agree well with the scaling expression over a wide range of operating conditions. From the expression, it is found that the decay time has a weak negative power law dependence on the incident ion flux ( $\Gamma_i^{-0.5}$ ). This may indicate that at higher fluxes, sputtered Be atoms are more likely to be ionized in the plasma, thereby increasing the re-deposited fraction of Be and thus leading to shorter decay time.

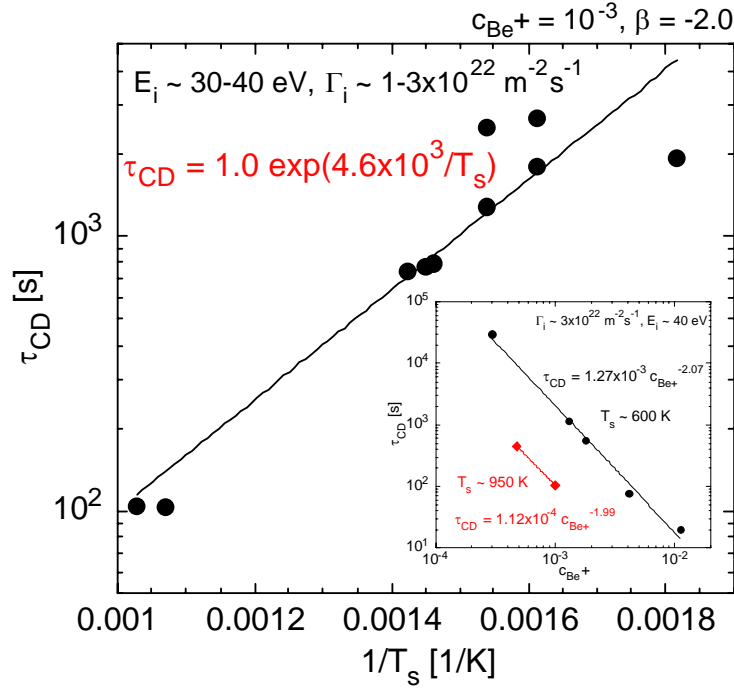


Fig. 11 - Surface temperature dependence of CD band decay time. An exponential fit is performed. The inlet shows the Be ion concentration dependence of CD band decay time at two surface temperatures  $T_s \sim 600$  K (black) and 950 K (red).

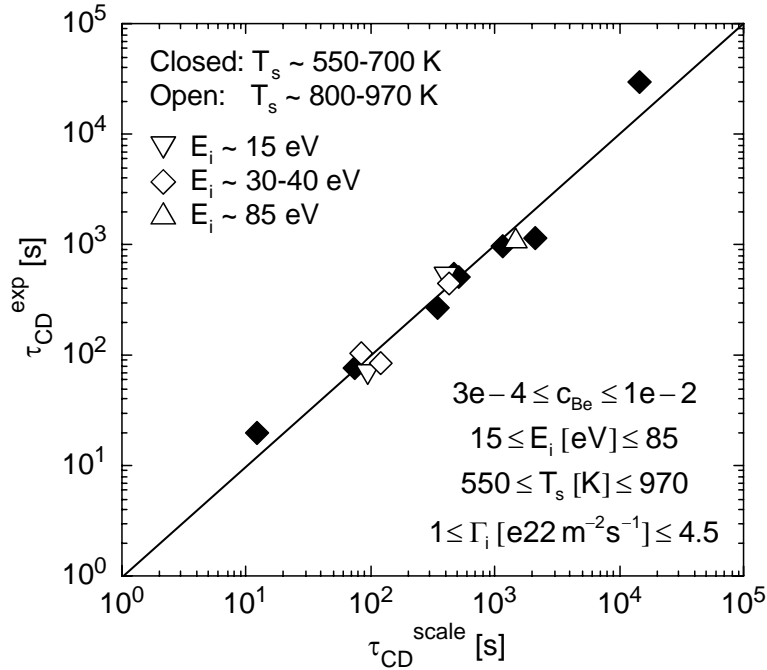


Fig. 12 - Comparison of experimental carbon chemical erosion mitigation time with the scaling expression in eqn. (1) above

## Implications of Be-C Mixed Material PMI Studies for ITER

These Be-C mixed material studies suggest that re-deposited films in ITER scenarios are likely to be rich in Be, provided that strike plate erosion is reduced by the influence of the Be-seeded SOL plasma on C chemical erosion. In contrast to a:C-H film growth, these Be rich deposited layers will form primarily in line-of-sight locations from the target due the high sticking probability (almost unity) for Be metal atoms. Tritium retention in such Be rich co-deposits displays a strong temperature dependence; these Be-containing coatings would then be expected to have a low hydrogen inventories in the operational range of ITER divertor PFCs. However, the difficulty in resolving the effect of O impurities in these co-deposits requires further experimental investigation.

Using typical values for ITER divertor carbon target plates [Federici:1999]  $\therefore f_{Be^+} = 0.05$ ,  $E_i = 20 \text{ eV}$ ,  $T_s = 1200 \text{ K}$  and  $\Gamma_i = 10^{23} \text{ m}^{-2} \text{ s}^{-1}$ ] with our scaling law for Be-C film formation, we estimate that  $\tau_{CD} \sim 9 \text{ ms}$  for these ITER conditions, which is much shorter than the predicted ITER Type I ELM period ( $\sim 1 \text{ s}$ ). These PISCES results therefore suggest that protective Be layers on C targets can be formed between ELMs in ITER, which would lead to a reduction of both chemical and physical erosion of the C divertor target. However, even though we might expect protective beryllium carbide surface layers to form in the ITER divertor between ELMs, one still must investigate the response of these surface layers to the harsh conditions expected during an ITER ELM. As discussed above, we have developed a technique to apply large heat loads to mixed-material surfaces during the plasma exposure in PISCES-B to measure the response of the mixed surface to the large temperature extremes encountered during an ITER ELM. A summary of these new capabilities is given later in Part I, while the planned experiments are be discussed in Part II of this document.

### *II.e. Beryllium-tungsten alloy formation on tungsten exposed to Be-seeded deuterium-plasmas*

Tungsten is known to interact chemically with beryllium to form the stable-alloy phases  $\text{Be}_2\text{W}$ ,  $\text{Be}_{12}\text{W}$  and  $\text{Be}_{22}$ , which all have melting points below  $2250 \text{ }^\circ\text{C}$ , significantly lower than that of pure W ( $\sim 3400 \text{ }^\circ\text{C}$ ) [Vasina:1970]. The chemical reactions leading to this alloy formation may not be limited to the near surface if bulk diffusion of Be in W is rapid enough; should such alloys form in ITER or JET (where Be/W PFC design are planned), W PFC's may show signs of reduced-mechanical strength, enhanced material loss during transient heating events or extreme failure under design conditions. PISCES is currently participating in a collaborative effort to address these concerns under ITER relevant PMI conditions. Other institutions such as IPP-Garching and Sandia-Livermore are investigating phase formation and reaction kinetics under high temperature  $800\text{--}1100 \text{ }^\circ\text{C}$  conditions of relevance to the upper-limit temperature range of the ITER tungsten armor.

Presently, experiments at 800 °C in PISCES, and at SNL and IPP are consistent with reaction kinetics that follow Fick's law and seemingly contradict earlier reported linear growth rates [Vasina:1970]. The rate of diffusion is found to be  $D_{800} \sim 2 \times 10^{-13} \text{ cm}^2 \text{ s}^{-1}$  and is somewhat faster than Be in C,  $\sim 10^{-15} \text{ cm}^2 \text{ s}^{-1}$  at the same temperature. Further studies are currently underway to determine the temperature dependence of the Be:W diffusivity in order to predict growth rates expected in ITER.

Under ITER PMI conditions, which have been simulated in PISCES-B, plasma and material effects can under certain conditions not favor the production of the Be-W alloy. In Fig. 13 below, cross-section SEM images are shown for two W targets that were exposed at 800 °C to plasma for ~1 h with  $f_{\text{Be}} = 0.0005$ . In the case on the left, the applied target bias was -75 V leading to ion bombardment with  $E_{\text{ion}} \sim 60 \text{ eV}$ , while the case on the right had a bias voltage of -17 V, resulting in  $E_{\text{ion}} \sim 10 \text{ eV}$ . The case on the left shows the formation of a deposited Be layer with a uniform ~300 nm  $\text{Be}_{12}\text{W}$  interlayer at the interface between the Be and W. The case on the right shows no deposited Be and only minor coverage of the surface in  $\text{Be}_{12}\text{W}$  nucleation zones. It is therefore believed that ion bombardment energy can significantly effect the production of the surface alloy through re-erosion of the deposited Be. Surface evaporation is found to produce a similar effect. For exposure temperatures above 1000 °C evaporation prevents the deposition of beryllium and hinders the formation of the surface alloy.

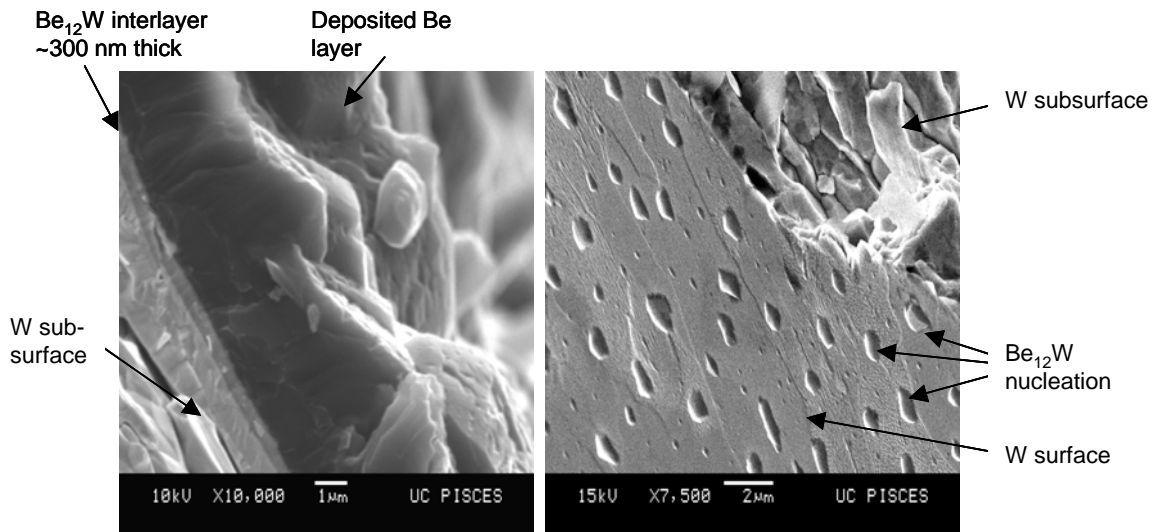


Fig. 13 – SEM images of W sample surfaces exposed to beryllium containing plasma, (a) beryllide interlayer formed, (b) only beryllide nucleation sites are observed on the plasma exposed surface.

A simple zero-dimensional surface particle balance model can be used to predict PMI conditions under which a deposited Be layer will form. The model results in Be layer formation occur when the incident flux of Be exceeds that lost by due to plasma-induced and surface processes. The incident flux  $\Gamma_{\text{Be}}$  is given by

$$\Gamma_{\text{Be}} = f_{\text{Be}} \Gamma_{\text{plasma}} (1 - R_f),$$

where  $f_{\text{Be}}$  is the fraction of Be in the plasma,  $\Gamma_{\text{plasma}}$  is the ion flux and  $R_f$  is the surface reflection coefficient for Be on W. The flux of Be lost from the surface,  $\Gamma_{\text{Loss}}$  is described by physical erosion and evaporation

$$\Gamma_{\text{Loss}} = Y_{\text{D-Be}} \Gamma_{\text{plasma}} (1 - R_d) + f_{\text{Be}} Y_{\text{Be-Be}} \Gamma_{\text{plasma}} (1 - R_d) + \Gamma_{\text{evap}} (1 - R_e)$$

where  $Y_{\text{D-Be}}$  and  $Y_{\text{Be-Be}}$  are sputter yields,  $R_d$  are the corresponding the redeposition fractions and  $R_e$  is the probability for evaporated Be to ionize and return to the target surface. Equating these two expressions and solving for  $f_{\text{Be}}$  leads to a simple equation describing the critical value of  $f_{\text{Be}}$  for which a deposited Be layer will form. Fig. 14 shows the critical  $f_{\text{Be}}$  value as a function of surface temperature for a set of constant ion energies 10, 25, 50 and 100 eV. The formation of a deposited Be layer in PISCES-B (full lines) is favored by low ion energy bombardment and surface temperatures below ~1200 K; as these parameters are increased, evaporation and re-erosion from the surface requires large plasma  $f_{\text{Be}}$  values to support the growth of a deposited Be layer on the W substrates.

### **Implications of Be-W Mixed Material PMI Studies for ITER**

Under the ITER conditions described above (dashed lines) the model predicts that tungsten beryllide can form if the W surface temperatures are below ~1300 deg K and  $f_{\text{Be}} > 0.04$ . However, further PMI data are necessary to validate this simple model. It is also further pointed out that this simple model is only applicable to plasma exposed normal surfaces. Other causes for concern, that need to be addressed, include the effects of trapped Be in tile gaps, transient heat loading which may or may not favor the production of alloys and the influence of C on Be-W PMI.

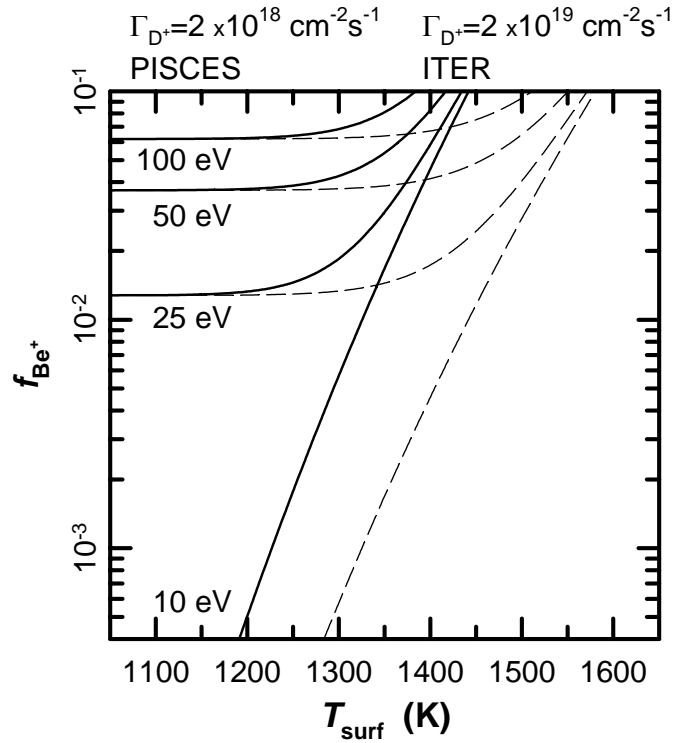


Fig. 14 – Conditions for tungsten beryllide formation in PISCES (solid lines) and predicted for ITER conditions (dashed lines). Beryllide formation occurs for conditions that lie above the ion energy curves.

### III. Mono-materials Investigations

The PISCES program has continued plasma-material research using mono materials, with a primary focus on the verification of PMI-related assumptions used within various plasma-surface interaction models. One assumption that has been investigated during the FY04-06 period is the angular distribution of atoms leaving a surface due to physical sputtering. This distribution has been measured both in PISCES-B (for Be targets) and in an offline plasma system for molybdenum and carbon targets. These results are compared to modeling of the plasma systems using the WBC code at Argonne National Laboratory and the TRIDYN surface interaction code.

#### III.a. Angular distribution of sputtered beryllium atoms from a beryllium target exposed to a deuterium plasma

The angular distribution of sputtered Be atoms from the ITER first wall will have an important effect in determining the penetration depth of Be atoms into the SOL plasma. When combined with cross-field and parallel transport, this distribution then affects the Be concentration in both the core and divertor plasmas. As shown above, the Be concentration is a key parameter in the formation of mixed material layers within the

divertor target region. In the last year the angular distribution of Be atoms sputtered and transported from a crystalline Be target exposed to a deuterium plasma with low incident ion energy was investigated. A schematic of the target region of PISCES-B is shown in fig. 15 below.

A Be target with a diameter of 21 mm, held with a clean tantalum (Ta) cap, was exposed to a steady-state deuterium plasma with electron density,  $n_e \sim 1-3 \times 10^{18} \text{ m}^{-3}$ , electron temperature,  $T_e \sim 8 \text{ eV}$  and ion flux,  $\Gamma_i \sim 1.5-3 \times 10^{22} \text{ m}^{-2}\text{s}^{-1}$ . Radial profiles of these plasma parameters, measured with a scanning double probe system at an axial distance of  $z = 152 \text{ mm}$  from the target, are nearly flat within the plasma diameter of around 50 mm. The incident angle of plasma ions is normal to the target. The incident ion energy,  $E_i$ , is controlled by biasing the target. The two-dimensional profile of eroded and transported Be atom density was determined spectroscopically. The light from the plasma is guided with a mirror and focused with a lens to the entrance slit of a 0.5 m Czerny-Turner type spectrometer equipped with a two-dimensional CCD camera. The whole optical system is absolutely calibrated with an integrating sphere. The spatial resolutions in the axial ( $z$ ) and vertical ( $y$ ) directions are approximately 1.0 mm and 1.4 mm, respectively. Vertical profiles of Be I line ( $2s2p \ ^1P-2s3d \ ^1D$ : 457.3 nm) intensity from eroded Be atoms were recorded every 2 mm in the  $z$  direction. From the vertical profile of the line-integrated intensity,  $I_{\text{Be}}$ , the radial profile of the local emissivity,  $\epsilon_{\text{Be}}$ , can be obtained by Abel inversion. Finally, the local ground state Be atom density,  $n_{\text{Be}}$ , is given as

$$n_{\text{Be}} = \frac{4\pi\epsilon_{\text{Be}}}{\langle\sigma\nu\rangle_{457.3\text{nm}} n_e} \quad \text{where } \langle\sigma\nu\rangle_{457.3\text{nm}} \text{ is the photon emission coefficient [ph m}^3\text{/s] of}$$

the Be I line at 457.3 nm taken from the ADAS data base. Fig. 16 below shows an example of two-dimensional profile of the Be atom density near the Be target at  $E_i \sim 140 \text{ eV}$ .

In fig. 17 below, these experimental Be density distributions are compared with WBC Monte-Carlo sputtered atom transport modeling that has been performed by ANL researchers [Brooks:2005]. After subtraction of the background Be originating from a thin Be coating formed on the Ta cap, the experimental angular distribution (solid diamonds) is found to be close to both cosine (black circles) and TRIM SP (blue squares) distributions. In very recent work, we have obtained the angular distribution of Be atoms sputtered from a crystalline Be sample due to deuterium plasma exposure. By comparing with the WBC modeling, this distribution is also found also to be close to the cosine distribution at low incident ion energy down to  $\sim 40 \text{ eV}$ . These results indicate that the cosine emission distribution assumption commonly used in erosion and redeposition modeling appears to be correct for D sputtering of Be surfaces.

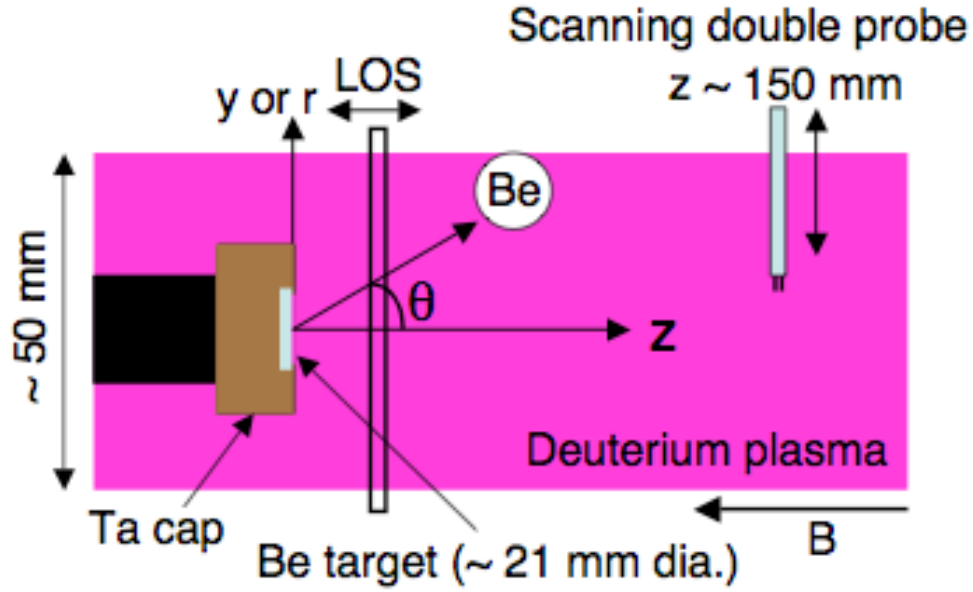


Fig. 15 - Schematic view of the target region in PISCES-B.

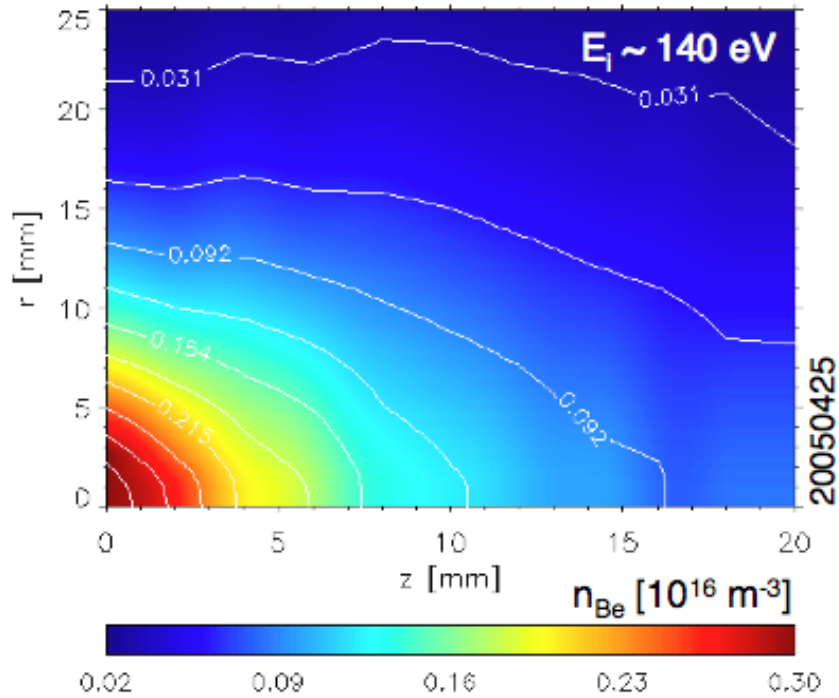


Fig. 16 - Two-dimensional profile of the Be atom density near the target.  $E_i \sim 140$  eV.

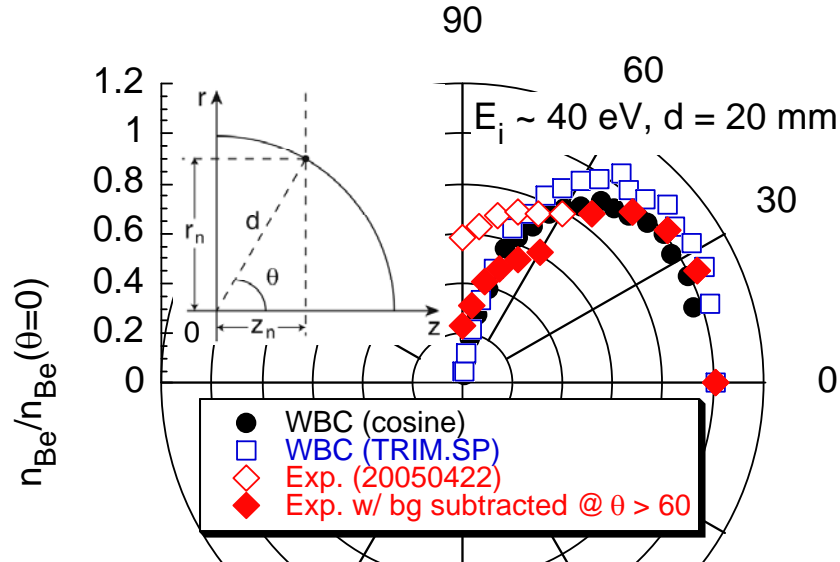


Fig. 17 - Angular distributions of sputtered Be at  $E_i \sim 40 \text{ eV}$ . Black circles and blue squares are derived from WBC modeling with cosine and TRIM.SP predicted distributions, respectively. Open diamonds are from an experiment, and closed diamonds are obtained by subtracting background Be density from open diamonds at  $\theta > 60$  degree.

### III.b. Angular distribution of sputtered carbon and metal surfaces

The main objective of this work is to *directly* measure the angular distribution of sputtered atoms and clusters produced by a surface undergoing ion bombardment, and compare these results with the more indirect Be results presented above. In order to avoid large chemical erosion effects when C surfaces are being examined, these experiments are carried out in a noble gas plasma discharge. Because the experiments are carried out in an off-line unmagnetized plasma device in the PISCES laboratory facility, a differentially pumped mass and energy spectrometer can be used to determine the angular distribution, sputtered particle mass, and particle kinetic energy in these experiments, providing new details of C PMI. This issue impacts erosion and redeposition modeling of ITER PFC erosion and redeposition.

The experiments are performed in an unmagnetized plasma device equipped with a radio-frequency inductively coupled plasma source. A material sample is inserted into the plasma, and normal incidence ion bombardment with controlled ion kinetic energy is achieved by biasing the sample with respect to the plasma. A differentially pumped quadrupole mass spectrometer with a sample orifice located a few cm away from the sputtering surface is then used to measure the relative flux of sputtered material from the surface. By changing the angle between the target normal and the QMS aperture then, we can obtain the angular sputtering distribution for the studied materials. For each data

point (target angle and incident energy), the QMS also measures the kinetic energy of the sputtered particles.

We first carried out experiments with metal surfaces to provide a comparison with the Be experiments discussed above. Fig. 18 below shows a polar plot of the directly measured angular distribution of sputtered Molybdenum flux for various incident ion energies. For all the incident energies studied in this work, the sputtering distribution is “under-cosine”, with a maximum at an angle of  $60^\circ$ . This maximum is less pronounced as the incident energy increases. Simulation of the angular distribution of Mo atoms sputtered by xenon bombardment using the Monte Carlo code TRIDYN [Moller:1988] predicts similar results, as can be seen in the polar plot in Fig. 19. For the lower energy ions, the collision process involves only a few target atoms and the resultant angular distribution is “under-cosine”. As the energy of the incoming ion increases and the collisional cascade develops, involving many target atoms, the angular distribution evolves towards the well-known cosine distribution. We expect that as the ion energy approaches 400-500 eV the distribution will become essentially cosine; experiments to confirm this are currently underway.

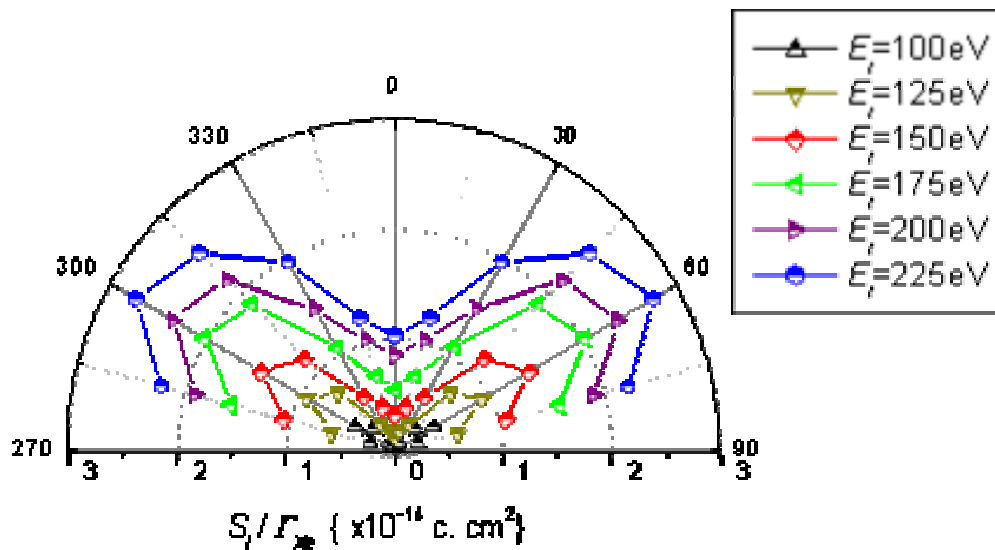


Fig. 18. Measured Mo ion angular distribution for different incident ion energies, normalized to incident ion flux. Data is mirrored around  $0^\circ$  for clarity.

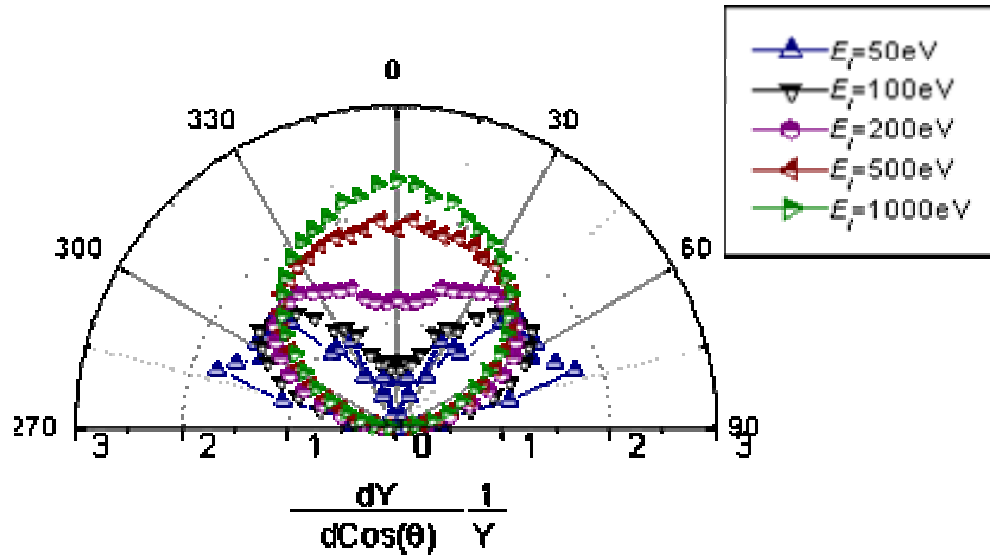


Fig. 19. Simulated Mo sputtering angular distribution for different incident ion energies. Data is mirrored around  $0^\circ$  for clarity.

For carbon sputtering the signal for the carbon ion is below the detection limit while the signals for  $C_2$  and  $C_3$  ions are detectable. This indicates a predominant sputtering of carbon as clusters for the case of low energy xenon ion bombardment. The measurements show an “under-cosine” angular distribution, with a maximum at around  $60\text{--}75^\circ$  for  $C_2$  and around  $60^\circ$  for  $C_3$ . Preliminary results suggest that as the ion mass is decreased, the erosion gradually becomes dominated by atomic C, and cluster emission becomes relatively smaller.

In summary, with high mass xenon ions at low incident ion energy, we observe “under-cosine” angular sputtering distributions with a maximum sputtered flux at around  $60^\circ$  for both Mo and carbon clusters. This indicates that the typically assumed cosine distribution of sputtered particles during low energy heavy ion bombardment of surfaces is incorrect. On the otherhand, deuterium sputtering of beryllium measurements presented earlier shows a clear cosine like distribution in agreement with numerical simulations of low energy, low ion mass sputtering processes. The Mo angular sputtering distribution evolution with incident energy is similar to the TRIDYN code predictions, and the results for the total sputtering of Mo are in good agreement with previous experiments. This gives us confidence in the experimental procedure and computational tools as we focus on the less extensively investigated sputtering behavior of carbon and beryllium surfaces in FY07-09.

### III.c. Temperature dependent erosion of beryllium

We carried out systematic study of D-induced physical sputtering of Be at elevated temperatures. The erosion rate exhibited a stronger than expected temperature

dependence, and forced the re-evaluation of physical sputtering at surface temperatures that approach, but do not exceed, the melting temperature. This led to the development of a model based on ion impact ad-atom production [Doerner:2005] to explain the temperature dependent erosion behavior. These surface ad-atoms are thought to be liberated from the lattice but still weakly bound to the surface via Van der Waals forces, and are thereby easier to remove via subsequent ion impact. A comparison of the total erosion rate from a beryllium sample with the temperature dependent erosion model is shown in Fig.20. These systematic measurements of the temperature dependent erosion behavior of beryllium samples have supplied the information necessary to quantify the enhanced erosion expected from solid beryllium material at elevated first wall temperature in ITER. This information has also aided in the development of a generalized model of temperature dependent erosion phenomenon that has been applied to a variety of solid and liquid materials.

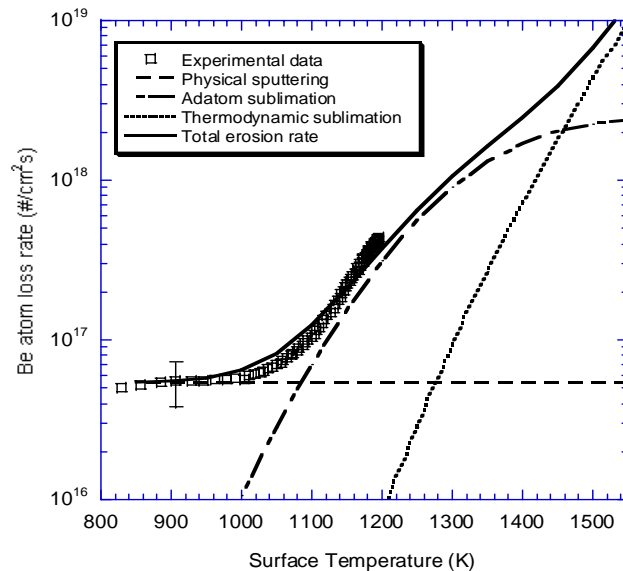


Fig. 20 - A comparison of each of the three terms in the temperature dependent erosion model to the high temperature erosion behavior of a beryllium sample exposed to deuterium plasma. As the surface temperature approaches 1000 K, the physical sputtering rate increases substantially due to the formation of weakly bound ad-atoms on the Be surface. Further increases in the Be surface temperature to ~1400 K then cause the Be loss rate to become dominated by thermal evaporation.

## Supporting Boundary Plasma Science and Hardware Development Accomplishments in FY2004-2006

### I. Introduction

As was discussed earlier, the PISCES Program contains both PMI-focused and Supporting Research elements. Within this latter category, work in the FY04-06 time period focused upon the following topics:

- Demonstration of the universal character of intermittent edge and scrape-off layer turbulence
- Origins of shear layers and transport barriers in edge plasmas
- Measurement of large-scale cross-field scrape-off layer flows from high speed imaging data
- Atomic and molecular physics and plasma-neutral interactions in divertor plasmas
- Enabling hardware development for new PMI research

In addition, graduate student research is considered to lie within this portion of the overall program. Key results from these efforts are summarized within this section.

## II. Edge and SOL Turbulence, Transport, and Flows

*Universality of Intermittent SOL Transport* In FY04-06, the detailed statistics of intermittent, bursty edge and SOL transport events were compared using data from three different tokamaks, ALCATOR C-MOD, Tore Supra and MAST, as well as the PISCES linear device. The comparison among the different turbulent signals was performed using different statistical analyses (see Fig. 21 below as an example). The probability distribution function (PDF) was the first statistical tool used for comparison. The same PDF features were observed in all four devices, that is, positively skewed density fluctuation PDFs. The power spectra were shown to be similar reflecting the same correlation properties (Fig. 21a), and the use of the conditional averaging revealed the same average temporal signature of avaloids for the four devices (Fig. 21b). This general similarity then suggests that the underlying dynamics of the events is similar across the different plasma devices.

Prior to the discovery of these bursty transport events, the SOL was thought to be fueled by cross-field diffusive transport, and as a result was thought to be confined to the region immediately surrounding the LCFS (Fig. 22a left panel). In the presence of a significant number of convective transport events, the SOL is no longer formed of a simple exponentially decaying layer close to the last closed flux surface; plasma is instead present intermittently far from the LCFS because of the high radial velocities of avaloids that allow them to compete with the parallel transport and thus to survive far from the LCFS point of origin (Fig. 22 right panel). As a result, the plasma can have a significant interaction with the first wall.

This first wall interaction naturally leads to the formation of a source of recycled neutrals; it has been suggested that the subsequent intrusion of these neutrals into the SOL may play a role in the plasma density limit, which has long been observed but poorly understood in tokamaks.

Work on C-Mod and DIII-D [LaBombard:2001, Whyte:2005] provided evidence for stronger intermittent convective SOL transport as the density limit was approached. In FY04-06, we performed a detailed study of the properties of avaloids or blobs as a function of the average density in a collaboration performed on the MAST device. In that

work, it was found that the relative fraction of the total radial particle flux carried by intermittent transport events increases with the line averaged density  $n/n_G=0.4$  (here  $n_G$  denotes the Greenwald density limit); as the line averaged density was increased further, this ratio of particle flux then began to decrease (see Fig. 22b below). In a recently published paper [Antar:2005], this was interpreted as the effect of the background turbulence on avaloids which increases with the density diminishing their size and thus their contribution. Moreover, the scaling of the various properties of avaloids were obtained. A more detailed understanding of this important issue requires further work; as discussed in Part II, we plan to use the linear devices as UCSD as well as collaborate with relevant tokamak groups in FY07-09 in order to make further progress on this issue.

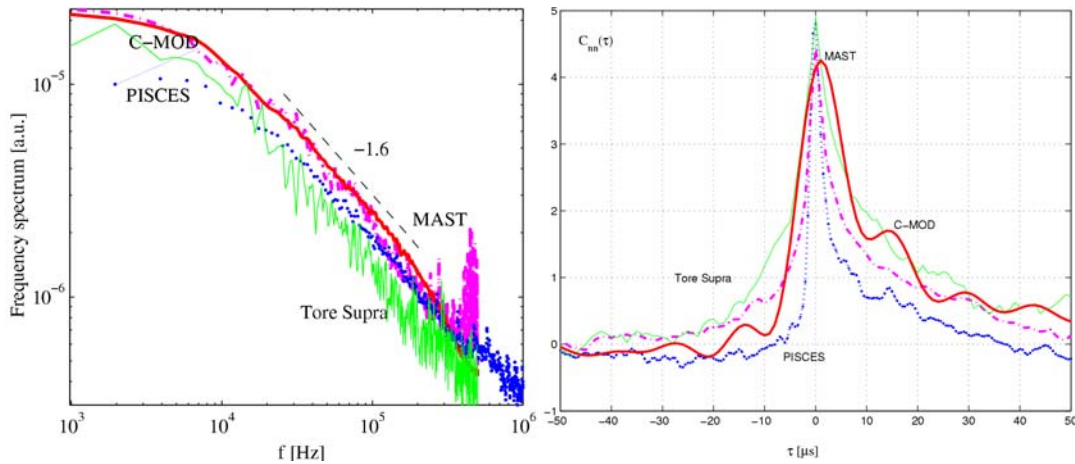


Fig. 21 - The left-hand plot shows the power spectra for the ion saturation current fluctuations taken in the SOL of PISCES, Alcator C-MOD, MAST and Tore Supra. The right-hand plot shows a typical temporal signature of avaloids in the four devices deduced from conditional averaging.

*Measuring Large-scale SOL Flows from the Propagation of Turbulent Density Fluctuations:* Measuring large scale convective flows in the edge and SOL of tokamaks is important in developing an understanding SOL plasma particle and heat transport. The development of a diagnostic capable of measuring SOL flows over a wide region of the plasma would significantly increase our capability to study SOL plasma and impurity transport across and along field lines. Motivated by these considerations, in FY06 we began the study of techniques that may allow such SOL flows to be inferred from fast framing imaging cameras that have recently been developed.

One such technique is known as time-delay estimation (TDE) which gives a measurement of the phase velocity of SOL plasma fluctuations. Two spatially separated measurements of e.g. fluctuating plasma density or potential are sampled with high time resolution ( $10^6$  samples/sec). The two signals are then cross-correlated on short time windows, and a time lag  $\tau_{\text{peak}}$  is found from the peak of the cross correlation function. From the known separation distance, the inferred velocity is estimated as simply  $V = \Delta x / \tau_{\text{peak}}$ .

Comparison of this measured velocity with Mach probe fluid velocity measurements, analytic theory, and numerical simulation shows that the TDE method infers the underlying plasma flow velocity where diamagnetic effects are weak (which are the dominant source of discrepancies between the fluid velocity and phase velocity of fluctuations).

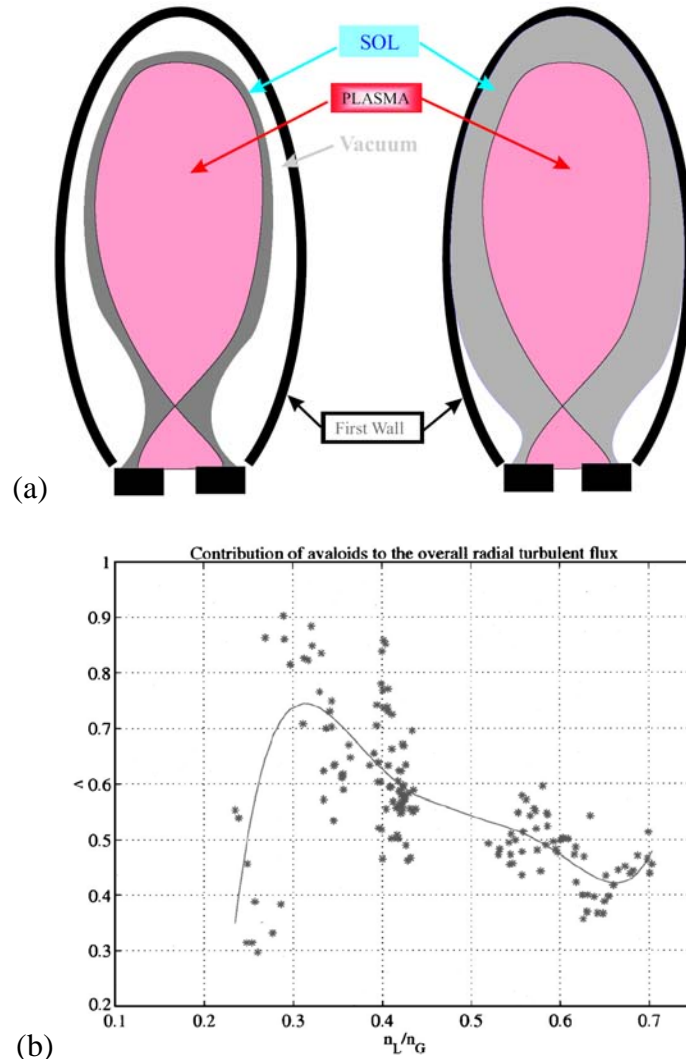


Fig. 22 – (a) The modification of our general view of the SOL. Instead of being a region that is localized around the separatrix where hot and dense plasma exists, it extends all the way to the outer walls. (b) Measured ratio of the cross-field particle flux due to avaloids or blobs to the total cross field particle flux as a function of the line-averaged plasma density in the MAST device. The relative significance of burstry transport first increases with line average desnty, and then decreases with further increases in density [Antar:2005].

As an illustration of this technique, we show the velocity profile measured with a multi-tip Mach probe that was scanned radially across the plasma in the CSDX linear plasma

device, which is also a part of the PISCES group. Following recent work by Shikama *et al.* [Shikama:2005], we then fit the data with a function of the form  $R_M = \exp[K \sin \Delta\alpha / \Delta\alpha (M_{par} \cos \theta + M_{perp} \sin \theta)]$ , where  $\Delta\alpha$  is the acceptance angle of each probe tip,  $M_{par}$  and  $M_{perp}$  are used as fitting parameters, and we use Hutchinson's model of ion collection [Hutchinson:2005] with  $K = 1.34$ . The Mach probe data shown as the green data points in Fig.23 below, indicate that a radially sheared azimuthal plasma flow exists in this plasma device. The results suggest that the fluid velocity is consistent with the TDE velocity profile, also shown in Fig. 23, provided that the diamagnetic drifts (not shown here due to space constraints) are accounted for. This result suggests, then, that high speed imaging diagnostics focused on the SOL region can be used to infer SOL plasma fluid flows transverse to the magnetic field in confinement devices.

*Studies of Turbulent Driven Shear Flows and Momentum Transport:* Recent theoretical work [Diamond:2005] suggests that sheared flows such as found in the H-mode transport barrier can be driven by turbulence, and that there is a mutual interaction between the turbulence and shear flow, leading to a self-regulated state of turbulence and shear. The results discussed above show that, in the absence of external momentum sources, a sheared plasma flow is sustained against dissipation within the CSDX plasma device. The question then arises: how is such a flow sustained against the dissipation? In order to answer this question, we examine the time-averaged azimuthal component of the steady-state turbulent fluid momentum equation, given by

$$\frac{1}{r^2} \frac{\partial}{\partial r} \left( r^2 \langle \tilde{V}_r \tilde{V}_\theta \rangle \right) = -\nu_{i-n} \langle V_\theta \rangle + \mu_{ii} \left( \frac{1}{r} \frac{\partial}{\partial r} \left( r \frac{\partial \langle V_\theta \rangle}{\partial r} \right) - \frac{\langle V_\theta \rangle}{r^2} \right),$$

where  $\nu_{i-n}$  is the ion-neutral collision rate,  $\mu_{ii}$  is viscosity due to ion-ion collisions,  $\langle \tilde{V}_r \tilde{V}_\theta \rangle$  is the turbulent Reynolds stress, the brackets denote a time average, and tildes denote fluctuating quantities, such that  $\langle V_\theta \rangle$  is the time-averaged azimuthal ion fluid velocity. Using a multi-tip probe assembly we measured the electrostatic turbulent Reynolds stress  $\langle R \rangle = \langle \tilde{E}_r \tilde{E}_\theta \rangle / B_0^2$ , which is equal to the correlation  $\langle \tilde{v}_r \tilde{v}_\theta \rangle$  under the assumption that the convecting velocity fluctuations are purely electrostatic. The fluctuating electric field  $\tilde{E}_r = \Delta V_f / \Delta x_r$  is taken as the difference between the floating potentials measured with two tips separated radially by a distance  $\Delta x_r = 0.5$  cm; the fluctuating azimuthal electric field  $\tilde{E}_\theta$  is measured similarly.

Using the measured Reynolds stress we can then numerically integrate this equation to find  $\langle V_\theta \rangle$ . Using reasonable boundary conditions (i.e.  $\langle V_\theta \rangle \rightarrow 0$  at  $r = 0$ ) and known damping rates, this turbulent momentum balance analysis then gives the time-averaged azimuthal ion fluid velocity profile shown as the solid black curve in Fig. 23 above. The azimuthal velocity has a strong radial variation and is peaked at  $r = 3.6$  cm, indicating the presence of a plasma shear layer at this location, consistent with the location of the particle flux transport barrier. Simulations of collisional drift turbulence in this device,

which are discussed in detail below, have also been carried out, and clearly show the formation of a shear flow (red line in Fig. 23) quantitatively similar to that observed experimentally. The agreement between the TDE velocity, measured velocity from the Mach probe, the self consistent  $V_\theta$  from azimuthal momentum balance, and numerical simulations demonstrates that the shear flow is maintained by the Reynolds stress against estimated damping. This result provides essential experimental support for the theoretical features of shear flow generation from drift-wave turbulence in magnetized plasmas – which is a leading candidate to explain the L-H transition.

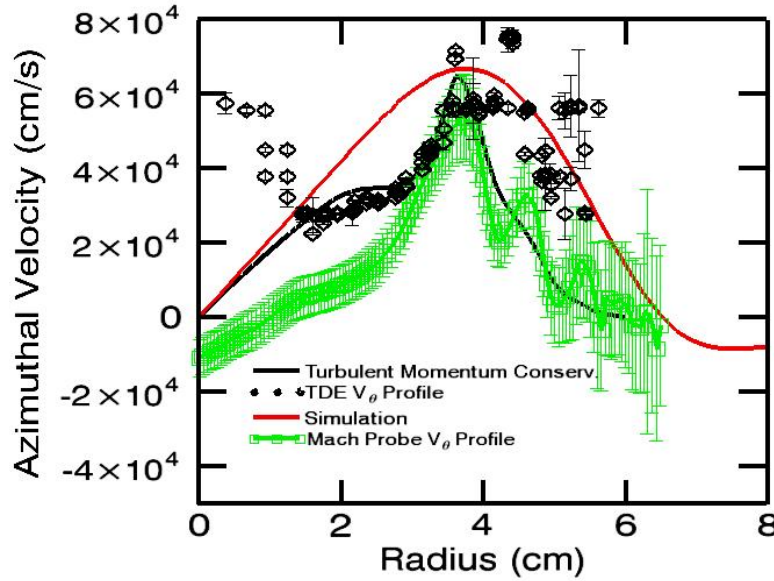


Fig. 23 - Azimuthal velocity found from 1D TDE method (black circles), Mach probe (green), turbulent momentum balance (black line), and simulation (red line).

*Two-fluid Edge and SOL Plasma Turbulence Model Development:* In FY04-06 we developed a numerical simulation of nonlinear collisional drift-wave turbulence to compare against experimental measurements and guide future PMI and boundary plasma investigations. The code describes the Hasegawa – Wakatani [Hasegawa:1983] model, which is generally considered to be the simplest self-consistent model for studying turbulent drift-wave transport. The equations are

$$\frac{\partial n}{\partial t} + \bar{V}_{\bar{E} \times \bar{B}} \cdot \bar{\nabla} n + \frac{V_*}{r} \frac{\partial \phi}{\partial \theta} + \omega_{||} (n - \phi) = D_n \nabla_{\perp}^2 n$$

$$\frac{\partial \Omega}{\partial t} + \bar{V}_{\bar{E} \times \bar{B}} \cdot \bar{\nabla} \Omega + \omega_{||} (n - \phi) = -v_{in} \Omega + \mu_{ii} \nabla_{\perp}^2 \Omega$$

where,  $n = \tilde{n}/n_0$  is normalized density fluctuation field, while  $\phi = |e| \tilde{\phi}/T_e$  is normalized electrostatic potential and  $\Omega = \rho_s^2 \nabla_{\perp}^2 \phi$  is the vorticity;  $\bar{V}_{\bar{E} \times \bar{B}} = -\rho_s C_s \bar{\nabla} \phi \times \hat{z}$  is the

fluctuating  $\vec{E} \times \vec{B}$  velocity, where  $C_s = \sqrt{T_e/M_i}$  is the sound speed and  $\rho_s = C_s/\Omega_{ci}$  is the ion gyroradius evaluated at the sound speed.  $V_* = \rho_s C_s/L_n$  is the diamagnetic velocity,  $L_n = -d \ln n_0/dr$  is the equilibrium density scale length.  $\omega_{\parallel} = k_{\parallel}^2 V_{Te}^2/v_{ei}$  is the so-called “adiabatic” parameter which measures the importance of parallel collisionality;  $k_{\parallel}$  is the parallel wavenumber,  $V_{Te} = \sqrt{T_e/m_e}$  is the electron thermal speed, and  $v_{ei}$  is the electron-ion collision rate. In the limit of  $\omega_{\parallel} \rightarrow \infty$ ,  $n \rightarrow \phi$  and the model reduces to the one-field Hasegawa-Mima [Hasegawa:1978] model, while in the limit of  $\omega_{\parallel} \rightarrow 0$  the system reduces to the advection of a passive scalar  $n$  by a two-dimensional incompressible flow.  $D_n$  represents particle diffusivity (included for numerical stability), while the  $v_{in}$  term describes the flow drag due to ion-neutral collisions [Gondarenko:1999] and  $\mu_{ii}$  is the ion fluid viscosity due to ion-ion collisions. A comparison between the predicted 2D density fluctuation and the measured 2D fluctuating plasma emission profile (proportional to density fluctuation amplitude) is given in Fig. 24 below, and shows reasonably good agreement. The simulations also predict that the turbulence sustains a radially sheared azimuthal flow, shown as the red line in Fig. 23 above. In FY07-09 we will incorporate a self-consistent plasma density source distribution, which we expect to then allow the simulation to capture the intermittent or bursty transport events that were discussed above. These plans are discussed in more detail in Part II below.

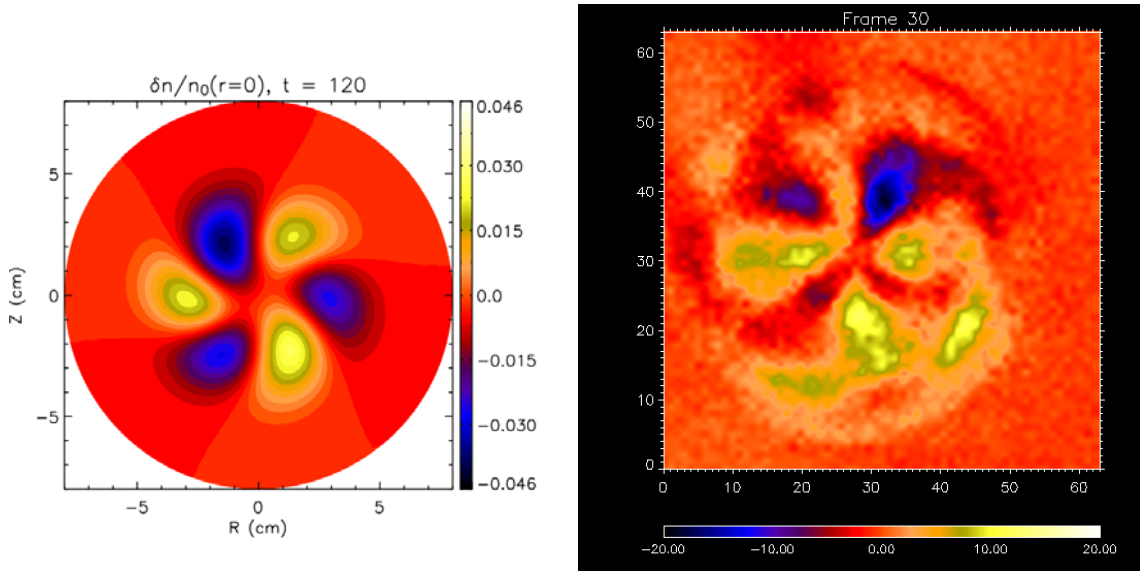
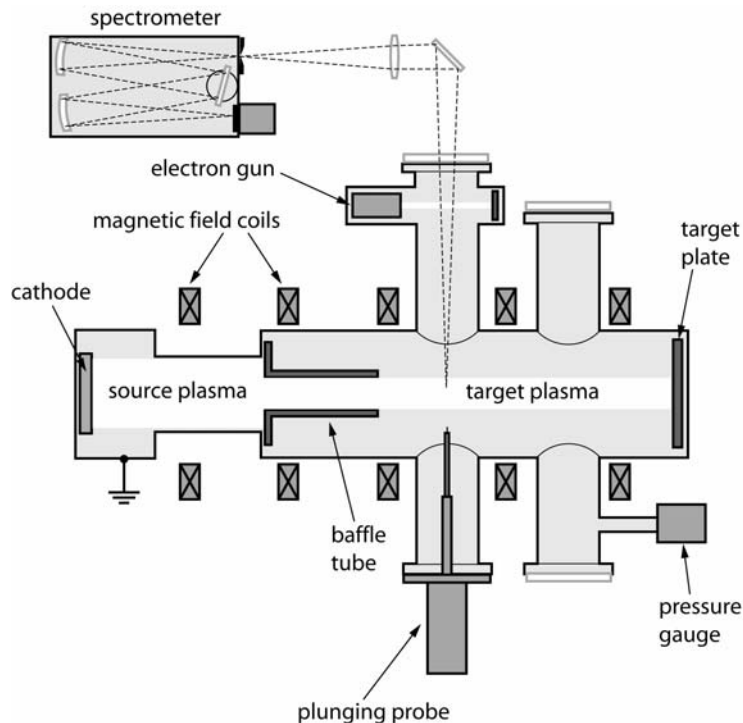


Fig. 24 - (a) Left panel: Predicted saturated density fluctuation distribution for typical CSDX plasma conditions, (b) Right panel: Measured fluctuating Ar plasma light emission in CSDX.

### III. Divertor Physics Studies

*Measurement of  $H_2$  accommodation rates in PISCES-A* Tokamak experiments have confirmed that  $H_2$  is found in large quantities in the divertor region of hydrogen

discharges [Fujimoto89, Hollmann06]. Almost all collision processes involving  $H_2$  are very sensitive to the  $H_2$  vibrational, rotational, and kinetic temperatures  $T_{\text{vib}}$ ,  $T_{\text{rot}}$ , and  $T_{\text{kin}}$  [Pigarov02]. Accurate modeling of collision processes involving  $H_2$  therefore requires knowledge of  $T_{\text{vib}}$ ,  $T_{\text{rot}}$ , and  $T_{\text{kin}}$ ; for this, it is important to know the degree of cooling during wall collisions, i.e. the probabilities  $\alpha_{\text{VS}}$ ,  $\alpha_{\text{JS}}$ , and  $\alpha_{\text{KS}}$  for relaxation of the temperatures  $T_{\text{vib}}$ ,  $T_{\text{rot}}$ , and  $T_{\text{kin}}$  to the wall temperature in a  $H_2$ -surface collision [Hollmann:2005]. Presently these accommodation coefficient probabilities are not well-known, experimentally or theoretically. Experiments done on PISCES-A (with stainless steel walls) in FY2005 have provided the groundwork for measurement of these probabilities in ITER-relevant wall materials by establishing the technique of spatial decay of  $H_2$  temperatures.



*Fig. 25 - Schematic of experimental setup used in PISCES-A for spatial decay measurement.*

An overview of the PISCES-A experimental setup used for these measurements is shown in Fig. 25 above. The discharge is operated in steady-state. Plasma visible line emission was measured using a 1.3 m Czerny-Turner visible spectrometer. This spectrometer was also equipped with a different (not shown in Fig. 25) terminated (to avoid reflections from the plasma) view of a weak electron beam mounted in a side port. This electron beam was used to diagnose molecular hydrogen temperatures in the side port. Small beam currents ( $I_{\text{beam}} \approx 0.3 \text{ mA}$ ) are used to ensure that the electron beam does not significantly perturb the local  $H_2$  temperatures. Electron-impact excitation is necessary to provide the line emission used to diagnose  $H_2$  temperatures. The  $H_2$  temperatures

$T_{\text{vib}}$ ,  $T_{\text{rot}}$  are obtained from molecular band line ratios [Lavrov:1999, Qing:1996], while the  $H_2$  translational temperature  $T_{\text{kin}}$  is obtained from molecular band line widths.

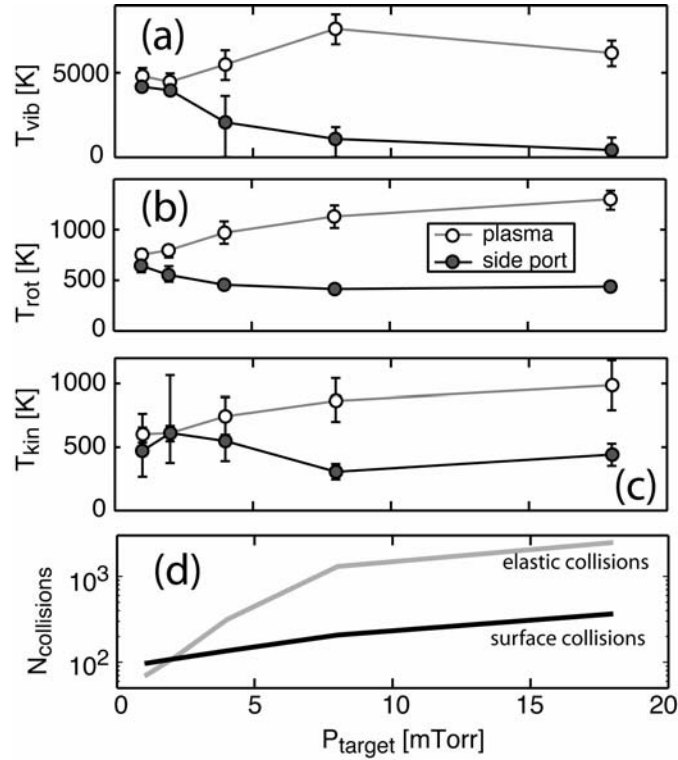


Fig. 26 -  $H_2$  temperature measurements in the plasma and in the side port as a function of neutral pressure  $P_{\text{target}}$  for (a)  $T_{\text{vib}}$ , (b)  $T_{\text{rot}}$ , and (c)  $T_{\text{kin}}$ ; as well as (d) Monte-Carlo simulations of number of elastic  $H_2 + H_2$  and surface collisions between the plasma and e-beam located within the pumping duct

Fig. 26 shows the  $H_2$  temperatures (a)  $T_{\text{vib}}$ , (b)  $T_{\text{rot}}$ , and (c)  $T_{\text{kin}}$  measured in the plasma (open circles) and in the side port (filled circles) as a function of the neutral pressure in the target region  $P_{\text{target}}$ . It can be seen that the temperatures in the main chamber and in the side port are quite close at low  $P_{\text{target}}$ , but diverge significantly as  $P_{\text{target}}$  is increased. Finally, in Fig. 26(d) the average number of  $H_2$ - $H_2$  and  $H_2$ -surface collisions experienced by an  $H_2$  molecule as it moves from the plasma to the e-beam location are shown, obtained from Monte-Carlo modeling, is shown. This number, together with the temperature differences of Fig. 26(a)-26(c) can be used to estimate the accommodation probabilities; the resulting estimates are shown in Fig. 27. It can be seen that accommodation probabilities tend to be small ( $\alpha \approx 10^{-3}$ ) for  $T_{\text{vib}}$  and  $T_{\text{rot}}$  and somewhat larger ( $\alpha \approx 10^{-2}$ ) for  $T_{\text{kin}}$ . The increasing trend in the probabilities with increasing target pressure could be a result of small increases in the wall temperature with increasing wall heat loads.

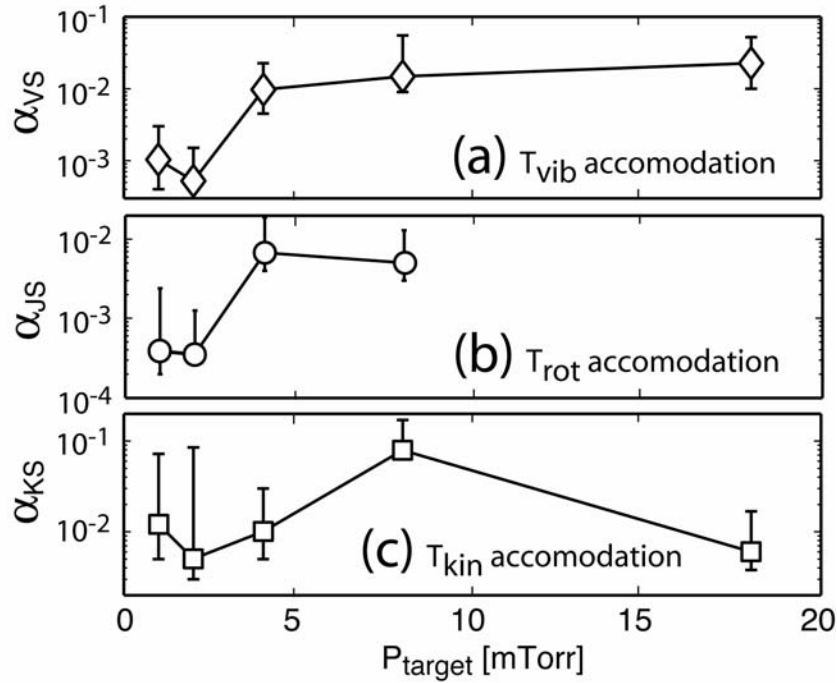


Fig. 27 - Accommodation probabilities (a)  $\alpha_{\text{VS}}$ , (b)  $\alpha_{\text{JS}}$ , and (c)  $\alpha_{\text{KS}}$  obtained from spatial decay experiments at different target region pressures.

*Measurement of radial heat loss during detachment in PISCES-A* The main role of a detached tokamak divertor is to spread out incoming heat loads. However, because of the complicated geometry and difficult diagnostic access, measurement of all the radial (cross field) heat loss terms in a tokamak divertor has not been done. In particular, it is not well-understood how the detaching divertor leg sheds energy in the intermediate temperature regime  $T_e < 4$  eV where ionizing radiation is small but recombination is not yet large. In the PISCES-A divertor simulator experiment, the measurement of the wall accommodation rates described previously have enabled, for the first time, evaluation of all important radial heat loss terms from a detaching hydrogen plasma (radiation, plasma, and neutral losses). Radiated power loss is measured using an absolutely calibrated AXUV photodiode array [Korde:1993] viewing the plasma column through a pinhole camera. Radial power loss due to plasma radial transport to the chamber walls is estimated by measuring the decay of plasma density and temperature into a side port. These plasmas are turbulent and radial (cross-magnetic-field) plasma flow to the outer chamber wall is relatively rapid, with average perpendicular flow speeds approaching 10% of the ion sound speed [Hollmann:2002]. Under these challenging conditions, it was found that best results for  $n_e$  and  $T_e$  measurements were obtained using a fast (1 MHz) swept single-tip Langmuir probe measurement technique [Boedo:1999].

Fast ring down measurements of the  $H_2$  temperatures were performed as an independent measurement of the plasma cooling rate due to ro-vibrational excitation of  $H_2$ . These experiments involve switching the discharge rapidly at  $t = 0$  to a lower power state; the basic setup is shown in Fig. 28. The low power state is chosen to be weak enough to allow a significant drop in the  $H_2$  temperatures from their initial condition, but strong enough to provide a good measurable signal of  $H_2$  molecular band emission. Fast measurements of  $H_2$  line ratios are obtained with an etalon/PMT setup.

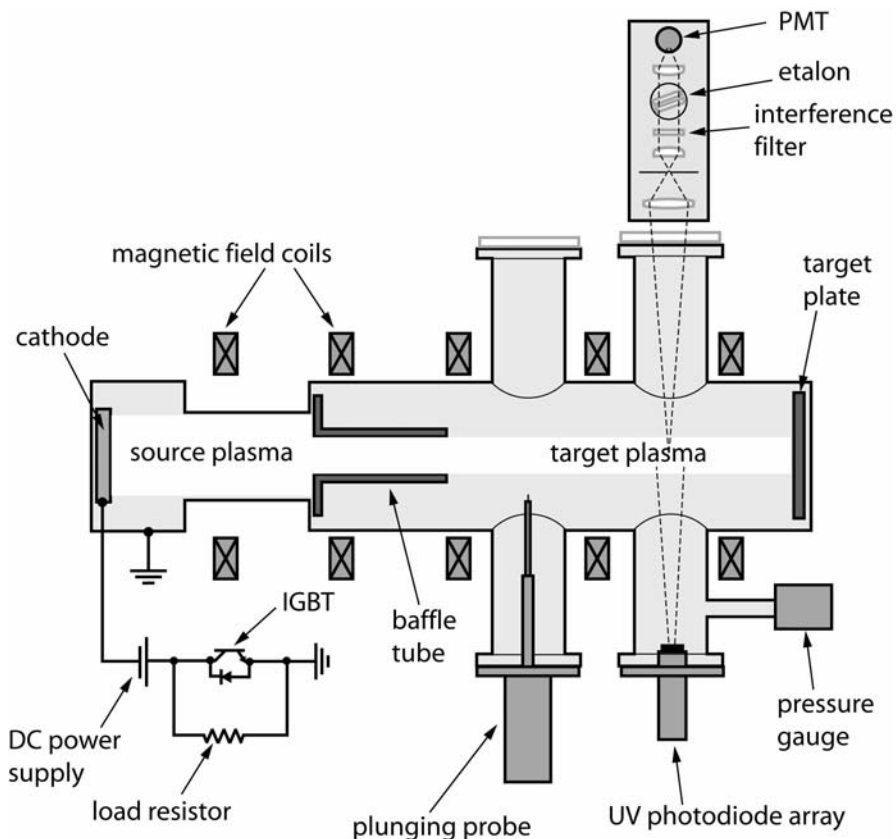


Fig. 28 - (a) PISCES-A experimental setup for time ring down measurements of neutral temperature.

A sample time ring down experiment is shown in Fig. 29. Central electron density (a), electron temperature (b),  $H_2$  vibrational temperature (c), and  $H_2$  rotational temperature (d) are shown. From the measured decay rates (exponential fits are shown in Fig. 29), the rate of plasma cooling into  $H_2$  rotational and vibrational degrees of freedom can be estimated.

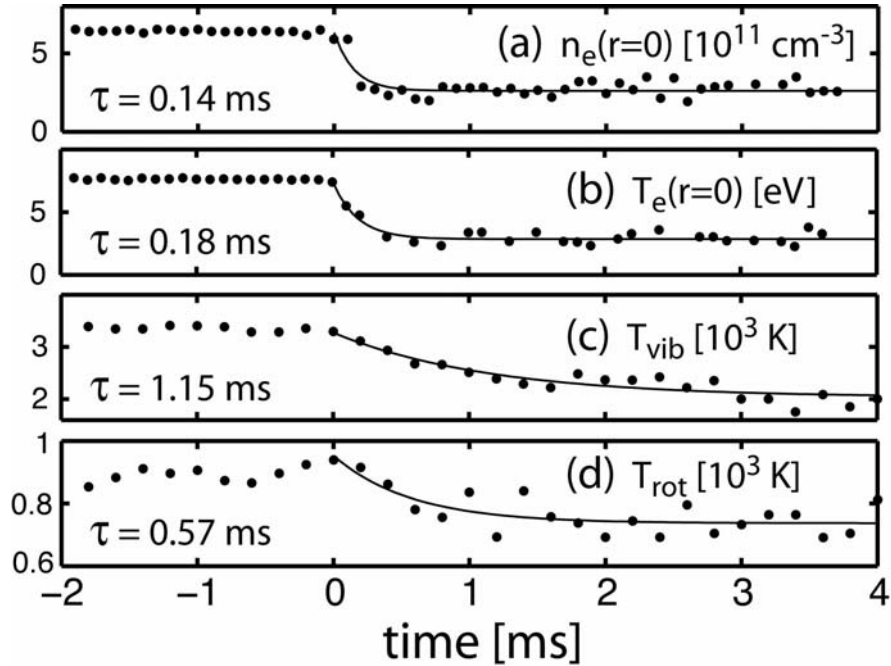


Fig. 29 - Time ring down experiment time traces for neutral pressure  
 $P_{\text{target}} = 1 \text{ mTorr}$ .

Fig. 30(a) shows the measured radial heat loss to the main chamber wall  $q_{\text{wall}}$  as a function of target pressure, while Figs. 30(b) and 30(c) show time-averaged electron density and temperature measured at the plasma center with a slow-swept single probe plunge. Radial heat flow due to radiation and plasma are shown as dark solid and light gray curves, respectively. Neutral heat flux to the walls obtained using the spatial decay data with Eq. (2) is shown with dashed curves. It can be seen that the radiation cooling is the largest loss term, but neutral cooling becomes significant (within a factor 2 of radiation) at higher neutral pressures that give a lower electron temperatures  $T_e < 4 \text{ eV}$ . The plasma heat flux to the walls is found to be much smaller ( $\approx 100\times$ ) than radiation loss for all conditions. Vibrational energy is the dominant loss channel for plasma cooling via  $H_2$ . The shaded squares and circles show the neutral cooling rates for  $T_{\text{vib}}$  and  $T_{\text{rot}}$  obtained from the time ring down experiments.

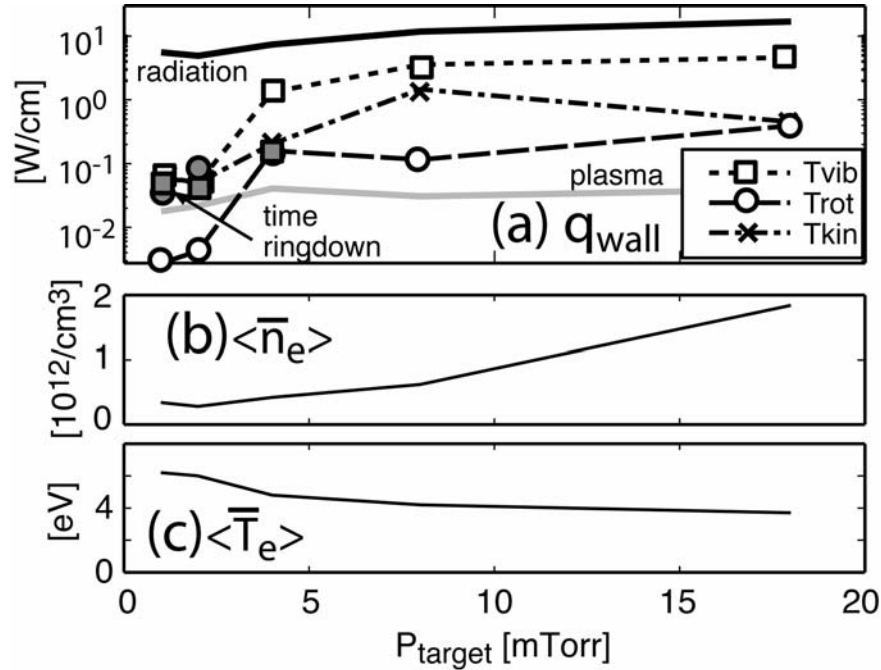


Fig. 30 - (a) Radial flux to chamber wall, (b) time-averaged electron density  $\langle \bar{n}_e \rangle$ , and (c) time-averaged electron temperature  $\langle \bar{T}_e \rangle$  as a function of neutral pressure  $P_{\text{target}}$ .

*Evaluation of  $H_2$   $T_{\text{rot}}$  as edge electron density diagnostic* Because the excitation energy of rotational quanta of  $H_2$  is so low ( $\Delta E_J \approx 0.02$  eV), the excitation rate of  $T_{\text{rot}}$  is expected to be almost independent of plasma temperature for typical edge plasmas. Furthermore, in most edge plasmas, the resulting  $T_{\text{rot}}$  is expected to be set by a balance between wall cooling and plasma excitation; under these conditions,  $T_{\text{rot}}$  becomes almost linearly dependent on density [Hollmann:2005]. This was confirmed by careful measurements of the equilibrium value of  $T_{\text{rot}}$  in PISCES-A. Fig. 31 shows the measured rotational temperature  $T_{\text{rot}}$  (gray circles) measured in PISCES-A. Also shown for comparison is data from  $D_2$  gas puffs in front of the TEXTOR limiter [Brezinsek:2002] and data obtained using  $D_2$  in the divertor of DIII-D [Hollmann:2006]. The dashed line is the (linear) prediction of modeling. The difference in  $T_{\text{rot}}$  between  $H_2$  and  $D_2$  is expected to be small because the electronic potentials are nearly identical [Brezinsek:2002]. These measurements confirm that the  $H_2$  rotational temperature, which is quite easily measured with a visible spectrometer, can serve as a valuable diagnostic of edge plasma density.

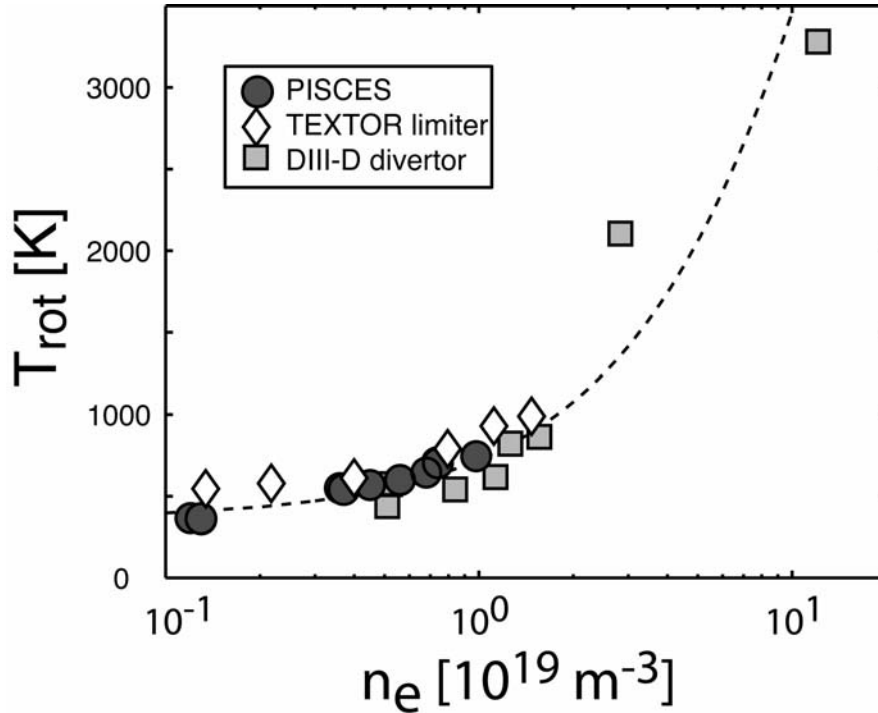


Fig. 31 - Molecular hydrogen rotational temperature  $T_{\text{rot}}$  measured as a function of local electron density  $n_e$  for PISCES-A and two tokamak experiments.

#### IV. Pulsed surface heat deposition system development

A pulsed power system has been added to Pieces-B to simulate the large PFC surface temperature excursions expected in the divertor region of ITER during ELMs. It is expected that the carbon divertor in ITER will reach transient temperatures of up to 3800° C. The question then arises as to whether the mixed Be<sub>2</sub>C layers that form on the C strike plates during steady-state plasmas will survive such dramatic temperature transients and continue providing erosion suppression of the divertor material.

The power pulsing is accomplished by applying a short-pulsed positive voltage to the material sample and drawing in plasma electrons to heat the sample surface. The voltage is applied by two power supplies and switched from the standard negative bias to the high-power positive bias and back using high-speed, high-power switches. The temperature of the sample surface is measured using an IR Pyrometry technique described below. The collimator to collect light from the sample is located 75 cm from the sample, and provides a 6mm diameter spot size.

Two separate non-invasive temperature diagnostics have been developed to measure the transient surface temperature of the sample using the blackbody thermal spectrum being emitted by the material surface. One is a fast (1MHz), two-color IR thermometer, originally developed by the UCSD Laser-Matter Interaction group led by Najmabadi and Tillack. Due to sensitivity limitations, this thermometer is only accurate down to about

1200° K. The other diagnostic is a slower IR photodiode array that measures a large portion of the emission spectrum on a much slower (100Hz) timescale, but is accurate down to room temperature. A diagram of the setup for the two thermometers is given in Fig. 32 below. Two beamsplitters are used to send the light to the photodiode array as well as the two photodiodes for two-color system. The prism in the photodiode array system is used to spread 0.9 to 1.6  $\mu\text{m}$  wavelength light across a linear detector array. The two-color system uses bandpass filters at 0.9 and 1.0  $\mu\text{m}$ . These wavelengths were chosen from the measured IR spectrum to give good temperature sensitivity and, at the same time, avoid absorption or emission lines from impurities in the plasma.

The slower array measures spectra that are in excellent agreement with the theoretical blackbody curve, demonstrating that the emissivity is constant across the wavelength and temperature ranges encountered here. In order to get a nearly real-time measurement using the two-color system, the Wien approximation to the blackbody equation, which assumes that the exponential is much greater than one, is used. The temperature is then given by the ratio of intensities at the two wavelengths

Preliminary measurements on a graphite sample without Be seeding have been made by pulsing the sample voltage to +75 V for 100 ms. The sample drew 15 A during this pulse. The resulting temperature curve taken with the two-color thermometer is shown in Fig. 33. The temperature rise time of 10 ms and decay time of ~20 ms can be seen. The oscillation in the plateau temperature is due to a 120 Hz fluctuation in the plasma source current. Systematic investigations using the positive pulsing apparatus to simulate transient heating effects on both carbon and tungsten targets during beryllium-seeded plasma exposure will be a large part of our proposed research effort and will be described in detail in Part II of this document.

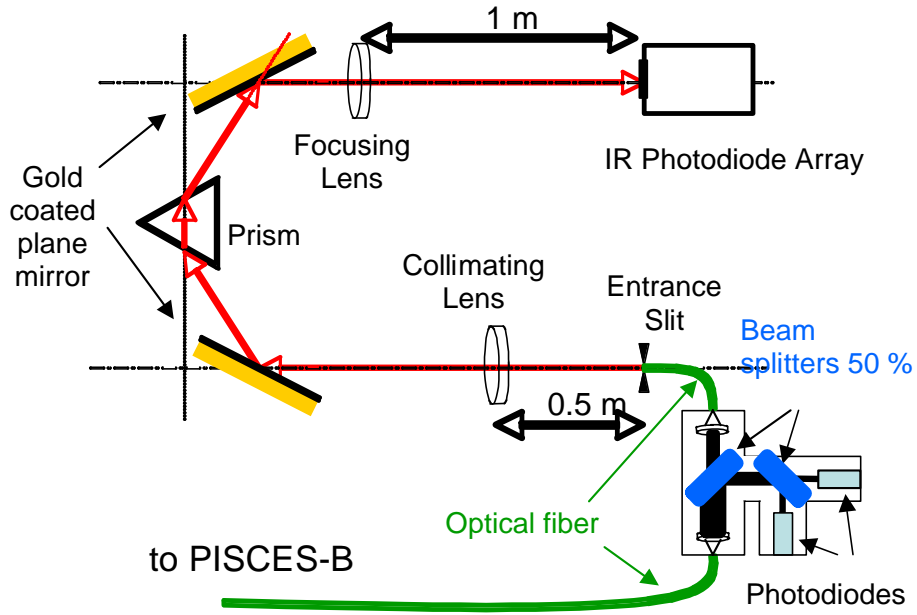


Fig. 32 - A diagram of the setup for the dual IR thermometers.

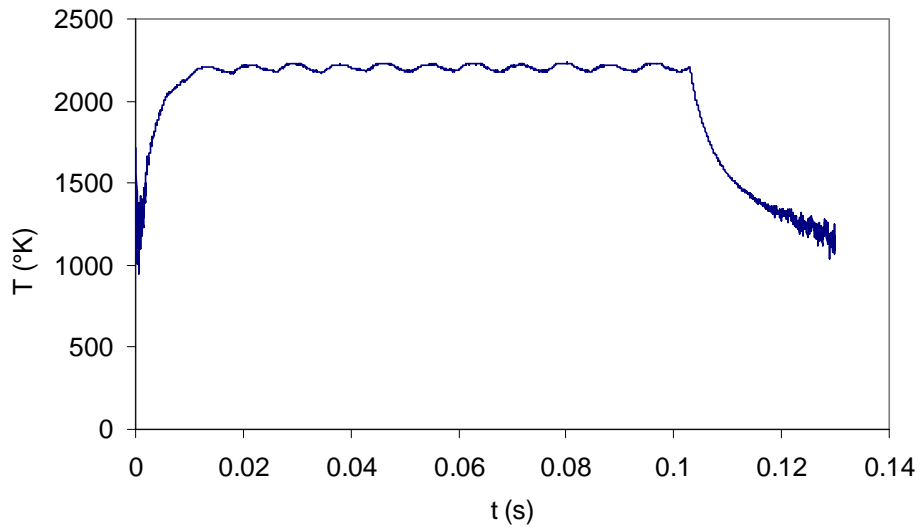


Fig. 33 - A plot of the sample surface temperature time history with 75 V pulsing.

## Part II: Proposed Work for FY07-09

### I. Introduction

During the proposed three-year grant period, the PISCES Program will continue to be centered on our existing collaborative work (primarily our US-EU Bilateral Collaboration) aimed at better understanding the role of mixed materials in the operation of ITER. The recently developed heat pulse deposition system will play a large role in the near-term experimental program (FY07) and will provide guidance toward the design, diagnostics and implementation of additional power and particle deposition systems for PISCES (FY08 & 09). In FY07, we also plan experiments that will identify the birth mechanisms of intermittent transport events, and modify an in-house fluid-based plasma turbulence simulation to include these dynamics. This work will then provide deeper understanding of the physics that leads to strong first wall PMI in confinement devices. In FY08, we expect to begin studying how vaporized wall material, liberated by thermal transients, transports back into the main plasma column. These experiments will be performed using both our existing pulsed thermal deposition system, and also by incorporating a modest-sized commercial laser ablation system onto the PISCES-B experiments. In addition to the experimental work being proposed, a significant effort will be directed toward interfacing with various PMI modeling experts and groups to incorporate the results of these experiments in benchmarking their codes. Finally, a modest effort will continue to be directed towards the understanding of certain high priority, or unique, plasma interaction with mono-material experiments.

A series of milestones for the PISCES Program for each of the three years of this proposal is listed below. Additional information on each milestone can be found in the pages that follow.

#### **FY07:**

- Document effects of heat pulse transient on formation conditions and deuterium retention characteristics of mixed-material surfaces
- Collect and characterize witness plate material and deuterium release behavior during various plasma conditions (Be deposition rate, oxygen content, incident energy)
- Develop and characterize Be erosion marker tiles for JET ITER-like wall experimental campaign
- Identify free-energy source(s) that lead to intermittent SOL structure formation and modify SOL turbulence model to produce SOL intermittent behavior.
- Incorporate impurity entrainment via passive scalar advection into turbulence model for simulating SOL impurity transport

#### **FY08:**

- Begin tertiary mixed-material investigations
- Install and commission laser power deposition system for vapor plume transport experiments

- Identify the birth mechanism(s) of SOL intermittent structures in linear plasma devices using experiment and turbulent simulation
- Develop engineering design of pulsed plasma source for ELM-like particle loading

**FY09:**

- Demonstrate and characterize pulsed plasma source system for ELM-like particle loading in PISCES-A
- Make first vapor shielding measurements using combined laser-ablation and pulsed particle sources in PISCES-A
- Test model for intermittent structure birth process in DIII-D & C-MOD tokamaks
- Simulate Be impurity distribution in PISCES-B using turbulence model and use result in time-averaged fluid code to predict Be flux during Be seeding experiments

***Planned Collaborations***

The PISCES program will continue a number of established formal and informal collaborations, and expects to establish several new collaborations during the FY07-09 time period.

*US/EU-EFDA Collaboration on Mixed Material PMI*

This formal collaboration, underway for several years, will continue in the coming period, and will focus upon ITER PFC mixed material PMI research. Work will also include erosion time marker development for the JET ITER-like first wall experiments.

*US/Japan Post-Jupiter II Collaboration (pending)*

Pending a final decision by the Japanese, PISCES anticipates becoming a formal participant in Post-Jupiter II research activities. Discussions with the US-DOE and with our Japanese partners have identified a number of opportunities in transient PMI science and technology issues relevant for both MFE and inertial fusion energy applications. These experiments would add significant new capability to the PISCES-B device, and would be performed at UCSD.

*US/Japan Collaboration on MFE PMI*

This more informal collaboration will continue, and will focus on retention issues within tungsten materials in the coming period. Joint experiments with the Nagoya University group are planned.

*Informal Domestic Collaborations*

We will broaden our domestic collaborations, and work with partners at:

- Argonne National Laboratory, (WBC erosion/redeposition model validation),

- *MIT ALCATOR C-Mod* (retention within Molybdenum surfaces),
- *PPPL* (support for LTX lithium first wall experiments),
- *DIID DIMES* (ITER-relevant first mirror parametric studies and other DIMES supporting experiments)
- *University of Wisconsin-Madison* (ARRIBA in-situ real-time PMI diagnostic in collaboration with Prof. Dennis Whyte).

In keeping with the program organization, we first present our detailed plans for PMI research, and then present our plans for the boundary plasma science and supporting development activities for the FY07-09 time period.

## **II. Mixed-Material Research**

Activities relating to mixed-materials can be broken down into three primary topics:

- 1) binary element issues,
- 2) tertiary element systems,
- 3) codeposited material behavior.

The activities in each of these areas will also integrate the key experimental results into the efforts of various US and International PMI modeling groups. The proposed research activities in each of these topics are described in detail below.

### **II.a. Binary element combinations**

#### *II.a.1. Beryllium-Carbon system*

In the area of binary mixed-material systems, our work will focus on the two primary mixed-material areas of interest to ITER, namely Be/C and Be/W. A significant amount of research into both of these systems has been described in the progress report section of this proposal, and while a great deal of insight and understanding into these systems has been acquired over the last few years, additional work is needed to resolve several key open issues.

One fundamental parameter that is lacking and is needed for input into the PMI surface sputtering codes is the sputtering yield for Be<sub>2</sub>C as a function of the incident ion energy. This value is critical for determining the Be particle balance in the codes and, once obtained, should facilitate the direct comparison of the models to the behavior of plasma exposed samples. The measurement of the beryllium carbide sputtering yield will be part of a broader effort to compare the sputtering yield of poly-crystalline beryllium to plasma deposited beryllium layers. We will also attempt to compare these values to the sputtering yield of beryllium-tungsten alloys that may form under various plasma conditions in PISCES-B.

The formation rate of beryllium carbide surface layers on graphite samples exposed to beryllium containing plasma has been well documented and a general scaling law has

been developed based on the parameters in the PISCES plasma column that can be systematically varied. This scaling relationship predicts the formation of beryllium-rich layers in the ITER divertor in the time between periodic transient events, such as ELMs. However, the response of these surfaces to extreme variations in surface temperature, such as those associated with ELMs, is still an open issue. By employing our newly commissioned heat-pulse deposition system during the exposure of graphite targets to beryllium-seeded plasma in PISCES-B, we will be able to systematically investigate the growth and response of beryllium carbide surface layers as a function of the transient power deposited on the sample surface. Such experiments will begin to address the stability, or robustness, of the beryllium surfaces to conditions associated with ITER. In Preliminary results indicate that the addition of short, high-temperature excursions of the surface increases the formation rate of beryllium carbide in the surface layer and thereby acts to inhibit chemical erosion of the graphite substrate more effectively. A comparison of two identical plasma discharges, one with and one without periodic temperature pulsing (up to about 1400°C) of the surface is shown in Fig. 34. In FY07 we will systematically investigate these effects in PISCES-B.

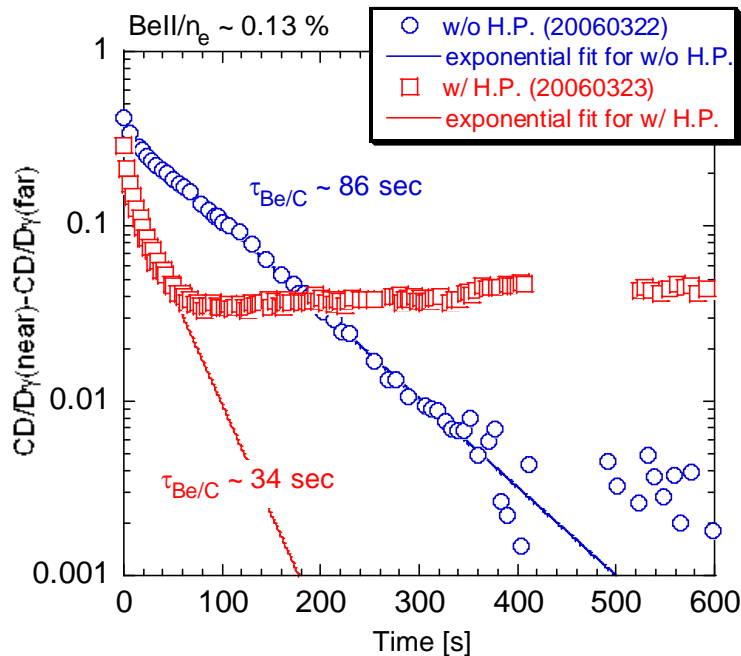


Fig. 34 – Suppression of chemical erosion of graphite exposed during heat pulsing (H.P.) of graphite targets occurs more rapidly.

The nature of the chemical bonding in the mixed surface layers and the surface morphology of the samples might be expected to change during transient heating exposure. The thickness of the resultant surface layers will also be compared to layers created under similar, but steady-state surface temperature, plasma exposures. In addition, the retention of hydrogen isotopes in the samples exposed to transient heating will be compared to non-transiently heated samples to ensure that no drastic alterations to

the tritium uptake of the carbon target plates in ITER should be expected. Again, we plan a series of controlled investigations of these topics in FY07 and early FY08.

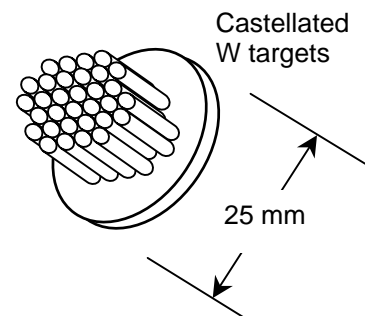
Whether protective beryllium carbide layers form in the ITER divertor will depend on many issues that are not possible to investigate in the PISCES geometry, such as SOL flow patterns. However, if the conditions of the divertor plasma are such that beryllium-rich layers form and carbon chemical erosion is suppressed, then another issue presents itself to ITER. The ITER divertor solution requires a certain amount of carbon impurities in the diverted plasma to radiate power from the plasma to allow detached divertor operation. Without chemical erosion of the divertor dump plates a radiating impurity, such as argon or neon, must be puffed into the divertor to achieve detached divertor operation. Because of this issue, PISCES will experimentally measure the impact of noble gas impurities added to the beryllium-containing deuterium plasma on the formation and longevity of the beryllium-rich surface layers.

The final step in our beryllium-carbon mixed-materials studies will be to acquire, through the US-EU Collaboration, some of the ITER reference material CFCs that will be used at the dump plates in ITER. It is important to verify that the somewhat different material structure associated with CFCs, and particularly the CFC proposed to be employed in ITER, behaves similarly to the more readily available ATJ graphite that has been used in the majority of the PISCES mixed-material studies.

### *II.a.2. Beryllium-Tungsten system*

Presently Be-W PMI experiments in PISCES-B span a limited range of plasma and target parameters. Further Be-W PMI experiments are planned that more aggressively span the range of operational conditions expected in ITER. These data will be used to determine operational conditions under which Be-W alloys will form and to validate the transport model used to predict the formation of deposited Be layers.

In previous PISCES experiments (Doerner:2005), W crucibles containing Be were observed to fail at temperatures below 1800 K. The crucible geometry, which allows evaporation in only a specific direction and is not exposed to plasma, crudely approximates a tile gap. Be trapped in W tile gaps in ITER will not be subject to intense plasma bombardment and will not evaporate as easily as with Be-W PMI conditions on W surfaces. Castellated W samples shown schematically here, will be used to assess the impact of Be-W alloy formation in such gaps. Be migration along cracks, alloy growth into castellation walls and grain boundary diffusion are to be examined. These experiments are particularly important should ITER need to adopt an all-metal W divertor where the strike points would be replaced with W brush structures.



The influence of transient heat loads on Be-W PMI will also be explored. In ITER the action of Type I ELM's, expected about once a second, will periodically flash heat divertor surfaces to in excess of 3000 K. Presently, it is unclear whether these heat loads will evaporate deposited Be layers, or deplete or assist in Be uptake in W. Using the transient heat pulse module onboard PISCES-B, experiments are planned to examine the effects of transient heat loads and then compare to the earlier Be-W PMI data set. An advantage of the use of W in a fusion reactor is its low retention of isotopic hydrogen. However deposited Be layers on graphite are known to increase retention and influences on retention due to transient heat loads are unknown. Thermal desorption studies will be performed in parallel with Be-W PMI experiments to assess the potential impact of deposited Be and transient heat loads on the desirable retention properties of W.

### *II.a.3. Beryllium-Nickel system (JET erosion tile marker development)*

The unique beryllium capabilities of the PISCES program have spawned a direct collaborative effort with the JET tokamak in England. The PISCES program will create a series of erosion tile markers for use at various locations inside JET. The tiles will consist of a beryllium tile substrate, supplied by the JET team. These tiles will be coated with a thin (~ 2 micron thick) layer of Ni in the PISCES-B enclosure using a magnetron sputter deposition chamber already operational and used for NIF target coating development work (in collaboration with General Atomics). The Ni coated beryllium tiles will then have an additional 5-6 microns of sputter deposited beryllium laid down over the Ni marker stripe, using the same magnetron facility. These erosion marker tiles will then be installed within JET for an experimental campaign. After the campaign the tiles will be removed and analyzed using ion beam techniques to determine the depth of the Ni layer beneath the resultant surface of the tile.

As part of the development work for this project, the erosion rate of the deposited beryllium layer will be measured in PISCES-B and compared to the erosion rate of 'standard' poly-crystalline Be targets. Additionally, some Be coated Ni substrates, created at the PISCES facility, will be analyzed at IPP-Garching as a function of temperature to determine the amount of Be-Ni inter diffusion. These two sets of data should make interpretation of the Jet erosion marker tiles more reliable.

### **II.b. Tertiary element combinations**

It is envisioned that sufficient understanding of the binary mixed Be-C and Be-W systems will be achieved during FY07 that a meaningful study of tertiary mixed systems will begin during FY08 and continue into FY09. Experiments will incorporate deuterated methane puffing while seeding PISCES-B plasmas with beryllium and interacting the resultant plasma with either graphite or tungsten targets. Another, practical, reason for delaying tertiary component experiments until after the binary component experiments have been concluded is the fact that methane injection into the PISCES-B device tends to contaminate regions of the machine that then act as carbon impurity sources during subsequent beryllium only injection experiments. While the intrinsic carbon impurity concentration after methane injection is still small, the impurities tend to restrict the

plasma source operational regimes available in the machine and therefore make comparisons between exposures difficult.

### *II.b.1 Beryllium and methane seeded plasma interactions with graphite targets*

Preliminary measurements involving deuterated methane puffing and beryllium seeding of deuterium discharges of graphite targets have been attempted, however no systematic results are yet available. The qualitative trend of beryllium-rich surface layer formation is still observed, but the systematically investigated time constants and surface concentrations are not available. Difficulties with measuring the absolute carbon concentration within the PISCES-B plasma column have been encountered, especially at higher target surface temperature where the IR radiation from the target interferes with measurement of the CI and CII line radiation profiles. A different set of carbon emission lines will be identified during subsequent experiments to eliminate this problem.

The same set of variables, as those investigated during beryllium seeded graphite exposures, will be investigated (namely surface temperature, ion flux and incident ion energy). In addition, the concentration of not just one, but two impurity species will have to be varied systematically. The ratio between the amounts of carbon to beryllium impurities will also need to be varied systematically.

Once trends in the behavior of exposed targets have been identified, perhaps the most important measurements will be to collect a series of mixed-material witness plate samples during such experiments. These codeposited materials will then be analyzed for both elemental composition and deuterium retention properties. It may reasonably be expected that any carbon contained in these samples will dominate both the retention and release behavior of deuterium. Vacuum thermal desorption spectroscopy (TDS) will be used to evaluate the temperature dependent release characteristics of codeposited samples. It may also be possible to perform TDS on codeposited samples (containing both Be and C) while a background of oxygen containing molecules are present in the vacuum oven. Such measurements could begin to address issues of collateral damage to beryllium containing surfaces in ITER if an oxygen bake is necessary to detritiate codeposited layers.

### *II.b.1 Tertiary element plasma interactions with tungsten targets*

Be-W work will be extended to include other effects relevant to an ITER scenario. Focus will shift from the influences caused by Be impurities to address the additional effects caused by a secondary impurity in the bombarding plasma. These experiments are summarized briefly as follows.

Controlled CD<sub>4</sub> injection will be used to study the influence of carbon impurities. Chemical erosion of the divertor strike plates may lead to carbon in the divertor plasma. With dual plasma impurities, Be-W PMI should be expected to dramatically differ. Both Be and W readily form carbides under elevated temperature PMI conditions and is

presently unclear whether Be-W or carbidic reactions will be favored. Should Be-W alloys form, the effects of C on alloy growth rates will be examined.

The impact of recycling impurities will also be investigated. Helium will be added to the deuterium plasma at levels up to 10 % to examine the impact of He ash. The addition of helium is expected to alter the erosion properties of Be-W PMI and will be compared to the deuterium only Be-W PMI data set. The inclusion of other noble gases, Ne and Ar, will be studied, should ITER require the use of noble gas injection to dissipate heat loads in the ITER divertor, the presence of heavy ions will nevertheless have a significant impact on divertor PFC PMI.

### *II.c. Codeposited material evaluations*

Understanding the codeposition properties of mixed materials as they interact with plasma is a high priority issue for ITER. The elemental composition of the codeposited material will have a large effect of the tritium inventory within these layers. Determining the inventory and understanding the effectiveness of various techniques to remove that inventory will be a focused research effort for the PISCES materials research group.

#### *II.c.1. Witness plate samples*

The witness plate manipulator, supplied by IPP-Garching during the first phase of our bilateral US-EU collaboration, is used to collect co-deposits of eroded material during mixed-material plasma interaction experiments. These codeposited layers can then be analyzed, both at IPP-Garching and at UCSD, to determine the elemental composition and their deuterium content. Initial analysis of PISCES codeposited material [Baldwin PSI 2004] has shown a strong inverse temperature dependence on the deuterium content with increasing temperature of the collecting sample. This trend is in agreement with similar, previous measurements. However, at the same time, due to difficulties with the embedded witness plate sample heaters, the oxygen content of these codeposited layers also increased with the temperature of the collecting sample. These PISCES codeposit measurements are contrary to conventional wisdom, which contends that tritium trapping in beryllium is dominated by the oxygen present in the codeposit.

In order to resolve these issues, we are working to develop a technique capable of varying the oxygen content of the PISCES discharges in a controlled fashion to further investigate this relationship. Simply puffing an oxygen containing molecule into the PISCES-B discharge results in several changes associated with the plasma parameters, the erosion of the target materials and subsequent cleanliness of non-oxygen contaminated discharges. Such changes make interpretation of results difficult. However, due to the unexpected nature of the results, it is important to verify and understand the parameters that dominate the retention properties of codeposited layers in ITER.

The witness plate manipulator will also be used in a piggyback fashion to collect eroded material during Be-W exposures and during heat-pulsing experiments. The role of tungsten sputtering by the beryllium impurity ions may lead to measurable tungsten

accumulating on the witness plate samples. While the tritium retention in plasma exposed polycrystalline samples is not thought to present a serious concern relating to the accumulation rate of tritium within the ITER vessel, recent results of tritium retention in plasma-sprayed tungsten surfaces show a much larger amount of retention (presumably due to voids in the resulting porous plasma sprayed material). The tritium content in codeposited tungsten, or tungsten containing, surfaces has never been experimentally explored. Finally, depending on the results of heat pulse deposition during plasma exposure of both tungsten and carbon targets in PISCES, there may be a change in the material lost from the target surface and therefore a change in the material collected on witness plate samples. Any such changes would be expected to impact the accumulation of deuterium in codeposited material.

Removal of deuterium contained within witness plate samples collected during PISCES-B mixed-material experiments has shown that most of the retained deuterium in beryllium-rich codeposits is released during baking of the samples to 375°C (the ITER maximum divertor bake temperature after a coolant drain). We will continue similar measurements during collection of mixed codeposit (for example during tertiary element exposures) to determine the effectiveness of baking the divertor as a means of tritium accumulation prevention in ITER. Similarly, if baking is insufficient to remove the majority of the retained deuterium, it may be possible to bake mixed codeposited samples in the presence of oxygen containing background gas in the vacuum ovens.

### *II.c.2. First mirror coatings*

A series of experiments concerning the evaluation of material deposited on first surface mirrors will be carried out by the PISCES program in conjunction with European experts in the area and also in collaboration with the DIII-D DIMES Program, which is also strongly affiliated with UCSD. The PISCES-B facility offers a unique possibility to investigate beryllium-containing deposits on mirror surfaces. The witness plate manipulator will be used to collect deposits on the mirrors. Analysis of the change in reflectance properties of the mirrors at different wavelengths may be investigated at UCSD, or perhaps in a separate facility dedicated similar measurements at the JET site in England.

Depending on the temperature of the substrate, deposited material can form into different types of surfaces with different physical properties (such as density, crystalline structure, grain size, etc). Any of these properties may affect the reflectance of the surface. A systematic approach to understanding the relationship of the surface temperature to the coating properties will be valuable for teams designing various diagnostics systems requiring mirrors in ITER.

## **III. Mono-Material Research**

### *III.a. Spectroscopic studies and model validation of plasma-material interactions with Be*

Beryllium (Be) is one of the key plasma facing component (PFC) materials in future fusion devices such as JET and ITER. In both devices Be will be used as the first wall material. For better prediction of Be behavior, validation of simulation codes, such as WBC and ERO etc, is required. This can be done with PISCES-B experiments, where controlled plasma-material interaction experiments with Be can be conducted. We plan to investigate sputtering yields of Be materials, angular and energy distributions of sputtered Be atoms, and importance of metastable state in Be I. The important point to note is that these will be investigated for both crystalline Be and deposited Be on Be, carbon (C) and tungsten (W) targets.

### III.a.1. Mixed material sputtering yield via spectroscopy

We will spectroscopically derive absolute sputtering yields of crystalline Be and deposited Be on Be, C ( $\text{Be}_2\text{C}$ ) and W (tungsten beryllide) with an aid of  $S/XB$  values for Be I lines from the ADAS database [1]. A preliminary measurement has been done. It is found that Be I (457.3 nm) line intensity of sputtered Be from deposited Be on a Be target is much stronger than that from crystalline Be as shown in fig. 35, where the plasma conditions are the same. This result indicates the higher sputtering yield of deposited Be on a Be target than crystalline Be. This may be explained by the lower surface binding energy of plasma deposited Be than that of crystalline Be (3.38 eV).

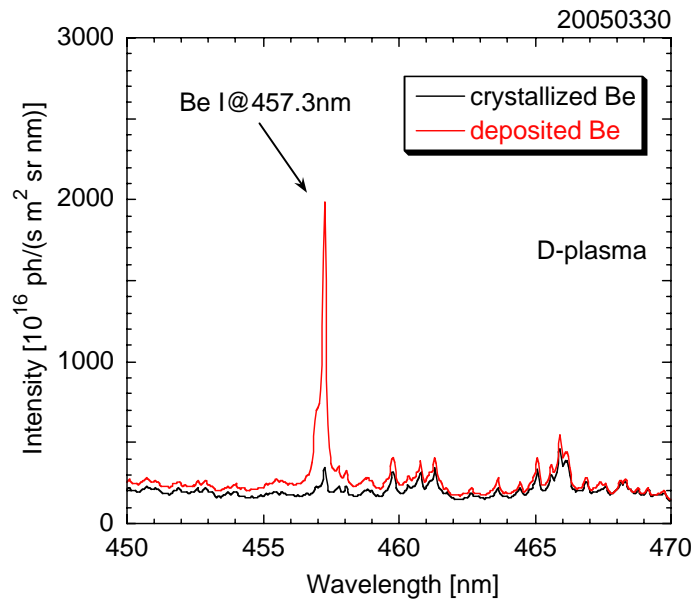


Fig. 35 - Be I (457.3 nm) line intensity of sputtered Be atoms from crystalline Be (black) and deposited Be on a crystalline Be target (red).

### III.a.2. Angular distribution of sputtered Be atoms

The sputtering yield angular distribution determines the penetration depth of sputtered atoms into plasmas as well as the redeposition profile. In FY06 we measured the two-dimensional profile of sputtered Be atom density near the target (crystalline Be) using

spectroscopic methods. From a comparison with WBC modeling, it has been found that the angular distribution is close to cosine for crystalline Be exposed to deuterium plasma. In FY07-08 we will investigate the incident ion energy and surface temperature dependences of angular distribution. In addition, differences in the angular distribution between crystalline Be and deposited Be will be explored.

### *III.a.3. Energy distribution of sputtered Be atoms*

The energy distribution of sputtered particles is also responsible for the penetration depth of sputtered particles into plasmas. We plan to obtain the energy distribution of sputtered Be atoms from a spectral line shape measured through a view port, which has nearly normal incidence to the target. For better resolution of line shape, the Be I (457.3 nm) line will be measured at the 2<sup>nd</sup> order (457.3 x 2 nm).

To see if the spectral line shape can be used in PISCES-B to estimate the energy distribution of sputtered Be atoms, we have examined the collision times of important processes. The ionization time of Be atom,  $\tau_i$ , is about  $10^{-5}$  sec at a typical plasma condition: electron density  $n_e = 3 \times 10^{18} \text{ m}^{-3}$  and electron temperature  $T_e = 8 \text{ eV}$ , where the ionization rate coefficient,  $\langle \sigma v \rangle_i$ , is around  $3 \times 10^{-14} \text{ m}^3/\text{s}$ . Because an experimental and/or theoretical cross section for elastic collision between Be and D<sub>2</sub> is not available, we made a simple calculation for the elastic collision time between Be and D<sub>2</sub>,  $\tau_{\text{ela}}$ , with the following assumptions; the radii of both Be and D<sub>2</sub> are  $10^{-10} \text{ m}$ , and the energy of sputtered Be atoms is a half of the surface binding energy ( $E_{\text{Be}} = E_s(\text{Be})/2 \sim 1.7 \text{ eV}$ ). A mean free path  $\lambda_m$  of about 0.05 m is obtained with a D<sub>2</sub> density,  $n_{\text{D}_2}$ , of  $10^{20} \text{ m}^{-3}$ .

The velocity of sputtered Be atoms,  $v_{\text{Be}}$ , is about  $6 \times 10^3 \text{ m/s}$  from  $v_{\text{Be}} = (2E_{\text{Be}}/m_{\text{Be}})^{0.5}$ . As a consequence,  $\tau_{\text{ela}} = \lambda_m / v_{\text{Be}} \sim 0.05/6 \times 10^3 \sim 10^{-5} \text{ sec}$ , which is of the same order as  $\tau_i$ . The energy transfer time,  $\tau_{\text{et}}$ , is typically longer than the elastic collision time when there is a mass difference between two particles, resulting in an estimated  $\tau_{\text{et}}$  between Be and D<sub>2</sub> that should be longer than the ionization time of Be atom. This then implies that the spectral line shape of the emission from sputtered Be should represent the energy distribution of sputtered Be atoms before they have a chance to thermalize with the background D<sub>2</sub>. In FY07-08, we plan to investigate the sputtered particle distributions as a function of the incident ion energy dependence and measure the differences between crystalline Be and deposited Be.

### *III.a.4. Importance of Be metastable states for Be spectroscopy in SOL plasmas*

There are two spin systems (singlet and triplet) in Be I. To date we have measured only a singlet line (457.3 nm) to derive the both the ground-state Be atom density and the sputtering yield of Be targets. The rate coefficient (shown in Fig. 36 below) of cross coupling between the ground and metastable states is larger than that of ionization from the ground state at  $T_e < 10 \text{ eV}$ . This indicates that a significant fraction of Be can be populated in the metastable state in typical SOL plasmas, making spectroscopic studies of Be more difficult. For example, if the metastable state population is significant, the

sputtering yield derived only from the singlet line becomes lower than the actual yield. In addition, in comparison with WBC and ERO modeling codes, where the metastable state is not taken into account, the experimental Be atom density in the ground state becomes lower. The metastable state contribution need to be included in both modeling codes.

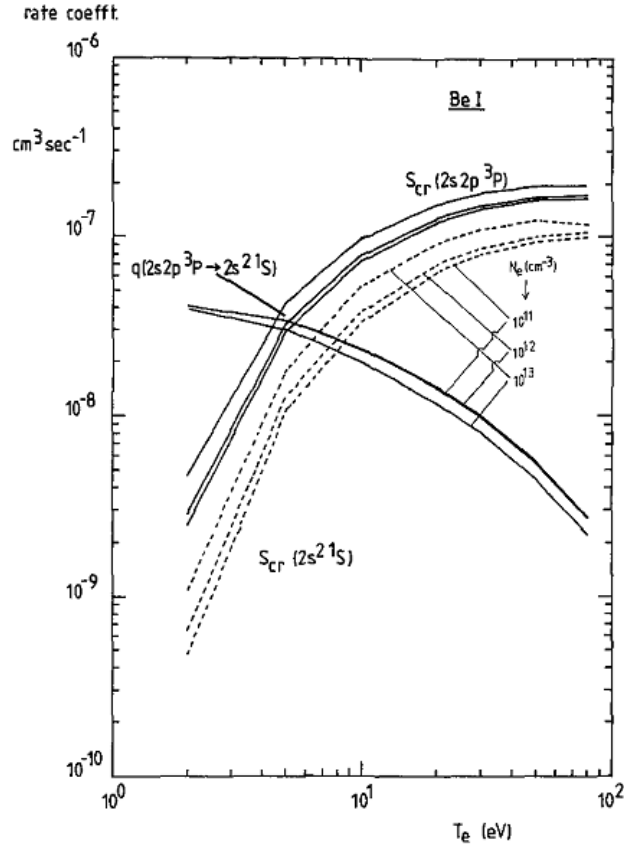


Fig. 36 – Rate coefficients for Be I singlet and triplet line radiation.

Recently, the spectroscopic windows on PISCES-B and in the wall of the Be enclosure were replaced with UV-grade fused silica to transmit light emitted from the plasma down to  $\sim 300$  nm. This improvement allows measurements of an intense Be I triplet line (332.1 nm) as well as an intense Be II (313.1 nm) line. We propose to perform thorough investigations of the metastable state of Be I in terms of the incident ion energy and surface temperature dependences, differences between crystalline and deposited Be, and plasma parameters dependences.

### III.a.5. Sticking coefficient of Be atoms

The sticking/reflection coefficient of sputtered beryllium atoms is an important quantity in being able to determine the location where beryllium-rich codeposits will accumulate. Values for the reflection coefficient can be obtained from binary collision modeling codes, such as TRIM, but these calculations are only reliable in energy ranges much above those of sputtered atoms. The sticking coefficient of sputtered beryllium atoms will

be measured in PISCES-B by using the well-developed technique of cavity probes. Cavity probes will be mounted on the witness plate manipulator and used to collect eroded material during the exposure of a beryllium target to deuterium plasma. The shape of the deposition pattern can then be used to determine the sticking coefficient. Such measurements with cavity probes can also be collected as a function of the temperature of the surface being deposited upon.

### *III.b. Tungsten plasma-material interactions*

This study will be done in collaboration with the NAGDIS group, Nagoya Univ., Japan (US-Japan collaboration). The linear divertor simulator NAGDIS-II will be used because of its ability to perform experiments on tungsten samples exposed to plasma bombardment at temperatures approaching the melting temperature of tungsten. There are three main topics for this collaboration: a) Angular and energy distributions of sputtered tungsten (W) atoms, b) Surface temperature dependence of sputtering yield of W, and c) Measurement of  $S/XB$  values for W I (400.9 nm) line emission.

A tungsten sample will be inserted into the plasma at the downstream ( $z = 1.72$  m). The angular distribution will be measured with a fast camera equipped with a filter for W I (400.9 nm) line. To obtain the energy distribution from a spectral line shape of sputtered W atoms, a line of sight, which is (nearly) normal to the sample, is necessary. For this purpose, a mirror will be installed at the midstream ( $z = 1.39$  m) or the upstream ( $z = 1.06$  m) ports. The purpose of topic (b) is to reveal if the erosion of W is enhanced at elevated surface temperatures below the W melting temperature via a process similar to that found on Be in FY05-06 and discussed in part I of this proposal. The surface temperature will be raised by plasma heating, and measured with a radiation pyrometer. For a measure of sputtering yield, W I (400.9 nm) line emission will be monitored. In topic (c), we will try to derive the ionization events/photon, i.e.,  $S/XB$  value for W I line (400.9 nm) by injecting evaporated tungsten oxide  $WO_3$ , and measuring both the W I line and an O I line. From the relation

$$\left. \frac{S}{XB} \right|_{WI} = \frac{1}{3} \left. \frac{S}{XB} \right|_{OI} \frac{I_{OI}}{I_{WI}}$$

the  $S/XB$  value for W I can be obtained with a known  $S/XB$  value for O I. Here, we assume that W and O atoms are injected into the plasma at a ratio of 1:3, which will be the case for fully dissociated  $WO_3$ . Although this parameter is critical to derive the W influx, experimental data are currently limited and are not in good agreement with preliminary calculations from the ADAS database.

### *III.c. Carbon mono-material investigation*

#### *III.c.1. Carbon cluster erosion*

One technique used to mitigate the intense heat flux encountered at the strike points in a divertor is to detach the divertor plasma from the strike point. Detachment is achieved by increasing the neutral gas pressure in the divertor chamber, allowing the incident power

to be radiated and thus cooling the divertor plasma. Often, seeding with noble gases is used to enhance the radiative properties of the plasma within the divertor. Depending on the incident plasma conditions, neon, argon or xenon can be used as the radiative gas.

As discussed previously in this proposal, we have observed a large amount of carbon cluster sputtering from graphite surfaces exposed to xenon plasma bombardment. We are currently extending these measurements to the other noble gases. Preliminary results show that the atom to cluster emission ratios change as the mass of the incident ion is increased. The largest ration of atoms/clusters is obtained during helium plasma bombardment and the lowest during xenon plasma bombardment. These measurements are made using a Hiden Ion Mass Spectrometer allowing measurements of not only the sputtered species, but also each species respective energy distribution and the angular distribution of each sputtered species. These sputtering measurements will be compared to simulation results obtained with the Monte Carlo TRIDYN code. Based on these results we will attempt to include the effects of C cluster erosion in the TRIDYN code.

### *III.c.2. Deuterium migration into CFCs*

Deuterium retention in graphite has been a well-studied issue for years. However, not all types of graphite show similar behavior. Carbon fiber composites (CFCs) are now being widely used in long-pulse devices (such as Tore Supra) and are planned for use in ITER. Recent results reported from Tore Supra were therefore particularly disturbing as significant deuterium seems to be retained in the CFC material after long-pulse discharges compared to short-pulse discharges. The deuterium was, at first, believed to be trapped in codeposits that form during the discharge, but this mechanism proved to be too small to account for the missing deuterium. A study of deuterium diffusion deep into the bulk of CFCs supplied by the Tore Supra team has recently begun. This collaboration involves Tore Supra, IPP-Graching and PISCES and is supported by the ITPA SOL and Divertor group. A series of initial sample exposures have been completed using the PISCES-A device and are currently being analyzed in Germany, and additional exposures are planned. The exact nature of the subsequent exposures will be determined based on the results from the initial experiments.

### *III.d. Deuterium migration into molybdenum*

Similar to the measurements proposed to examine the issue of deep penetration of plasma deposited deuterium into CFCs, we will also expose a series of Mo samples to different conditions of deuterium plasma. Preliminary measurements using C-Mod supplied Mo samples have already been exposed in the PISCES-A facility and are undergoing detailed analysis at the University of Wisconsin. Additional systematic exposures of C-Mod relevant Mo samples will be conducted at PISCES to further investigate the similarities and differences between migration of deuterium deep into Mo and CFC structures.

#### IV. PMI Modeling Code Validation

An important and active part of each of the measurements described above is their comparison to the predictions of PMI modeling tools, such as WBC and ERO. Some of this work, relating to the comparison of the energy and angular distributions of sputtered particles has already been described. In addition, the PISCES group, in collaboration with modeling teams at ANL and KFA, are validating the predictive capabilities of these codes with respect to mixed material interactions. Neither of these codes includes chemical effects in the surface of materials interacting with the incident plasma, so issues like the impact of beryllium carbide formation must be added in a manner that can be extrapolated to other scenarios, such as ITER.

For example, the binding energy of beryllium atoms in the beryllium carbide molecule plays a large role in determining the erosion yield of beryllium from mixed-material samples and thereby determines the amount of beryllium that should be detectable on the surface of plasma exposed targets. Typically the PMI modeling codes use a concentration-weighted average of the pure material binding energies to model the binding energy of alloys in the surface. The parametric studies involving the formation time of carbides in the surface, or alternatively the suppression time of chemical erosion, can be used to test this binding energy model. The temporal evolution of the surface composition is also a critical test of the ability of these codes.

Both the WBC and ERO codes have been successfully applied to deuterium on beryllium plasma surface interaction experiments to verify the plasma physics inputs for the codes are correct and to test their abilities before they are exercised on mixed-material surfaces. An example of the comparison of the absolute intensity and sputtered beryllium mean free path between ERO and PISCES-B is shown in Fig. 37. Comparisons with WBC show similar results. During this proposal period we will continue collaborating with both these modeling teams with the aim of including mixed-material effects into each of these models, both for the Be/C system as well as the Be/W system.

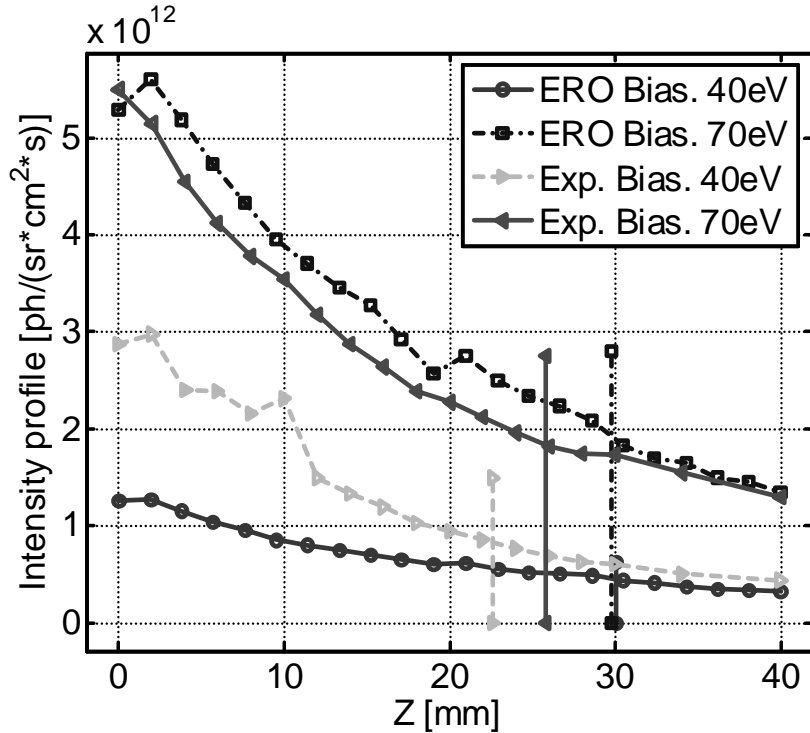


Fig. 37 – Comparison between ERO model results and PISCES-B measurements show good agreement at higher bias voltage, uncertainty of the magnitude of plasma potential at lower energy makes for larger experimental error bars in the 40 eV case. Vertical lines in the figure mark the  $e$ -folding distance for each case.

## V. Boundary Plasma Science and Supporting Hardware Development Tasks

In FY07-09, these supporting research elements will focus upon

- Experimental and numerical studies of intermittent SOL plasma transport
- Divertor physics
- In-situ PMI diagnostic development
- Hardware development for transient PMI experiments

Our plans in each of these areas are detailed below.

*Origins of Intermittent SOL Transport:* The objective of this work is to identify the physic mechanism(s) that lead to the formation of bursty SOL transport, first in the linear plasma devices at UCSD and on tokamaks. The work on the PISCES-A and CSDX linear plasma devices will be performed using the using a combination of multipoint Langmuir probe and fast imaging diagnostics (see Fig. 38 below from a sequence of images obtained with the fast camera). Once the essential origin(s) of these events are clearly understood, we will work collaboratively on confinement devices to search for the

presence of similar physics in the SOL region, and to develop physics-based projections of the role and significance of intermittent SOL transport for ITER first wall PMI.

In FY07-08, we will use fast imaging on PISCES and CSDX using an existing fast camera device in parallel to with Langmuir probes on PISCES and CSDX in order to complement our knowledge of the SOL intermittent structures and to so accurate assessment of their role of these structures in ITER can be made. We will use these instruments to characterize the spatio-temporal properties of the blobs in the SOL of PISCES and CSDX at a given magnetic field and gas pressure, see how their scale changes with the ion gyroradius using scans of the magnetic field strength and ion mass. We also want to identify under what conditions the detachment process of these bursts takes place using fast imaging. We will also examine the role that pressure gradient, plasma rotation, and flow shear play in triggering these events, and make detailed comparisons of the experimental results with the turbulence simulation work that is described below. Once these experiments on the PISCES-A and CSDX devices have been completed and published, we will then seek to collaborate with one or more tokamak devices and test the physics picture developed here using tokamak SOL data in the FY08-09 time period.

In FY07, we will modify a simulation that was developed in FY05-06 via other OFES-DOE grants in such a way that the plasma density gradient can self-consistently evolve in time in response to the turbulent transport by incorporating a particle source term into the turbulence model. Previous studies of similar models where the “background” profile is allowed to evolve have shown evidence of intermittent behavior analogous to the experimental observations. Therefore, the first step in our research will be to change our numerical model from one which describes the evolution of finite  $k_\theta$  density fluctuations  $\tilde{n}$  in the presence of steady  $k_\theta = 0$  background  $n_0$  to a “source-driven” model of the density which would be given as

$$\frac{\partial n}{\partial t} + \bar{V} \cdot \bar{\nabla} n + \omega_\parallel (n - \phi) - D \nabla_\perp^2 n = S_n$$

where  $n$  now contains all  $k$  modes, and  $S_n$  is an azimuthally symmetric source term. Based upon the recent experience of other modeling groups, we then expect that that simulations will then lead to bursty transport phenomena. The first objective of this work will then be to test whether this is indeed true and then compare these bursts with what is seen in the experiments.

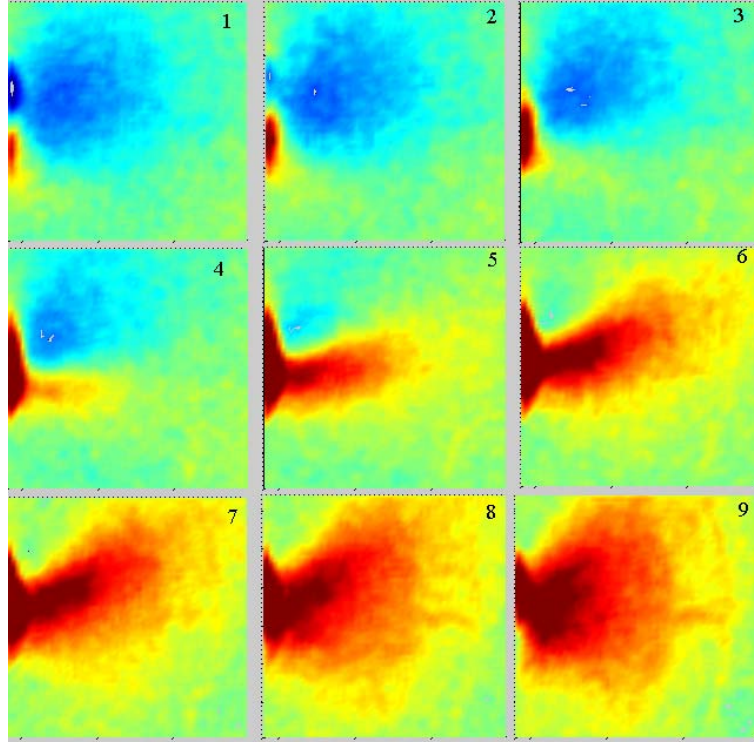


Fig. 38 - Preliminary results from imaging the SOL of the linear CSDX showing the birth and subsequent evolution of a burst of plasma escaping into the outer low density SOL-like region. The integration time is  $1 \mu\text{s}$  and the time between frames is  $10 \mu\text{s}$ . The structure seems to remain attached to the main plasma while having long excursions far from the main plasma column.

In FY08, we will then take this turbulence model and use it to study the entrainment of first wall impurity ions in the turbulence, under the assumption that the impurities are a passive scalar from the point of view of the turbulence dynamics. The approach here would be to add an additional equation to the model, of the form

$$\frac{\partial \psi}{\partial t} + \vec{V}_{E \times B} \cdot \vec{\nabla} \psi = S_{\psi} + L_{\psi}$$

Where  $\psi$  is the local density of impurity ions,  $S_{\psi}$  is a source of impurity ions located at the outer edge of the plasma, and  $L_{\psi}$  is a model of the depletion of impurity ions due to parallel transport to the endplates / divertor region. What we hope to develop is a physics-based model for the rate at which impurity ions are effectively transported or mixed into the plasma center from the edge region where they are generated. Although the assumption of treating the impurities as a passive scalar will have to be verified *a posteriori*, it will step represent a step forward in the modeling of their dynamics in the edge region. It should be emphasized that understanding these impurity fluxes is important not

only for predicting the rate at which they will enter the core plasma, but the rate at which they will be eroded from the first wall, and their rate of deposition in the divertor region.

We will then link these simulations to the mixed material PMI studies by predicting the incorporation of Be impurities into the PISCES-B plasma column, and try to predict the effect of turbulence on the transport of ionized sputtered Be atoms in the PISCES-B plasma column.

## Divertor Physics

*Measurement of  $H_2$  accommodation rates in PISCES-A for ITER wall materials*  
Measurements in 2005 done in PISCES-A and discussed previously in this document have demonstrated the use of spatial decay of molecular hydrogen vibrational, rotational, and kinetic temperatures  $T_{\text{vib}}$ ,  $T_{\text{rot}}$ , and  $T_{\text{kin}}$  as  $H_2$  travels from the plasma down a side port to obtain the accommodation rates for  $H_2$ -surface collisions. These measurements are important because wall collisions are typically the dominant cooling term for the  $H_2$  temperatures and therefore must be included to accurately model the effect of  $H_2$  in detached divertors [Hollmann05]. In FY07 we propose to continue this work to allow independent control of the wall temperature and wall material in these experiments.

Fig. 39 below shows a schematic of the proposed experimental layout. The main modification to existing experimental hardware is the addition of an insert tube made of the material to be tested (e.g. carbon, tungsten, or aluminum). The tube needs to be actively cooled and heated to allow control of the tube temperature independently from the plasma conditions. Mounting inside the vacuum chamber will need to be done via thermally and electrically isolated hardware. High-temperature thermocouples embedded in the tube will allow monitoring of the tube temperature. An electron gun (already constructed) can be used to aim a weak diagnostic electron beam down the insert tube to provide electron-impact excitation of  $H_2$  necessary for diagnosis of the  $H_2$  temperatures. Thermally isolated optical mounts must be installed with views across the insert tube. Several views are envisioned to better constrain the interpretation of the spatial decay data (unlike the proof-of-principal experiments of 2005 where only two views were used). These views need to be carefully terminated to ensure that reflections from the main plasma discharge do not perturb the measurements. The electron beam will be fired along the normal PISCES-A axial magnetic field, so it is anticipated that the beam will be well-collimated. The optical signals will be run with optical fibers out of the vacuum vessel and be imaged onto the existing PISCES-A visible spectrometer to obtain the  $H_2$  temperatures along the inside length of the drift tube. Analysis of this spatial decay data with the help of the existing PISCES-A neutral Monte-Carlo code is expected to give first measurements of  $H_2$  accommodation rates for ITER-relevant wall materials and under controlled wall temperatures. These probabilities are expected to be valuable for input into edge modeling codes.

*Impurity flow study and comparison with UEDGE:* A major emphasis of the PISCES program is studying the effects of mixed ITER wall materials, e.g. Be-W alloy formation,

Be overlayer suppression of C chemical sputtering, and so on. These mixtures are expected to come about as a result of sputtered wall materials becoming ionized and captured in the background plasma flow, then carried to a different part of the tokamak. An essential aspect of tokamak wall material migration is therefore the degree to which impurities become entrained in a background plasma flow, i.e. to what extent do heavier impurities accelerate up to the (often near sound speed) light background ion flow (as opposed to staying near their own slower sound speed flow). This fundamental problem has not been well-studied previously. PISCES-A, with its easy diagnostic access, is an excellent test platform for checking the accuracy of the parallel flow physics included in edge fluid codes. Here, we propose to use PISCES-A to validate the parallel flow physics contained in the UEDGE edge modeling code [Rognlien:1992], which is routinely used in the fusion edge physics community. UEDGE uses the Braginskii equations to model the parallel flow of ions [Braginskii:1965]. This work will be done in collaboration with A. Pigarov (UCSD), who will perform the UEDGE modeling..

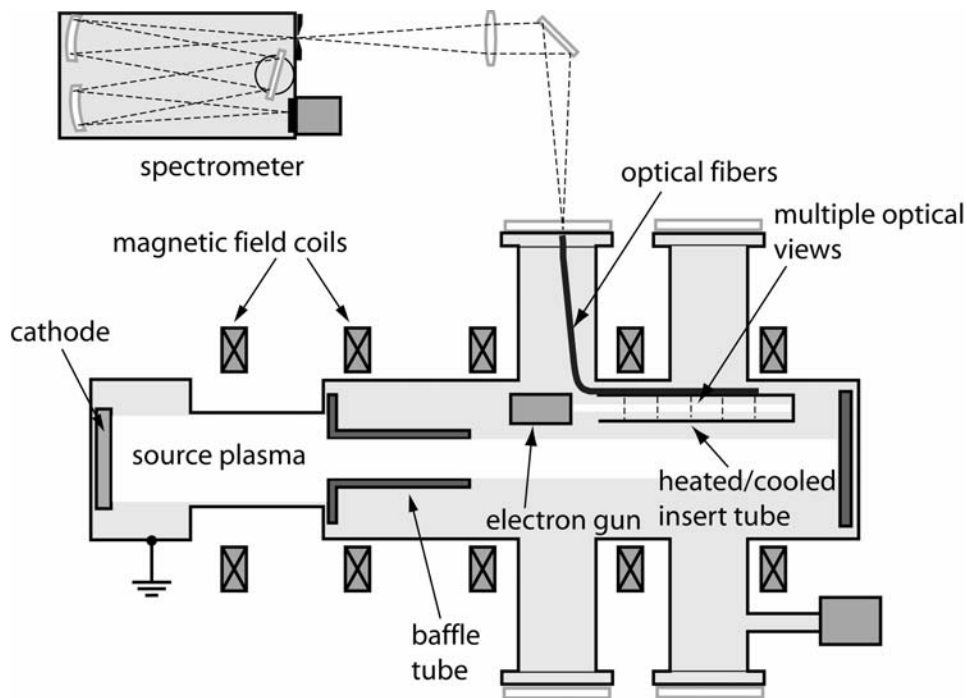


Fig. .39 - Schematic of proposed spatial decay experiment for measuring  $H_2$  accommodation coefficients in PISCES-A

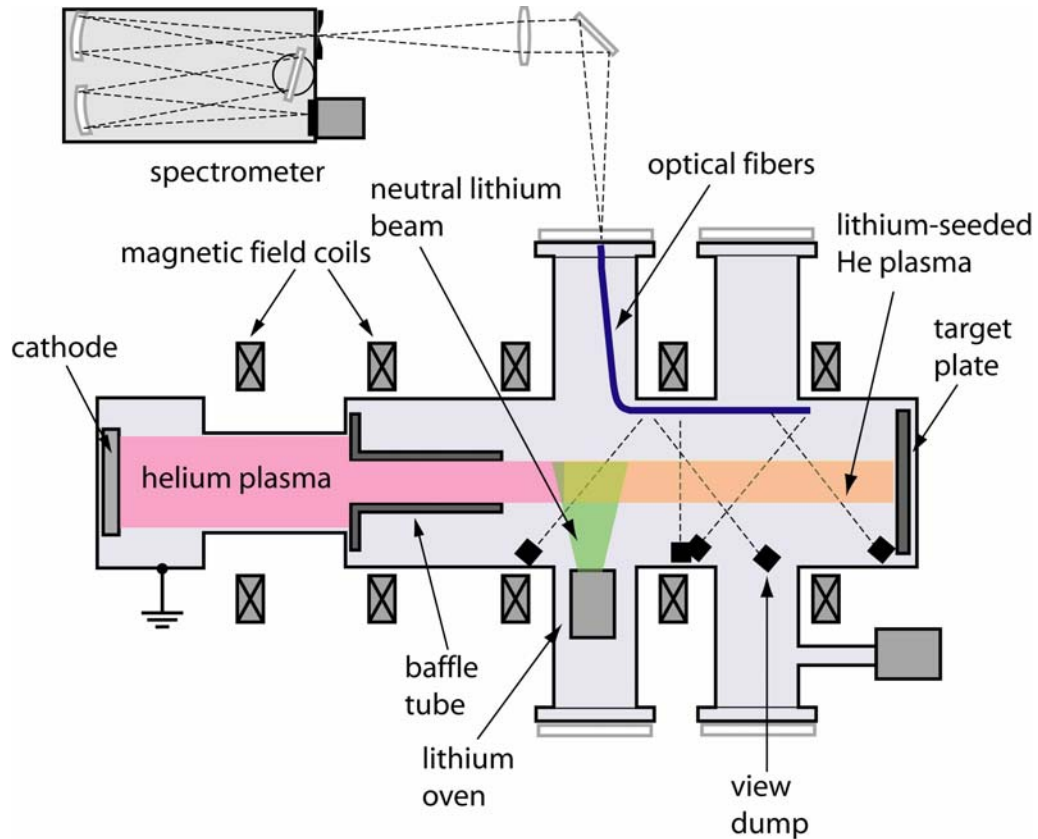


Fig. . 40 - Schematic of experiment for measuring impurity flow in PISCES-A

A basic schematic of the proposed experiment is shown in Fig. .40. A lithium oven would be used to create a beam of neutral Li used to seed a He plasma in PISCES-A. He would be used as the main species to allow spectroscopic measurement of the background plasma flow. Li would be used as an impurity because it is non-recycling and is light (making it easier to measure velocities and making finite gyro-radius effects less of a concern). Measurements of the impurity and background flow would be done steady-state using passive spectroscopy. Collimated fiber views across the plasma column would be used. One or more perpendicular views would be used as wavelength references to get at the parallel flow velocities. Fiber views would be terminated with viewing dumps to avoid reflections.

The experimental plan would consist primarily of varying the plasma conditions and measuring the degree to which the Li ions accelerate up to the background He ion flow. The most important parameters in this study are background flow velocity (varied dominantly by varying the source region neutral pressure, which changes the plasma pressure gradients) and the background ion temperature (varied dominantly by varying the discharge power). After successful experiments with Li, it would be useful to repeat these experiments with a different mass impurity (e.g. Na) to study the mass scaling in the impurity flow.

## In-situ Real-time PMI Diagnostic Development

*Direct chemical erosion measurement:* Chemical erosion via emission of volatile hydrocarbons from graphite surfaces under hydrogen plasma bombardment is a significant concern for the graphite divertor of ITER because of the possibility of significantly enhanced erosion of the divertor plates even during detached divertor operation, and also because of the possibility of co-deposition of tritium into carbon layers [Federici:2001]. Presently, although the importance of chemical erosion of carbon is well-recognized in the tokamak community [Roth:2004], many uncertainties remain in the rate at which chemical erosion actually occurs as a function of surface temperature, surface composition, and plasma flux. One of the main sources of this uncertainty is thought to be the indirect method by which carbon chemical erosion is currently measured. Presently, the presence of carbon chemical erosion (i.e.  $CH_4$  and/or  $C_2H_6$  emission from carbon under hydrogen plasma bombardment) is inferred by passive visible spectroscopy using either  $CH$  Gero band emission ( $A-X$  band head at 431 nm) to infer  $CH_4$  emission or  $C_2$  Swan band emission ( $d-a$  band head at 516 nm) to infer  $C_2H_6$  emission. In either case, the measured radical is the result of a long breakup chain, so calculating the original neutral emission from the surface is a challenging undertaking. Additionally, the measured emission intensity depends on the local plasma conditions ( $n_e$  and  $T_e$ ), which are frequently not known well. Traditionally, the experimental method used to attempt to circumvent these problems has been to calibrate the measured  $CH$  emission by injecting a known quantity of  $CH_4$  into the plasma [Whyte01]. However, this technique itself has associated difficulties, such as the short mean free path of  $CH_4$  and the need to inject a large enough amount to get a good signal yet not perturb the plasma.

Here, it is proposed to use near infra-red (NIR) absorption spectroscopy to directly measure the  $CH_4$  production from chemical erosion of graphite targets under various plasma bombardment conditions. The advantages of this method over existing methods are: 1) the  $CH_4$  column density is measured directly without resorting to complicated and uncertain modeling, 2) the measurement is spatially localized, allowing study of the  $CH_4$  mean free path under different plasma conditions, and 3) the technique is non-perturbative.

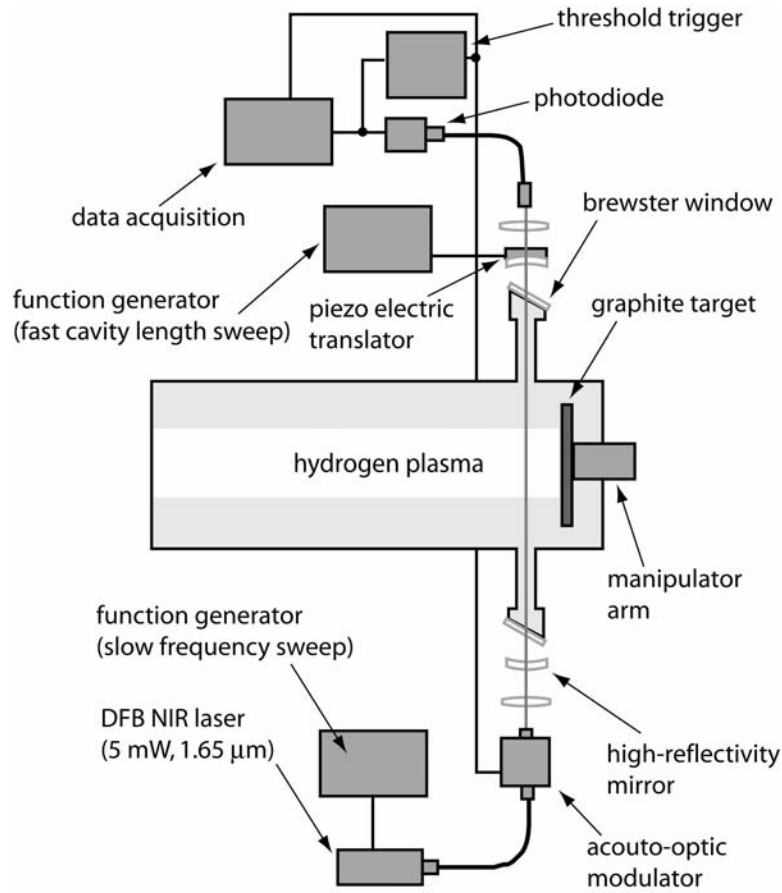


Fig. .41 - Schematic of proposed experiment for measuring line-averaged  $CH_4$  density due to chemical erosion of graphite target in PISCES-A.

An overview of the proposed experimental setup is shown in Fig. .41. The basic experimental idea is to use a linear cavity consisting of two high-reflectivity dielectric spherical mirrors isolated from the vacuum by Brewster windows. An optical cavity of some sort is necessary here because the column densities of  $CH_4$  are expected to be too low to detect easily in a single absorption pass. Multi-pass mirror cells such as a White Cell or Herriott cell are not desirable here because we wish to diagnose a very thin column immediately in front of the graphite target (the mean free path of  $CH_4$  is expected to be only several mm in typical edge plasma conditions). Additionally, multi-pass cells are usually limited to  $< 50$  bounces, while a well-tuned optical cavity can have a much higher  $Q$  than this. For example, using high-quality multilayer mirrors with a reflectivity  $R = 0.999$  gives an optical cavity finesse

$$Q \approx \frac{\pi\sqrt{R}}{1-R} \approx 3000$$

and so thousands of passes can be achieved, giving the potential to measure very small column densities of  $CH_4$ .

A challenge with high  $Q$  optical cavities is that length alignment must be maintained to accuracies better than the wavelength (of order 1  $\mu\text{m}$  here). In many precision optics experiments, active feedback is used to maintain optical cavities on resonance. This can be challenging to implement, however, particularly in a noisy environment. For simplicity, we propose to use cw cavity ring down spectroscopy here. In this technique, the cavity length is not locked on resonance, but is swept in length intentionally through resonance. A piezo electric translator and function generator can be used for this purpose. When the cavity passes through a resonance, power is coupled efficiently into the optical cavity, and an intensity buildup is registered by a photodiode monitoring the cavity output. When this intensity reaches a predetermined threshold, the input optical power is switched off. Here, we propose using an acousto-optic modulator to accomplish this switching. Typical AO modulator switching times are  $< 0.1 \mu\text{s}$ , which is expected to be sufficiently fast for these experiments. Empty cavity ring down rates in these experiments are expected to be  $\tau = \frac{QL}{c} \approx 5 \mu\text{s}$ , where  $L = 50 \text{ cm}$  is the cavity length. If the light in the cavity is at the correct wavelength to be resonantly absorbed by  $\text{CH}_4$ , then the cavity losses increase and ring down becomes faster. By comparing the measured ring down times to the empty cavity rate (measured before any  $\text{CH}_4$  is introduced), an absorption spectrum can be constructed.

As an optical source, we propose to use a solid state distributed feedback (DFB) laser at 1.65  $\mu\text{m}$ . This wavelength is chosen to correspond to the  $2\nu_3$  overtone band of  $\text{CH}_4$ . This band is weaker than the fundamental band near 3.4  $\mu\text{m}$ , but is much easier to access from a hardware perspective (i.e. readily available telecommunications optics function well at 1.65  $\mu\text{m}$ ). The DFB laser can be tuned in frequency either by changing the injection current (which changes the diode temperature) or by directly heating/cooling the diode. Injection tuning has the advantage that the laser frequency can be swept quickly (up to MHz) but the laser intensity changes and mode-hops are often experienced. Here, we expect to use temperature tuning, which is slower ( $< 1 \text{ Hz}$ ) but more stable. The width of the scan is of order 0.004  $\mu\text{m}$  for DFB lasers at 1.65  $\mu\text{m}$ ; this is sufficiently wide to measure three rotational lines of the  $\text{CH}_4$   $2\nu_3$  band structure. These three lines can be fit to obtain the rotational temperature, estimate the absorption of the entire band, and obtain the column density of  $\text{CH}_4$  along the laser path.

Previous work has been done using cavity ring down NIR absorption spectroscopy of  $\text{CH}_4$ , primarily for studying trace quantities of  $\text{CH}_4$  in the atmosphere. In [Fawcett02] an absorption detection limit of  $\alpha_{\text{min}} \approx 1.5 \times 10^{-8} / \text{cm}$  was reported, while in [Morville04], a detection limit of  $\alpha_{\text{min}} \approx 1.9 \times 10^{-9} / \text{cm}$  was achieved by averaging 256 times. The second case corresponds to a number density of  $\text{CH}_4$  (in a low pressure environment where the peaks are narrow) of roughly  $n_{\text{CH}_4} \approx 3.7 \times 10^{10} \text{ cm}^{-3}$ . Assuming an  $\text{CH}_4$  erosion yield  $Y = 0.015$  [Janev95], a plasma flux  $\Gamma \approx 10^{18} / \text{cm}^2 / \text{s}$ , and room-

temperature methane with  $v \approx 4 \times 10^4$  cm/s, we have a near-surface density of  $CH_4$  in front of the PISCES-A graphite target of:

$$n_{CH_4} \approx \frac{Y\Gamma}{v} \approx 3.8 \times 10^{11} \text{ cm}^{-3} \quad ,$$

which is an order of magnitude above the expected detection limit. We conclude that  $CH_4$  emitted due to chemical erosion in PISCES-A should be detectable with this technique.

The ability to directly measure chemical erosion is expected to provide a valuable tool to the PISCES laboratory, and may also be extendable to tokamak experiments. Important experiments which are planned are studies of the validity of  $CH$  band emission measurements for inferring  $CH_4$  release; studies of the mean free path and temperature of  $CH_4$  released from the surface; and direct measurement of changes in  $CH_4$  release as a function of plasma flux, plasma temperature, and surface temperature. Additionally, this technique is expected to be valuable in present studies of chemical erosion suppression due to Be deposition on C being done on PISCES-B. Assuming this technique works well for  $CH_4$ , the technique can readily be extended to other important molecules, such as  $C_2H_6$  (most molecules tend to have strong fundamental bands in the range 3-4  $\mu\text{m}$  and weaker overtone bands in the range 1-2  $\mu\text{m}$ ). This would require the purchase of a different DFB laser tuned to a different wavelength; however, much of the remaining hardware shown in Fig. 241 could be retained.

*Real time net erosion/redeposition and D/T retention diagnostic development* The goal of the Alpha Radioisotope Remote Ion Beam Analysis (ARRIBA) diagnostic, under development at the University of Wisconsin by Prof. D. Whyte, is to provide in-situ, time-resolved measurements of erosion/deposition and hydrogenic retention on plasma exposed surfaces. A Curium-244 radioisotope provides steady-state source of high energy ( $\sim 6$  MeV) alpha ions. These alphas are a proxy for high-energy ion beams used for Rutherford Backscattering Spectroscopy (RBS) and Elastic Recoil Detection (ERD), which respectively provide depth-resolved measurements of solid elements and hydrogen isotopes. We propose to field ARRIBA on PISCES-B to provide in-situ real-time PMI data during Be mixed material experiments. A schematic of the diagnostic arrangement is shown in Fig. 42.

The UW group has modeled the performance of ARRIBA for a PISCES-specific case: coating of Beryllium films on tungsten, and the results indicate that good performance should be achievable. Count deficiencies in the energy spectrum (Fig. 43) of backscattered alpha particles impinging on a Be/W surface can be used to find the elemental ratio of Be to W in the near surface and the thickness of the mixed-material layer (provided that the spectrum obtained from the pure W surface is also acquired.) Integration of the peak counts in ERD energy spectra (Fig. 44) provides a relative measure of the hydrogenic retention in deposited layers. Initial simulations indicate that

an ARRIBA diagnostic could measure PISCES relevant deposits of Be on W surfaces with a resolution of  $.05\mu\text{m}$  and 5 at. % Be for film thicknesses up to  $\sim 3\mu\text{m}$ . The sensitivity to retained hydrogenic species is  $\sim 1 - 5$  at. % for film thicknesses up to  $\sim 1\mu\text{m}$ . The resolution and sensitivity can be improved by increasing the time allowed for acquiring the energy spectra, which is here assumed to be  $\sim 1000\text{s}$ . This is only meant as an example, the ARRIBA device has wide flexibility in its ability to measure different elemental combinations. The ARRIBA diagnostic is well-suited to a steady-state device like PISCES, since it exploits the magnetic field to control exposure and analysis of samples surfaces using  $J \times B$  with an internal coil embedded within the sample holder device. Furthermore, the radio-isotope alpha source allows for continuous monitoring of erosion, deposition and hydrogenic retention.

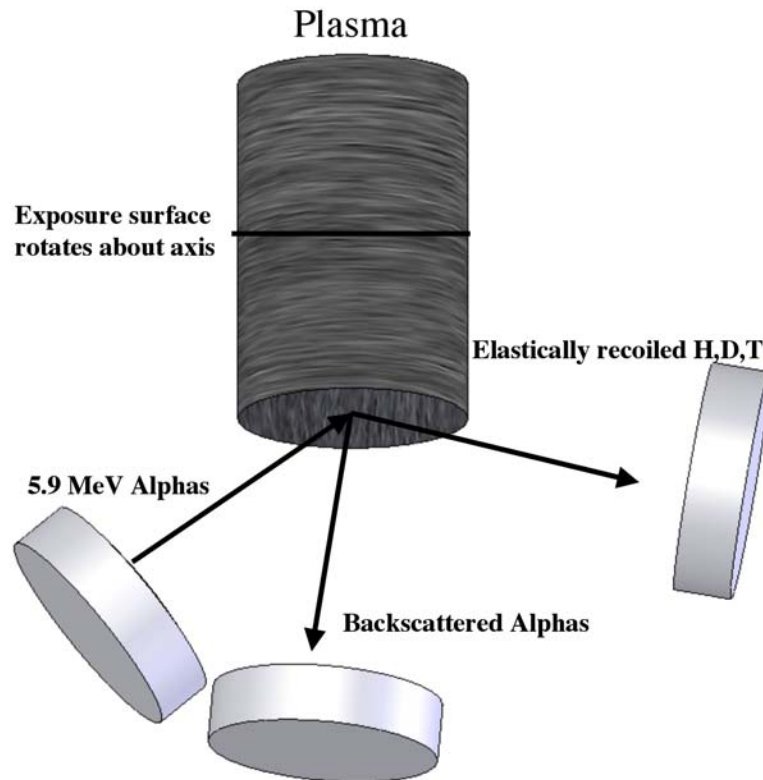


*Fig. 42: The ARRIBA surface rotates between the exposure and analysis positions.*

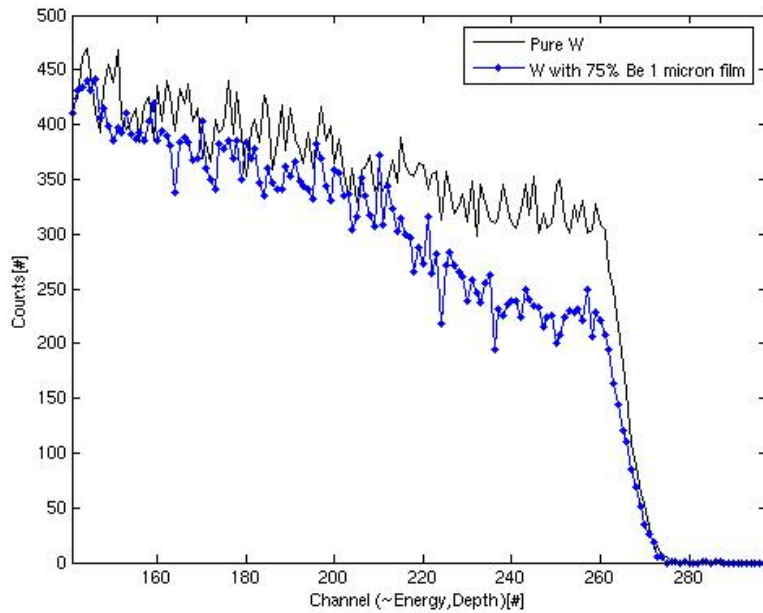


Fig. 43: The deficiency of counts between the two spectra provide a measure of the deposition and relative atomic fraction of Be on W.

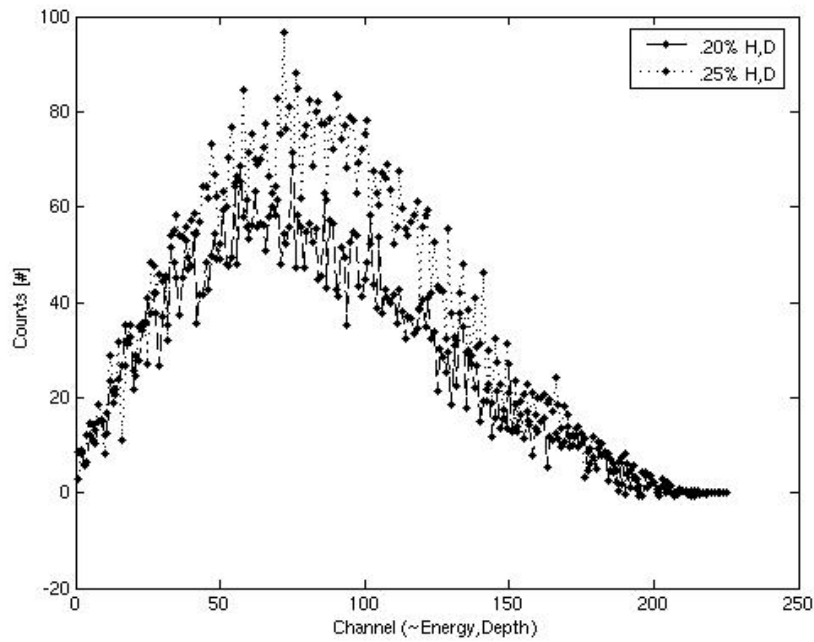


Fig. 44: Integration of the H,D peaks in ERD spectra provide a measure of retained hydrogenic species. The data shown here is for 1000nm thick deposited layer (Be,W) containing equal amounts of hydrogen and deuterium.

## Hardware Development for Transient PMI Experiments

The pulsed biasing thermal transient system described above was developed in FY06 and will be used in FY07 and FY08 to investigate the response of mono-material and mixed material systems to ELM-like thermal transients. This pulsed biasing scheme inherently perturbs the plasma discharge conditions, and in particular results in a non-thermal electron distribution function within the plasma column. As a result, the emission-based spectroscopy diagnostic techniques used for e.g. in-situ erosion measurements become difficult or impossible to use. Thus this thermal transient apparatus can be used to study the material response to such events, but cannot be used to study equally important issues such as the transport of ablated material into and through the background plasma, or the trapping of such material by a dense plasma particle load arriving on the material surface due to upstream ELM-driven plasma transients.

In order to enable the study of these plasma effects, we propose to add a laser ablation system to the PISCES facilities in FY07-08. Experience within the UCSD Center for Energy Research indicates that a modest-scaled (<1J) commercially available laser pulse focused to a 1cm spot is capable of heating relevant material surfaces (e.g. W) to ablation conditions (see. Fig. 45 below for data from the laboratory of F. Najmabadi/M. Tillack showing the measured surface temperature v. laser pulse energy). This heated surface can then eject a few 10's-100's of monolayers of surface atoms at roughly surface thermal energies. Since the laser does not perturb the background PISCES plasma, the subsequent transport of these particles can be followed using our existing diagnostics. By combining this technique with the existing pulsed biasing technique, we would expect to be able to study both the response of mixed material PMI to thermal transients, and then also study the subsequent transport of ablated mixed material layers into the background plasma. This laser system would be integrated into the experiment using the experience and expertise that already exists at UCSD, thus minimizing the time and cost needed to make such a system operational for MFE PMI research applications.

During ELM transients in ITER, the thermal load is also accompanied by a significantly increased transient plasma particle flux and, as a result, ablated surface material vapor clouds may become trapped in the near-surface region by this transient plasma. The complex issues of reionization, transport, and self-consistent interactions with the plasma present a modeling challenge, and thus controlled experiments on this issue would also be useful. In FY08, we propose to make a detailed engineering investigation into the feasibility of using a small pulsed plasma source, capable of producing plasma densities of  $10^{14} \text{ cm}^{-3}$  at electron temperatures of 3-10 eV for ~1msec. At these conditions, the mean-free path of vapor plume atoms would be a few mm or less, sufficient to induce significant vapor trapping effects. Such plasma sources have been demonstrated and can be reasonably constructed and integrated with the PISCES devices. If this evaluation demonstrated that this approach does indeed appear to be viable, then in FY09 we would propose to develop the pulsed plasma source capability using an off-line plasma chamber located within our laboratory space. When combined with the laser ablation system

described earlier, then one could envision carrying out controlled ELM thermal and particle load transient experiments using ITER relevant mixed materials. These experiments would then be used to validate vapor-trapping models that are in development for ITER divertor evaluations. With suitable material sample holder arrangements, surface currents could also be induced in the material samples being exposed in these experiments, and the resulting melt-layer loss from such samples could also be examined.

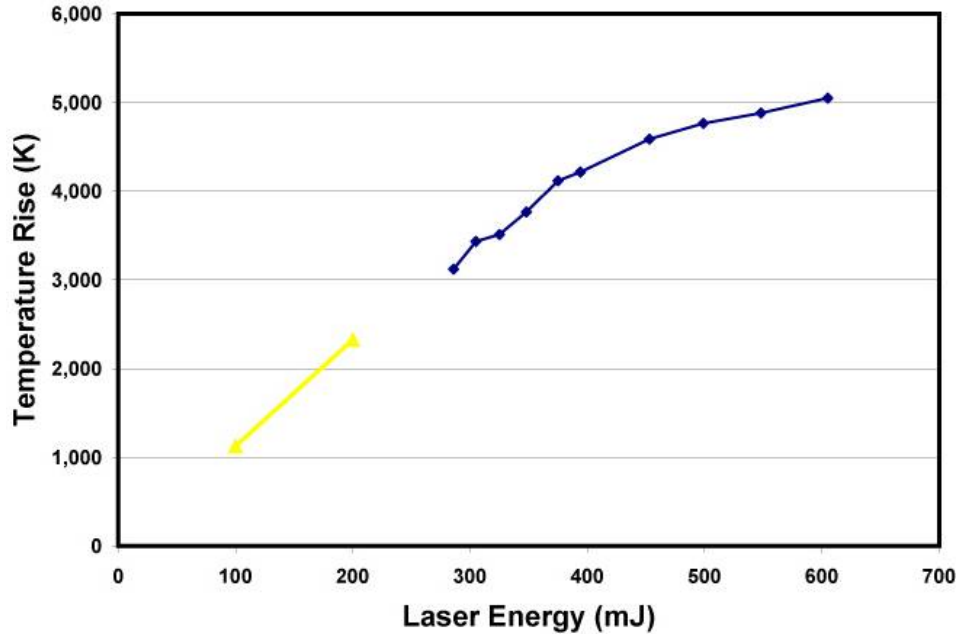


*Fig. 45: Measured tungsten (W) surface temperature rise v. laser pulse energy. A Nd:YAG laser is focused to a 1cm<sup>2</sup> spot, and a two-color thermometer system is used to measure surface temperature. Data courtesy of the UCSD Laser-Matter Interaction Laboratory (Najmabadi/Tillac)*

## References

- [Arakawa:1966] A. Arakawa, J. Comp. Phys. 1 119 (1966)
- [Antar:2005] GY Antar, GCounsell, JW Ahn, Phys. Plasmas 12 082503 (2005)
- [Beyer:2000] P Beyer, S Benkadda, X Garbet, et al, Phys. Rev. Lett. 85 4892 (2000)
- [Biskamp and Zeiler:1995] D. Biskamp, A. Zeiler Phys. Rev. Lett. 74 (1995) 706.
- [Boedo:1999] J. A. Boedo, D. Gray, R. W. Conn, et al, Rev. Sci. Instr. 70, 2997 (1999).
- [Braginskii:1965] S. I. Braginskii, "Transport Processes in a Plasma," Rev. of Plasma Phys. Vol 1 (Consultants Bureau, NY, 1965).
- [Brezinsek:2002] S. Brezinsek, PhD thesis, Forschungszentrum Julich, 2002.
- [Carreras:1996] BA Carreras, D Newman, VE Lynch et al Phys. Plasmas 3 2903 (1996)
- [Causey:1996] R A Causey et al., Proc. Int. Workshop Status/Prospect of Tritium PMI Studies, July 18–19, (1996), Toyama, Japan]
- [Causey:1998] R A Causey and D S Walsh, J. Nucl. Mater. 254, (1998) 84,
- [Coad:2001] J.P. Coad et al., 290-293 (2001) 224]
- [Diamond:1998] P.H. Diamond, M.N. Rosenbluth, F. Hinton, et al Proc. 17th IAEA Fusion Energy Conference (19-24 October 1998, Yokohama, Japan), 2000, IAEA-CN-69/TH3/1.
- [Diamond:2005] P.H. Diamond et al., Plasma Phys. Cont. Fusion 47, R35 (2005).
- [Doerner:1999] R P Doerner, et al., J. Nucl. Mater. 266–9 (1999) 392].
- [Doerner:2005] R. Doerner et al., J. Nucl. Mater. (2005) 342, 63
- [Fawcett:2002] B. L. Fawcett, A. M. Parkes, D. E. Shallcross, and A. J. Orr-Ewing, Phys. Chem. Chem. Phys. 4, 5960 (2002).
- [Federici:1999] G. Federici et al., Journal of Nuclear Materials 266-299 (1999) 14-29
- [Federici:2001] G. Federici, C. H. Skinner, J. N. Brooks, et al., Nucl. Fusion 41, 1968 (2001).
- [Fujimoto:1989] T. Fujimoto, K. Sawada, K. Takahata, et al., Nucl. Fusion Lett. 29, 1519 (1989).
- [Garcia:2005] OE Garcia, V Naulin, AH Nielsen et al, Phys. Plasmas 12 062309 (2005)
- [Goldstrass:2001] P Goldstrass, et al., J. Nucl. Mater. 290–3 (2001) 76,
- [Gondarenko:1999] N.A. Gondarenko, P.N. Guzdar, Geophys. Res. Lett. 26, 3345 (1999)
- [Haasz:1996] A Haasz & J Davis, J. Nucl. Mater. 232 (1996) 219]
- [Hasegawa:1978] A. Hasegawa, K. Mima, Phys. Fluids 21, 87 (1978).
- [Hasegawa:1983] A. Hasegawa, M. Wakatani, Phys. Rev. Lett. 50 682 (1983)
- [Hasegawa:1987] A. Hasegawa, M. Wakatani, Phys. Rev. Lett. 59, 1581 (1987).
- [Hitchinson:2005] I. H. Hutchinson, Plasma Phys. Cont. Fusion 47, 71 (2005).
- [Holland:2003] C. Holland, P.H. Diamond, S. Champeaux, et al, Nuc. Fusion 43 761 (2003)
- [Hollmann:2002] E. M. Hollmann, A. Yu. Pigarov, R. Seraydarian, et al., Phys. Plasmas 9, 1226 (2002).
- [Hollmann:2005] E. M. Hollmann, A. Yu. Pigarov, and K. Taylor, J. Nucl. Mater. 337, 451 (2005).
- [Hollmann:2006], E. M. Hollmann, S. Brezinsek, N. H. Brooks, et al., to be submitted to Plasma Phys. Contr. Fusion (2006).

- [Janev:1995] R. K. Janev, “Atomic and Molecular Processes in Fusion Edge Plasmas,” (New York: Plenum Press, 1995).
- [Karniadakis:1991] G.E. Karniadakis, M. Israeli, S.A. Orszag, J. Comp. Phys. 97 414 (1991)
- [Korde:1993] R. Korde, J. S. Cable, and L. R. Canfield, IEEE Trans. Nucl. Sci. 40, 1655 (1993).
- [LaBombard:2001] B LaBombard, RL Boivan, M Greenwald et al, Phys. Plasmas 8 2107 (2001)
- [Lavrov:1999] B. P. Lavrov, A. S. Melnikov, M. Kaening, and J. Roepcke, Phys. Rev. E 59, 3526 (1999).
- [Linsmeier:2001] Ch. Linsmeier, et al., J. Nucl. Mater. 290–3 25 (2001).
- [Mayer:1996] M Mayer, R Behrisch et al. J Nucl Mater., 230,67 (1996)
- [Möller:1988] W. Möller, W. Eckstein and J. P. Biersack, Computer Physics Communications, 51 (8) 355 (1988).
- [Morville:2004] J. Morville, D. Romanini, A. A. Kachanov, and M. Chenevier, Appl. Phys. B 78, 465 (2004).
- [Pigarov:2002] A. Yu. Pigarov, Phys. Scripta T96, 16 (2002).
- [Qing:1996] Z. Qing, D. K. Otorbaev, G. J. H. Brussaard, et al., J. Appl. Phys. 80, 1312 (1996).
- [Rognlien:1992] T.D. Rognlien, J.L. Milovich, M.E. Resink, and G.D. Porter, J. Nuclear Materials 196-198 347 (1992)
- [Rognlien:1992], TD Rognlien, JL Milovich, M Rensink et al, J. Nuc. Matls 196
- [Rognlien:1999] T.D. Rognlien, D.D. Ryutov, N. Mattor, and G.D. Porter, Phys. Plasmas 6 1851 (1999)
- [Rognlien:1992] T. D. Rognlien et al., J. Nucl. Mater. 196, 347 (1992).
- [Rohde:2001] V. Rohde et al., J. Nucl. Mater. 290-293 (2001) 317]
- [Roth:2004] J. Roth, R. Preuss, W. Bohmeyer, et al., Nucl. Fusion 44, L21 (2004).
- [Shikama:2005] Shikama et al., Phys. of Plas. 12, 044504 (2005).
- [Vasina:1970] E A Vasina, et al., Matall. (Metally) 1 (1970) 119
- [Whyte:2005] DG Whyte Plasma Physics and Controlled Fusion 47 1579(2005)
- [Whyte:2001] D. G. Whyte, G. R. Tynan, R. P. Doerner, and J. N. Brooks, Nucl. Fusion 41, 47 (2001).
- [Xu:1998] X.Q. Xu and R.H. Cohen, Contrib. Plasma Phys. 36 158 (1998)